ChPT Rechnungen zur Analyse von Gitter-QCD-Daten

Dissertation

zur Erlangung des Doktorgrades (Dr. rer. nat.)

Fakultät für Physik
–Institut für theoretische Physik–
Universität Regensburg

vorgelegt von

Ludwig Greil

aus Runding

07. März 2014

"In physics, you don't have to go around making trouble for yourself – nature does it for you."

—**Frank Wilczek**

Vorsitzender: N. N.

1. Gutachter: Prof. Dr. A. Schäfer
2. Gutachter: Prof. Dr. V. Braun

weiterer Prüfer: N. N.

Das Promotionsgesuch wurde gestellt am 07.03.2014.
Die Arbeit wurde angeleitet von Prof. Dr. A. Schäfer.

Contents

1 Theoretical Background

1.1 Quantum Chromo Dynamics (QCD)

Theoretical physicists believe that all visible matter in the universe is made up of three families of quarks and leptons and that matter is formed due to the interaction between these particles. Of the four interactions – strong, weak, electromagnetic interaction and gravity – the first three are collected in what is called the Standard model of particle physics. The quantum field theory that describes the strong interaction is called quantum chromodynamics, in short QCD, which is a non Abelian gauge theory with an $SU(3)_c$ symmetry group. The fundamental fields contained in the theory are called quarks (fermions) and gluons (gauge bosons) and the QCD Lagrangian is given by

$$\begin{aligned}\mathscr{L}_{\mathrm{QCD}} = &\sum_f \bar{q}_f^i \left(i \not{D}_{ij} - \delta_{ij} m_f\right) q_f^j - \frac{1}{4} G^a_{\mu\nu} G^{a,\mu\nu} - \frac{g^2\theta}{64\pi^2} G^a_{\mu\nu} \tilde{G}^{a,\mu\nu} \\ &- \frac{c}{2} \left(\partial_\mu A^{a,\mu}\right) \left(\partial_\nu A^{a,\nu}\right) - \bar{\xi}^a \partial^\mu \partial_\mu \xi^a + g f_{abc} \bar{\xi}^a \partial^\mu \left(A^c_\mu \xi_b\right).\end{aligned} \tag{1.1}$$

The expression above contains the covariant derivative D, which is defined as

$$\not{D}_{ij} = \gamma^\mu D_{\mu,ij} = \delta_{ij} \gamma^\mu \partial_\mu - i g t^a_{ij} \gamma^\mu A^a_\mu. \tag{1.2}$$

Eq. (1.1) contains both quark fields q_f and the gluon fields A^a_μ. There are six different flavors of quarks, called up, down, charm, strange, top and bottom, or in short $\{u, d, c, s, t, b\}$. Each of those flavors has a different mass, denoted by the mass parameter m_f in the Lagrangian. The experimentally measured masses and electric charges can be found in tabs. 1.1, 1.2. The term proportional to c is called the gauge-fixing term. The fields ξ are so-called ghost fields. Both ghost terms and gauge-fixing term only appear in the quantized version of the QCD Lagrangian.
There is another quantum number, called color, assigned to each of the quark fields, denoted by the indices $\{i, j, \ldots\}$ in the Lagrangian, which can take the values r, g, b. It is this so-called color charge that is the origin of the strong interaction mediated

Table 1.1: The light quarks u, d and s: these masses are estimates of the *current-quark masses* in the $\overline{\text{MS}}$ scheme at a scale $\mu \approx 2\,\text{GeV}$, taken from [1].

	u	d	s
charge $[e]$	$2/3$	$-1/3$	$-1/3$
mass [MeV]	$2.3^{+0.7}_{-0.5}$	$4.8^{+0.7}_{-0.3}$	95 ± 5

Table 1.2: The heavy quarks c, t and b: c- and b-quark masses are the *running* masses in the $\overline{\text{MS}}$ scheme, taken from [1].

	c	t	b
charge $[e]$	$2/3$	$2/3$	$-1/3$
mass [GeV]	1.275 ± 0.025	$173.5 \pm 0.6 \pm 0.8$	4.18 ± 0.03

by the gluons and the interaction strength of which is measured by the coupling parameter g. As mentioned before, the gauge group is $SU(3)_c$, the group of special unitary transformations that, in this case, acts in color space. The associated Lie Algebra is generated for the fundamental representation $t^a = \lambda^a/2$, where the λ^a are the Gell-Mann matrices. The defining algebra is $[t^a, t^b] = if^{abc}t^c$ where the f^{abc} are the $SU(3)_c$ structure constants. Using the gluon fields A^a_μ we can construct the gauge invariant field strength tensor, which is proportional to the commutator $[D_\mu, D_\nu]$:

$$G^a_{\mu\nu} = \partial_\mu A^a_\nu - \partial_\nu A^a_\mu - g f^{abc} A^b_\mu A^c_\nu. \tag{1.3}$$

We can also define the *dual* field strength tensor

$$\tilde{G}^{a,\mu\nu} = \epsilon^{\mu\nu\alpha\beta} G^a_{\alpha\beta}. \tag{1.4}$$

Thus, the term proportional to θ in the Lagrangian shown in eq. (1.1) would result in parity and CP violation due to strong interaction. Since so far there is no experimental evidence for parity violation withtin QCD we can omit this last term, i.e. from now on we set $\theta \equiv 0$.
What is most important about this theory is that the coupling g is not a constant, it always depends on the energy-momentum scale of the process that is under investigation. It is, just like the quark masses, subject to renormalization, due to quantum loop contributions to QCD matrix elements. In 1973, Wilczek, Gross and Politzer [2, 3] discovered that QCD is an asymptotically free theory, i.e. that the higher the energy scale μ, the smaller the coupling $g(\mu)$, which leads to the possibility of perturbatively expanding QCD matrix elements in powers of g. Formulated differently, it means that at high energies, the quarks effectively behave like free particles. On the other hand, at low energies (below 1 GeV) the coupling g is large, so it renders a perturbative treatment of QCD impossible. There are several non-

perturbative approaches to QCD: Lattice QCD (LQCD) [4, 5], effective field theories (EFTs) [6–8], Shifman–Vainshtein–Zakharov sum rules [9, 10] and many more.
As is clearly visible from tabs. 1.1, 1.2, there is a hierarchy in the masses of quarks, namely

$$m_{u,d} \ll m_s < 1\,\mathrm{GeV} < m_{c,b} \ll m_t, \tag{1.5}$$

which means that if we are interested in the properties of hadrons at low energies, the heavy quarks can be integrated out and the only dynamical degrees of freedom left are the light quarks and the gluons. Sometimes, even the s-quark is integrated out, which leaves only the two lightest quarks and the gluons as explicit degrees of freedom. The contribution of the quark flavors that have been integrated out is encoded in the (local) couplings of the other fields of the theory.
In this work we are interested in the low energy properties of hadrons and our non-perturbative method of choice is Chiral Perturbation Theory (ChPT) combined with data obtained from lattice QCD (LQCD) simulations.

1.2 Chiral Perturbation Theory (ChPT)

At low energies, the effective degrees of freedom are not quarks and gluons, but rather hadrons (mesons and baryons) formed from quarks and gluons. This observation combined with the assumption that QCD is the theory describing strong interactions leads to the idea of constructing an effective quantum field theory that has the same symmetries as QCD, is Lorentz invariant, satisfies the principles of quantum mechanics and the cluster decomposition principle [11, 12], i.e. distant experiments should give uncorrelated results. This most general effective quantum field theory will be written down in a Lagrangian with infinitely many terms and is unrenormalizable in the usual sense (and has consequently infinitely many counterterms for which one can, however, find an appropriate ordering scheme). Before we concern ourself with renormalizability and the construction of the effective Lagrangian we have to take a look at the symmetries (broken and unbroken) of QCD.

1.2.1 Chiral symmetry breaking

Since we are only interested in the low energy properties of our theory we are allowed to only keep the three lightest degrees of freedom. Additionally for now, we only consider the massless part of the QCD Lagrangian,

$$\mathscr{L}^0_{\mathrm{QCD}} = i\bar{q}\not{D}q - \frac{1}{4}G^a_{\mu\nu}G^{a,\mu\nu}, \tag{1.6}$$

while treating the mass term as a small perturbation to the massless case. Here we have used that $q^T = (u, d, s)$ and we have dropped all color and flavor indices. Using the chirality projectors we can now decompose the quark spinor into left- and

right-handed spinors so that $q = q_L + q_R$:

$$q_L = \frac{1-\gamma_5}{2}q, \qquad q_R = \frac{1+\gamma_5}{2}q. \tag{1.7}$$

Using the properties of the matrix $\gamma_5 = i\gamma^0\gamma^1\gamma^2\gamma^3$ one finds that in $\mathscr{L}^0_{\mathrm{QCD}}$ left- and right-handed quarks do not interact, i.e. they completely decouple from each other:

$$i\bar{q}\not{D}q = i\bar{q}_L\not{D}q_L + i\bar{q}_R\not{D}q_R. \tag{1.8}$$

This means $\mathscr{L}^0_{\mathrm{QCD}}$ is invariant under global, separate transformations in flavor space, e.g.

$$q_L \mapsto Lq_L, \quad q_R \mapsto Rq_R, \tag{1.9}$$

where $L \in U(3)_L$ and $R \in U(3)_R$, and we can now rewrite the whole symmetry group to

$$\begin{aligned} U(3)_L \times U(3)_R &= SU(3)_L \times SU(3)_R \times U(1)_L \times U(1)_R \\ &= SU(3)_V \times SU(3)_A \times U(1)_V \times U(1)_A, \end{aligned} \tag{1.10}$$

where the subscript V stands for the vector- and A for the axialvector-transformations (where we have used $R = L$ and $R = L^\dagger$ respectively). The symmetry associated with this set of transformations is called *chiral symmetry* while the limit of vanishing quark masses is usually referred to as the *chiral limit*.
Experiments indeed show that QCD has this invariance under $U(1)_V$ transformations, which corresponds to baryon number conservation, whereas the axial $U(1)_A$ symmetry is anomalously broken, which means that the symmetry is broken when quantizing the theory.
When looking at the hadron spectrum we find that a $SU(3)_L \times SU(3)_R$ symmetry cannot be realized, not even approximately, since the expected (approximate) parity-doubling of hadron states is not at all observed in nature. On the other side one finds that the lowest-lying baryons are arranged in approximate multiplets of this $SU(3)_V$ symmetry. Since the symmetry of the Lagrangian is not shared by the ground state it is spontaneously broken, which according to Nambu and Goldstone leads to the appearance of massless spin zero particles, so-called Goldstone bosons [13, 14]. To be exact, for every generator of the broken symmetry one Goldstone boson emerges, so in our case where $SU(3)_L \times SU(3)_R$ is broken down to just the vectorial group, we should have $3^2 - 1$ Goldstone bosons with the quantum numbers of the $SU(3)_A$, i.e. an octet of pseudoscalar mesons. In the idealized case of $\mathscr{L}^0_{\mathrm{QCD}}$ they would be massless, but since chiral symmetry is also explicitly broken by the mass term, we expect them to have small masses, at least small compared to the first particle that is not an approximate Goldstone boson, namely the vector meson $\rho(770)$ with mass $M_\rho \approx 775\,\mathrm{MeV}$. Looking at the eight lowest-lying pseudoscalar mesons (see tab. 1.3) we find that this is indeed the case, although the supression factor $M_K/M_\rho \approx 0.64$ is

Table 1.3: Masses and quantum numbers of the lowest-lying octet mesons, taken from [1]

	$\pi^\pm$	π^0	$K^\pm$	$K^0, \bar{K}^0$	η
J^P	0^-	0^-	0^-	0^-	0^-
approx. mass [MeV]	140	135	494	498	548

quite large compared to the two-flavor case, where one only has a triplet of pion states and thus a supression factor of $M_\pi/M_\rho \approx 0.18$. Hence a better convergence behavior for a perturbative expansion around the chiral limit is expected for the two-flavor case. In the purely mesonic sector which we are considering now, the suppression factors appear in even powers, i.e. $(M_K/M_\rho)^2 \approx 0.41$ and $(M_\pi/M_\rho)^2 \approx 0.033$, hence we expect a better convergence for this setup than when e.g. baryons or vector mesons are included.

1.2.2 Constructing ChPT

In this section we will describe how to construct an effective field theory of QCD based on the symmetries and symmetry breaking patterns described in the last subsection. This effective theory will then describe the interaction between mesons at low energies. As a first step we add external vector ($v^\mu(x)$), axialvector ($a^\mu(x)$), scalar ($s(x)$) and pseudoscalar ($p(x)$) sources to eq. (1.6):

$$\mathscr{L} = \mathscr{L}^0_{\mathrm{QCD}} + \bar{q}\Big[\gamma_\mu(v^\mu + \gamma_5 a^\mu) - (s - i\gamma_5 p)\Big]q. \tag{1.11}$$

All these external fields are Hermitian in flavor space and we have only included the octet components of a^μ and v^μ, i.e. $v_\mu = v^i_\mu \lambda^i/2$ and $a_\mu = a^i_\mu \lambda^i/2$ where the λ^i with $i = 1, \ldots, 8$ are the well known Gell-Mann matrices. Hence the traces in flavor space $\langle v^\mu \rangle$ and $\langle a^\mu \rangle$ are zero. We can now write down the generating functional

$$e^{iZ[v,a,s,p]} = \left\langle 0 \left| \mathrm{T}\left\{ \exp\left(i \int d^4x\, \hat{\bar{q}}\Big[\gamma_\mu(v^\mu + \gamma_5 a^\mu) - (s - i\gamma_5 p)\Big]\hat{q} \right) \right\} \right| 0 \right\rangle, \tag{1.12}$$

which is invariant under $SU(3)_L \times SU(3)_R$ transformations if the external sources transform in the following way:

$$r^\mu \mapsto R r^\mu R^\dagger + iR\partial^\mu R^\dagger, \tag{1.13}$$

$$l^\mu \mapsto L l^\mu L^\dagger + iL\partial^\mu L^\dagger, \tag{1.14}$$

$$s + ip \mapsto R(s + ip)L^\dagger \tag{1.15}$$

Here, again, $L \in SU(3)_L$ and $R \in SU(3)_R$ and we have used the linear combinations l^μ and r^μ defined as $r^\mu = v^\mu + a^\mu$ and $l^\mu = v^\mu - a^\mu$. We also have made use of the ordinary time ordering $\mathrm{T}\{\ldots\}$ in the definition of the generating functional. The

scalar source s usually contains the quark mass matrix $\mathscr{M} = \mathrm{diag}(m_u, m_d, m_s)$ in such a way that $s = \mathscr{M} + \ldots$ and is thus treated, as mentioned before, as an external perturbation of the otherwise massless theory.
Introducing these external fields is useful in two different ways: on one hand, this formalism is very well suited for adding a broad variety of interactions, e.g. adding the coupling of photon fields to the quark fields. On the other hand all Greens functions for quark currents can be derived by taking functional derivatives with respect to the external sources.
The key idea of an effective theory is now to write eq. (1.12) as a path integral over the effective degrees of freedom, in our case the Goldstone bosons:

$$e^{iZ[v,a,s,p]} = \int [dU] \exp\left(i \int d^4x \, \mathscr{L}_{\text{eff}}(U, v, a, s, p)\right). \tag{1.16}$$

Note that here, the path-integral measure is denoted as $[dU]$ while the field U collects the Goldstone bosons in a suitable way which will be specified below. By rewriting eq. (1.12) we have made the assumption that the low-energy behavior of QCD is dominated by the interactions of these Goldstone bosons and hence eq. (1.16) is not applicable in an energy regime where other degrees of freedom like the $\rho(770)$ vector meson or baryons become important for the dynamics. What has also been assumed is that quarks and gluons never appear as asymptotic states, because due to confinement free quarks or gluons do not contribute to long-range dynamics at low energies.
The rest of this subsection will be concerned with the construction of $\mathscr{L}_{\text{eff}}$ and will closely follow [15] whereas the fundamental principles are explained in [16, 17]. We start from the fact that our initial symmetry group G is spontaneously broken to H, which is a proper subgroup of G. Note that according to the Goldstone theorem [13, 14] we then have $\dim(G) - \dim(H) = n$ Goldstone boson fields which we will collect in a vector $\vec{\Phi} = (\phi_1, \ldots, \phi_n)^T$. We find that G acts on $\vec{\Phi}$ in the following way:

$$g \in G: \qquad \vec{\Phi} \mapsto \vec{\Phi}' = \vec{f}\left(g, \vec{\Phi}\right), \tag{1.17}$$

where $\vec{f}$ fulfills the group homomorphism property

$$\vec{f}\left(g_1, \vec{f}\left(g_2, \vec{\Phi}\right)\right) = \vec{f}\left(g_1 g_2, \vec{\Phi}\right). \tag{1.18}$$

Now we consider the subgroup H that leaves the ground state ($\vec{\Phi} \equiv \vec{0}$) invariant, i.e.

$$h \in H: \qquad \vec{f}\left(h, \vec{0}\right) = \vec{0}. \tag{1.19}$$

In our case, the subgroup H is to be identified with $SU(3)_V$. Using the group homomorphism property eq. (1.18) again we find that for all $h \in H$, $g \in G$,

$$\vec{f}\left(gh, \vec{0}\right) = \vec{f}\left(g, \vec{0}\right), \tag{1.20}$$

and thus we have found an invertible mapping from the coset space G/H onto the space of Goldstone boson fields. Also, the dimension of G/H is the same as the number of generators that do not leave the ground state invariant, i.e. the dimension of the space of Goldstone boson fields. So now we have found a one-to-one correspondence of the elements of G/H to the Goldstone boson fields. Looking at the action of G on G/H one finds, as elaborately described in [15], that each element of G/H and thus the Goldstone bosons can be uniquely characterized by a unitary matrix $U(x)$ that contains all 8 Goldstone bosons and transforms under chiral transformations in the following way:

$$U(x) \mapsto RU(x)L^\dagger, \quad L \in SU(3)_L, \quad R \in SU(3)_R. \tag{1.21}$$

There is still a freedom of choice regarding the coordinates on the group manifold G/H and the standard choice for $U(x)$ is

$$U(x) = \exp\left(i\frac{\phi(x)}{F_0}\right), \tag{1.22}$$

where $\phi(x) = \lambda^a\phi^a(x)$ is a Hermitian 3×3 matrix

$$\phi(x) = \sqrt{2}\begin{pmatrix} \frac{1}{\sqrt{2}}\pi^0(x) + \frac{1}{\sqrt{6}}\eta(x) & \pi^+(x) & K^+(x) \\ \pi^-(x) & -\frac{1}{\sqrt{2}}\pi^0(x) + \frac{1}{\sqrt{6}}\eta(x) & K^0(x) \\ K^-(x) & \bar{K}^0(x) & -\frac{2}{\sqrt{6}}\eta(x) \end{pmatrix}, \tag{1.23}$$

and F_0 is a dimensionful constant. One finds that the matrix element of the axial vector current between a one-boson state and the vacuum can be expressed as

$$\langle 0 \left| A_a^\mu(0) \right| \phi_b(p) \rangle = ip^\mu \delta_{ab} F_0, \tag{1.24}$$

by expanding the axial current to lowest order in powers of ϕ. One calls F_0 the pseudoscalar meson decay constant in the chiral limit.
Now that we have chosen a representation for the Goldstone boson fields we can construct the corresponding effective Lagrangian. Lorentz invariance dictates that derivatives of the Goldstone fields can only appear in pairs and for now we neglect all the external fields v, a, s, p. Since we are talking about a low energy expansion all the appearing Goldstone boson momenta q have to be small compared to a typical hadronic scale of $\approx 1\,\mathrm{GeV}$. This expansion of matrix elements in powers of q goes by the name of Chiral Perturbation Theory. As mentioned above the effective Lagrangian will have infinitely many terms and we can cluster them according to the number of derivatives acting on the Goldstone boson fields:

$$\mathscr{L}_{\text{eff}} = \mathscr{L}^{(0)} + \mathscr{L}^{(2)} + \mathscr{L}^{(4)} + \dots . \tag{1.25}$$

Since U is a unitary matrix, $\mathscr{L}^{(0)} = U^\dagger U = \mathbb{1}$ and can therefore be neglected. Thus, the leading order term in the effective Lagrangian is $\mathscr{L}^{(2)}$ and takes the form

$$\mathscr{L}^{(2)} = \frac{F_0^2}{4} \left\langle (\partial_\mu U) (\partial^\mu U)^\dagger \right\rangle + \dots , \tag{1.26}$$

where $\langle \dots \rangle$ still stands for a trace in flavor space and the prefactor $F_0^2/4$ has been chosen in such a way that the lowest order expansion of the Lagrangian reproduces the well known kinetic terms

$$\mathscr{L}^{(2)} = \left(\partial_\mu \pi^+\right) \left(\partial^\mu \pi^-\right) + \left(\partial_\mu K^+\right) \left(\partial^\mu K^-\right) + \dots . \tag{1.27}$$

Since we want our theory to be invariant under local chiral transformations (Leutwyler showed in [18] that this is neccessary to have a theoretically sound construction of ChPT), we have to introduce a covariant derivative that contains the external fields l^μ and r^μ,

$$\nabla^\mu U = \partial^\mu U - i r^\mu U + i U l^\mu . \tag{1.28}$$

We want to have a consistent power counting scheme, thus we need the external fields a^μ and v^μ to also be counted as $\mathcal{O}(q)$. So far we have dealt with the chiral limit of the theory, i.e. all quark masses were zero. Once we switch on the quark masses we have explicit chiral symmetry breaking in form of the mass term which in full QCD behaves as follows under a decomposition into left- and right-handed quarks:

$$\bar{q} \mathscr{M} q = \bar{q}_L \mathscr{M} q_R + \bar{q}_R \mathscr{M} q_L . \tag{1.29}$$

Since we want to have the exact same explicit symmetry breaking pattern as in QCD, we can now construct the full lowest order chiral Lagrangian, which contains the scalar field $s = \mathscr{M} + \dots$, the field U and derivatives acting thereon:

$$\mathscr{L}^{(2)} = \frac{F_0^2}{4} \left\langle (\nabla_\mu U) (\nabla^\mu U)^\dagger + 2B_0 (s U^\dagger + U s^\dagger) \right\rangle , \tag{1.30}$$

where B_0 is related to the quark condensate in the chiral limit. One can clearly see that we have counted the quark masses, and thus the scalar field that contains the quark masses, as $\mathcal{O}(q^2)$, which can be understood when we expand eq. (1.30) to lowest order. We then find the famous Gell-Mann-Oakes-Renner relation [19] that the squared Goldstone boson masses are proportional to the quark masses:

$$M_{\pi^\pm}^2 = B_0 (m_u + m_d), \tag{1.31}$$
$$M_{\pi^0}^2 = B_0 (m_u + m_d) + \mathcal{O}((m_u - m_d)^2), \tag{1.32}$$
$$M_{K^\pm}^2 = B_0 (m_u + m_s), \tag{1.33}$$
$$M_{K^0}^2 = B_0 (m_d + m_s), \tag{1.34}$$

$$M_\eta^2 = \frac{B_0}{3}(m_u + m_d + 4m_s) + \mathcal{O}((m_u - m_d)^2). \tag{1.35}$$

All the contributions proportional to the mass difference between m_u and m_d disappear in the isospin symmetric case $m_u = m_d$ but have to be taken into account if one allows for isospin breaking. Throughout this thesis we will work in the approximation of isospin symmetry and thus $M_{\pi^\pm}^2 = M_{\pi^0}^2$, $M_{K^\pm}^2 = M_{K^0}^2$. Employing eqs. (1.31)-(1.35) and again assuming isospin symmetry we can verify the famous Gell-Mann-Okubo mass formula

$$4M_K^2 = 3M_\eta^2 + M_\pi^2, \tag{1.36}$$

which is fulfilled up to a few percent in nature. Using the Lagrangian eq. (1.30), at leading order one can reproduce the results that are already known from current algebra [20]. The effective Lagrangian method is advantageous in the sense that higher order corrections can be systematically calculated.
The unknown constant can be connected to the quark condensate and the decay constant F_0 via eq. (1.16) and one finds the following (lowest order) relation:

$$\langle 0|\bar{u}u|0\rangle = \left\langle 0|\bar{d}d|0\right\rangle = \langle 0|\bar{s}s|0\rangle = -F_0^2 B_0 + \dots . \tag{1.37}$$

Later on we will also need $\mathscr{L}^{(4)}$, which was first constructed by Gasser and Leutwyler [7], so it is convenient to present it in its entirety at this point:

$$\begin{aligned}
\mathscr{L}^{(4)} = {} & L_1 \left\langle (\nabla^\mu U)^\dagger (\nabla_\mu U)\right\rangle^2 + L_2 \left\langle (\nabla_\mu U)^\dagger (\nabla_\nu U)\right\rangle \left\langle (\nabla^\mu U)^\dagger (\nabla^\nu U)\right\rangle \\
& + L_3 \left\langle (\nabla^\mu U)^\dagger (\nabla_\mu U) (\nabla^\nu U)^\dagger (\nabla_\nu U)\right\rangle \\
& + L_4 \left\langle (\nabla^\mu U)^\dagger (\nabla_\mu U)\right\rangle \left\langle \chi^\dagger U + \chi U^\dagger\right\rangle \\
& + L_5 \left\langle (\nabla^\mu U)^\dagger (\nabla_\mu U) (\chi^\dagger U + \chi U^\dagger)\right\rangle \\
& + L_6 \left\langle \chi^\dagger U + \chi U^\dagger\right\rangle^2 + L_7 \left\langle \chi^\dagger U - \chi U^\dagger\right\rangle^2 + L_8 \left\langle \chi^\dagger U \chi^\dagger U + \chi U^\dagger \chi U^\dagger\right\rangle \\
& - iL_9 \left\langle F_{\mu\nu}^R (\nabla^\mu U) (\nabla^\nu U)^\dagger + F_{\mu\nu}^L (\nabla^\mu U)^\dagger (\nabla^\nu U)\right\rangle \\
& + L_{10} \left\langle U^\dagger F_{\mu\nu}^R U F^{L,\mu\nu}\right\rangle + H_1 \left\langle F_{\mu\nu}^R F^{R,\mu\nu} + F_{\mu\nu}^L F^{L,\mu\nu}\right\rangle + H_2 \left\langle \chi^\dagger \chi\right\rangle ,
\end{aligned} \tag{1.38}$$

where we have introduced new building blocks

$$\chi = 2B_0(s + ip), \tag{1.39}$$
$$F_{\mu\nu}^L = \partial_\mu l_\nu - \partial_\nu l_\mu - i[l_\mu, l_\nu], \tag{1.40}$$
$$F_{\mu\nu}^R = \partial_\mu r_\nu - \partial_\nu r_\mu - i[r_\mu, r_\nu]. \tag{1.41}$$

The last two terms in eq. (1.38) do not have any physical relevance, they are counterterms to the renormalization of one-loop graphs and are hence often omitted. All these constants L_i and H_i are in no way restricted by the theory and basically they

encode all the information about the integrated out heavier quarks. They are free parameters of the theory and have to be fixed with input from experiments or LQCD. Since the number of terms in the effective Lagrangians gets large pretty fast one might say that the theory loses predictive power when doing higher order analyses. But for a given process only subsets of low energy constants (LECs) contribute at a given order, hence it is not neccessary to pin down all the LECs appearing in the effective Lagrangians to said order.

1.2.3 Power counting and renormalization

Since we have a proper power counting scheme for the effective Lagrangian we now want to translate said scheme to a power counting scheme for Feynman diagrams. We start with the propagator for the Goldstone boson fields in momentum space,

$$i\Delta(q) = \frac{i}{q^2 - M_\phi^2}, \tag{1.42}$$

which we obviously count as $\mathcal{O}(q^{-2})$. This will always be the case, also if $\Delta(q)$ appears inside of a loop integral with its momentum q integrated up to infinity. This will still lead to a consistent counting scheme if we use dimensional regularization. Let I be the number of internal Goldstone boson lines, V_n the number of vertices from $\mathscr{L}^{(n)}$ and L the number of loops, then any given amplitude $\mathscr{A}$ expressed in momenta q takes the following form:

$$\mathscr{A} \propto \int (d^d q)^L \frac{1}{(q^2)^I} \prod_n (q^n)^{V_n}. \tag{1.43}$$

If we now want $\mathscr{A}$ to be of chiral dimension D, i.e. $\mathscr{A}$ is of order $\mathcal{O}(q^D)$, then we find that

$$D = dL - 2I + \sum_n n V_n, \tag{1.44}$$

and using the identity $I = L - 1 + \sum_n V_n$ we can eliminate I and end up with a counting formula for our perturbative expansion in Feynman diagrams:

$$D = (d-2)L + 2 + \sum_n (n-2)V_n. \tag{1.45}$$

We see that for $d \geq 2$ the chiral dimension D is non-negative; for definiteness we set $d = 4$ from now on. For an increasing number of loops, the amplitude $\mathscr{A}$ will be supressed since q is a small momentum and the lowest order contribution is of $\mathcal{O}(q^2)$. The graphs associated with an $\mathcal{O}(q^2)$ amplitude consist of no loops and an arbitrary number of vertices originating from $\mathscr{L}^{(2)}$. At next to leading order we have one loop graphs with vertices from $\mathscr{L}^{(2)}$, tree level graphs with exactly one vertex from $\mathscr{L}^{(4)}$ and tree level graphs with several insertions from $\mathscr{L}^{(2)}$. Combining

eq. (1.45) with the earlier mentioned fact that every Lagrangian of fixed order has only a finite number of terms leads to the conclusion that at fixed chiral order, only a finite number of Feynman diagrams contribute to a process at a certain chiral order. Since all loop graphs contain ultraviolet (UV) divergences as the dimension $d \to 4$ they require renormalization, which is only possible if a theory contains counterterms that can absorb these divergences. The effective Lagrangian of ChPT as we have presented it here contains all possible terms that are consistent with the required symmetries, thus every UV divergence created by loop graphs will be absorbed by a LEC from the same Lagrangian. Of course we need to employ a regularization scheme that keeps all symmetries relevant for the theory intact, as is the case for dimensional regularization. As presented in [7] all one-loop divergences can be absorbed in the L_i and H_i of eq. (1.38):

$$L_i = L_i^r(\mu) + \Gamma_i \lambda, \qquad i = 1, \ldots, 10, \tag{1.46}$$

$$H_i = H_i^r(\mu) + \Delta_i \lambda, \qquad i = 1, 2, \tag{1.47}$$

where prefactors Γ_i and Δ_i are known from the associated β-function while the divergence is contained in λ:

$$\lambda = \frac{\mu^{d-4}}{(4\pi)^2}\left[\frac{1}{d-4} - \frac{1}{2}(\log 4\pi + \Gamma'(1) + 1)\right]. \tag{1.48}$$

Here we have introduced a mass scale μ, called the scale of dimensional regularization. Subtracting terms proportional to λ from one-loop amplitudes is commonly known as the modified minimal subtraction scheme (for short $\overline{\text{MS}}$ scheme), which is a certain scheme within dimensional regularization. There also exists the minimal subtraction (MS) scheme where only the term proportional to the $(d-4)$ pole is subtracted from the amplitude. As one can see from eqs. (1.46), (1.47) the renormalized LECs depend on the scale μ, as is the case for the subtracted loop graphs, while the full amplitude in combination of both effects is independent of the scale μ.
Up to now we have only considered the interactions between mesons, which gives insight into a variety of interesting quantities like meson decay constants, meson-meson scattering amplitudes and many more. So far we cannot investigate any processes that include baryons or vector mesons and thus our current framework needs to be extended. The next sections will show how to introduce baryons in the theory and how to systematically calculate baryonic observables in this framework.

1.3 Baryon Chiral Perturbation Pheory (BChPT)

In this section we systematically want to introduce baryons into the framework of ChPT (we closely follow [21]) so that transition amplitudes

$$\mathscr{F}(\vec{p}, \vec{p}', v, a, s, p) = \langle B'(\vec{p}')|B(\vec{p})\rangle^c_{v,a,s,p}\,, \tag{1.49}$$

can be calculated in terms of a low-energy expansion. B' and B stand for outgoing and incoming baryon states and they carry three momenta $\vec{p}'$ and $\vec{p}$ respectively. We will only consider contributions from connected Feynman diagrams, which is indicated by the superscript c and analogously to the mesonic sector we again want these matrix elements to be evaluated in the presence of external fields. Here, we only need to consider single-baryon-states, so we will neglect all possibilities of multiple baryon states as incoming or outgoing particles, hence processes like baryon-baryon scattering cannot be described by our theory. We will extend the theory of ChPT by the lowest-lying octet baryons which we collect in a 3×3 Hermitian matrix B,

$$B = \begin{pmatrix} \frac{1}{\sqrt{2}}\Sigma^0 + \frac{1}{\sqrt{6}}\Lambda & \Sigma^+ & p \\ \Sigma^- & -\frac{1}{\sqrt{2}}\Sigma^0 + \frac{1}{\sqrt{6}}\Lambda & n \\ \Xi^- & \Xi^0 & -\frac{2}{\sqrt{6}}\Lambda \end{pmatrix}, \tag{1.50}$$

that transforms nonlinearly under chiral transformations, i.e.

$$B \to K(L,R,U)BK^\dagger(L,R,U), \tag{1.51}$$

where again $L \in SU(3)_L$, $R \in SU(3)_R$ and the compensator field K is a non-linear function of the field U and L, R, which is defined by its action on the field $u = \sqrt{U}$:

$$u \to KuL^\dagger = RuK^\dagger. \tag{1.52}$$

We can now construct building blocks $\mathscr{X}$ that transform under chiral transformations as $\mathscr{X} \to K\mathscr{X}K^\dagger$, which will be the main building blocks of our effective Lagrangian:

$$u_\mu = iu^\dagger(\nabla_\mu U)u^\dagger, \tag{1.53}$$

$$\chi_\pm = \frac{1}{2}\left(u\chi^\dagger u \pm u^\dagger \chi u^\dagger\right), \tag{1.54}$$

$$F^\pm_{\mu\nu} = u^\dagger F^R_{\mu\nu} u \pm u F^L_{\mu\nu} u^\dagger. \tag{1.55}$$

We find that in this chosen representation, the covariant derivative takes the form

$$D_\mu B = \partial_\mu B + [\Gamma_\mu, B], \tag{1.56}$$

where the chiral connection Γ_μ is given by

$$\Gamma_\mu = \frac{1}{2}\left[u^\dagger, \partial_\mu u\right] - \frac{i}{2}\left(u^\dagger r_\mu u - u l_\mu u^\dagger\right). \tag{1.57}$$

So far we can tell that u_μ has to be counted as $\mathcal{O}(q)$ since it contains a derivative acting on a meson field. We also find that $F^\pm_{\mu\nu}$ is of $\mathcal{O}(q^2)$. However, it is not yet clear how the baryon field B and the covariant derivative thereof should be counted, since the baryon octet mass in the chiral limit, m_0, does not vanish. An analysis of the behavior of free baryon fields as performed in [21] shows that only the baryon

three-momentum $\vec{p}$ can be counted as $\mathcal{O}(q)$ and thus we end up with the following important counting rules:

$$B,\, \bar{B} = \mathcal{O}(1), \qquad D_\mu B = \mathcal{O}(1), \qquad i\not{D}B - m_0 B = \mathcal{O}(q). \tag{1.58}$$

Furthermore we present the counting rules for baryon bilinears of elements of the Clifford algebra, since these will also be used for writing down the effective meson-baryon Lagrangians:

$$\bar{B}\left\{\mathbb{1}, \gamma_\mu, \gamma_5\gamma_\mu, \sigma_{\mu\nu}\right\} B = \mathcal{O}(1), \qquad \bar{B}\gamma_5 B = \mathcal{O}(q). \tag{1.59}$$

Using the building blocks eq. (1.53)-(1.55) and counting rules eqs. (1.58), (1.59) we can write down the lowest order effective Lagrangian for the meson-baryon interaction:

$$\mathscr{L}_{\mathrm{MB}}^{(1)} = \left\langle \bar{B}(i\not{D} - m_0)B \right\rangle + \frac{D}{2}\left\langle \bar{B}\gamma_5\gamma^\mu \left\{u_\mu, B\right\}\right\rangle + \frac{F}{2}\left\langle \bar{B}\gamma^\mu\gamma_5 \left[u_\mu, B\right]\right\rangle. \tag{1.60}$$

As already mentioned before, m_0 is the baryon octet mass in the chiral limit and D and F are the axial meson baryon couplings. In the chiral limit $D + F = g_A^0$, where g_A^0 is the axial coupling constant in the chiral limit from $SU(2)_f$ BChPT. The constants D and F can in principle be determined by fitting to semileptonic baryon decays [22, 23] or fitting to hyperon axial coupling data obtained through LQCD simulations [24]. The values obtained from the semileptonic baryon decays do not match the ones obtained from fits to LQCD simulation data and thus, we will employ a very common choice for the $SU(3)$ axial couplings, namely $D = 0.75$, $F = 0.5$.
Analogously to the derivation of eq. (1.45) we can obtain the ordering for a perturbative expansion within our theory by considering the fact that the baryon propagator is counted as $\mathcal{O}(q^{-1})$ and hence we end up with an expression for the chiral dimension D that also includes baryons:

$$D = 2L + 1 + \sum_n (n-2)V_n^{\mathrm{MM}} + \sum_n (n-1)V_n^{\mathrm{MB}}. \tag{1.61}$$

We have attached superscripts to the number of vertices per chiral order depending of whether they originate from the meson-meson or the meson-baryon Lagrangians. Eq. (1.61) implies that the chiral ordering starts at $\mathcal{O}(q)$, as one would expect since we also have a Lagrangian of first chiral order.
The $SU(2)_f$ version of this theory was first worked out by Gasser, Sainio and Švarc [25] and is in general called Baryon Chiral Perturbation Theory (BChPT). It is noted in the aforementioned publication that, in contrast to meson ChPT, where the $\overline{\mathrm{MS}}$ renormalization scheme is used, one now has to use a different renormalization scheme since dimensional regularization combined with the $\overline{\mathrm{MS}}$ scheme does not maintain power counting when including baryons. The evaluated loop graphs will in general contain terms of lower chiral order than suggested by naïve power counting, so that we can speak of a break down of chiral power counting when using this

renormalization scheme. This behavior can be explained with the appearance of a non-vanishing mass scale in this theory, namely the baryon mass in the chiral limit, m_0. This lead to several suggestions of renormalization schemes that keep chiral power counting intact: the non-relativistic heavy baryon approach (HBChPT) [26, 27], the relativistic infrared regularization (IR) scheme [28], based on ideas presented in [29, 30], and the newer, also Lorentz-invariant, extended-on-mass-shell scheme (EOMS) [31]. We will give a short introduction to the IR scheme after this section.
Since we will perform a full one-loop calculation and analysis of the baryon octet masses we need additional terms for the effective baryon-meson Lagrangian which we shall present here. The second order Lagrangian differs from the one in [33] as one term was eliminated in [34, 35]:

$$\begin{aligned}
\mathscr{L}^{(2)}_{\mathrm{MB}} &= b_{D/F}\left\langle \bar{B}\left[\chi_+, B\right]_\pm\right\rangle + b_0\left\langle \bar{B}B\right\rangle\langle\chi_+\rangle \\
&\quad + b_{1/2}\left\langle \bar{B}\left[u_\mu,\left[u^\mu, B\right]_\mp\right]\right\rangle + b_3\left\langle \bar{B}\left\{u_\mu,\left\{u^\mu, B\right\}\right\}\right\rangle + b_4\left\langle \bar{B}B\right\rangle\langle u_\mu u^\mu\rangle \\
&\quad + ib_{5/6}\left\langle \bar{B}\sigma^{\mu\nu}\left[\left[u_\mu, u_\nu\right], B\right]_\mp\right\rangle + ib_7\left\langle \bar{B}\sigma^{\mu\nu}u_\mu\right\rangle\langle u_\nu B\rangle \\
&\quad + \frac{i\,b_{8/9}}{2m_0}\Big(\left\langle \bar{B}\gamma^\mu\left[u_\mu,\left[u_\nu,\left[D^\nu, B\right]\right]_\mp\right]\right\rangle + \left\langle \bar{B}\gamma^\mu\Big[D_\nu,\left[u^\nu,\left[u_\mu, B\right]\right]_\mp\Big]\right\rangle\Big) \\
&\quad + \frac{i\,b_{10}}{2m_0}\Big(\left\langle \bar{B}\gamma^\mu\left\{u_\mu,\left\{u_\nu,\left[D^\nu, B\right]\right\}\right\}\right\rangle + \left\langle \bar{B}\gamma^\mu\left[D_\nu,\left\{u^\nu,\left\{u_\mu, B\right\}\right\}\right]\right\rangle\Big) \\
&\quad + \frac{i\,b_{11}}{2m_0}\Big(2\left\langle \bar{B}\gamma^\mu\left[D_\nu, B\right]\right\rangle\langle u_\mu u^\nu\rangle + \left\langle \bar{B}\gamma^\mu B\right\rangle\langle\left[D_\nu, u_\mu\right]u^\nu + u_\mu\left[D_\nu, u^\nu\right]\rangle\Big),
\end{aligned} \tag{1.62}$$

$$\begin{aligned}
\mathscr{L}^{(4)}_{\mathrm{MB}} &= d_1\left\langle \bar{B}[\chi_+,[\chi_+, B]]\right\rangle + d_2\left\langle \bar{B}[\chi_+,\{\chi_+, B\}]\right\rangle + d_3\left\langle \bar{B}\{\chi_+,\{\chi_+, B\}\}\right\rangle \\
&\quad + d_4\left\langle \bar{B}\chi_+\right\rangle\langle\chi_+ B\rangle + d_5\left\langle \bar{B}[\chi_+, B]\right\rangle\langle\chi_+\rangle + d_6\left\langle \bar{B}B\right\rangle\langle\chi_+\rangle\langle\chi_+\rangle \\
&\quad + d_7\left\langle \bar{B}B\right\rangle\left\langle\chi_+^2\right\rangle + \ldots.
\end{aligned} \tag{1.63}$$

1.4 Infrared regularization for baryons

The goal of Becher and Leutwyler was, as they wrote in the introduction of [28], to find a regularization procedure that is Lorentz invariant and reproduces the HBChPT result when performing a non-relativistic expansion, without having to deal with the problems associated with a purely non-relativistic treatment, i.e. problems with convergence of the heavy baryon expansion in certain energy regions as presented in sec. 3 of [28]. The basic idea of the regularization scheme is to separate the 'soft' parts that come from the meson propagator from the 'hard contribution' that stems from the baryon propagator and absorb the latter into the local couplings while keeping the 'soft' part which does not violate chiral power counting, as was first formulated by Tang and Ellis [29, 30].
We will illustrate the basic idea of Becher and Leutwyler for the easiest scalar one-loop

integral

$$H = -i \int \frac{d^d l}{(2\pi)^d} \frac{1}{[M^2 - l^2]\,[m^2 - (P-l)^2]}, \tag{1.64}$$

which contains the meson propagator with meson mass M of $\mathcal{O}(q)$ and the baryon propagator with mass m and momentum P. Using the power counting as was explained before we would assign a chiral order of $\mathcal{O}(q^{d-3})$. We now need to extract the 'soft' part or, as called in [28], the infrared singular part, which has d-dependent powers of the mass M, i.e. M^{d-3}, M^{d-2}, etc.
We start with the standard Schwinger-Feynman parametrization to combine the two propagators, i.e.

$$H = -i \int \frac{d^d l}{(2\pi)^d} \int_0^1 \frac{du}{\left[(1-u)(M^2 - l^2) + u(m^2 - (P-l)^2)\right]^2}, \tag{1.65}$$

and after carrying out the l integration we find the following result:

$$H = \frac{m^{d-4}}{(4\pi)^{d/2}} \Gamma\left(2 - \frac{d}{2}\right) \int_0^1 du \left[u^2 - 2\alpha\Omega u(1-u) + \alpha^2(1-u)^2\right]^{\frac{d}{2}-2}. \tag{1.66}$$

Here we have introduced the dimensionless quantities

$$\alpha = M/m, \qquad \Omega = \frac{P^2 - m^2 - M^2}{2mM}. \tag{1.67}$$

For very small α, i.e. approaching the chiral limit, the integral has an infrared singularity which arises in the limit of small u. From eq. (1.65) we can already see that the low energy behavior is connected to $u \approx 0$ (the infrared singular part) while at $u \approx 1$ the hard momentum structure of the baryon propagator dominates. Hence we will isolate the divergent part by rescaling the integration variable u as $u = \alpha x$. Again, in the limit of small α, the upper integration limit becomes large, hence we artificially extend the integration to infinity and we define the infrared singular part of the integral as

$$\begin{aligned} I &= \mathscr{K} \int_0^\infty du \left[u^2 - 2\alpha\Omega u(1-u) + \alpha^2(1-u)^2\right]^{\frac{d}{2}-2} \\ &= \mathscr{K}\, \alpha^{d-3} \int_0^\infty dx \left[1 - 2\Omega x + x^2 + 2\alpha x(\Omega x - 1) + \alpha^2 x^2\right]^{\frac{d}{2}-2}, \end{aligned} \tag{1.68}$$

where we have introduced the abbreviation $\mathscr{K}$ to collect the d-dependent coefficients. As can be derived from eq. (1.68) by expanding in the meson mass parameter α for a fixed Ω, the infrared sigular integral exclusively contains d-dependent powers of α while what Becher and Leutwyler call the remainder and which is often also called

the regular part R,

$$R = -\mathscr{K} \int_1^\infty du \left[u^2 - 2\alpha\Omega u(1-u) + \alpha^2(1-u)^2\right]^{\frac{d}{2}-2}, \tag{1.69}$$

is an ordinary Taylor series in the parameter α, i.e.

$$I = \frac{m^{d-4}}{(4\pi)^{d/2}} \alpha^{d-3} \left(c_0 + \alpha c_1 + \alpha^2 c_2 \ldots\right), \tag{1.70}$$

$$R = \frac{m^{d-4}\Gamma\left(2-\frac{d}{2}\right)}{(4\pi)^{d/2}(d-3)} \left(1 - \alpha\Omega + \alpha^2 \frac{1+(d-6)\Omega^2}{d-5} + \ldots\right), \tag{1.71}$$

where the coefficients c_i depend on Ω. In the case of on-shell baryons ($P^2 = m^2$), they reduce to

$$c_i = \frac{1}{2i!}\Gamma\left(\frac{i+1}{2}\right)\Gamma\left(\frac{3-d+i}{2}\right). \tag{1.72}$$

One can find that this artificial extension of the integration interval introduces new divergencies for higher dimensions d. If we now take the limit $d \to 4$ (again for on-shell baryons) we find that the infrared singular part I produces a leading oder term

$$I(d \to 4) = -\frac{1}{16\pi}\left(\frac{M}{m}\right) + \mathcal{O}(\alpha^2), \tag{1.73}$$

which is of $\mathcal{O}(q)$ and thus obeys chiral power counting, whereas the regular part contains power counting violating terms and already starts at $\mathcal{O}(q^0)$:

$$R(d \to 4) = -2\lambda + \frac{1}{16\pi^2} + \mathcal{O}(\alpha). \tag{1.74}$$

The regularization prescription given by Becher und Leutwyler is to employ the decomposition $H = I + R$. Since the regular part of the integral is polynomial in the small expansion parameter q all contributions from R can be absorbed in the low energy constants while for the infrared part we again use the $\overline{\text{MS}}$ scheme for the treatment of UV divergencies appearing in I.
The generalization of this method to tensorial integrals and integrals with more than two propagators is presented in the original article and for deeper and more comprehensive discussion of infrared regularization the reader is referred to [28]. This method has been reformulated in [36] analogously to their own EOMS scheme.

1.5 Vector mesons in ChPT

After systematically introducing baryons into the framework of ChPT we now aim to do the same for vector mesons so that we can calculate transition amplitudes

$$\mathscr{V} = \langle V'(p')|V(p)\rangle^c_{v,a,s,p}\,, \tag{1.75}$$

where V' and V stand for the outgoing and incoming vector mesons and p' and p stand for the four momenta carried by the vector mesons. Over the years, a variety of methods to incorporate vector mesons have been proposed: the so-called massive Yang-Mills approach [37], vector mesons as Goldstone bosons of a spontaneously broken hidden local symmetry [38, 39], the approach brought forth by Weinberg, Callan, Coleman, Wess and Zumino [16, 17, 40] and the formulation using antisymmetric tensor fields to describe the vector mesons, formulated in [41, 42]. See [43] for a recent review on the effects and problems of additional degrees of freedom in the context of effective field theories. For a comprehensive review we refer the reader to [44] while a brief but concise overview is presented in [45].
We will extend ChPT by the lowest-lying octet of massive vector mesons making use of the formulation in terms of flavor singlet (S_μ) and octet (V_μ) vector fields

$$V_\mu = V^a_\mu \lambda^a = \begin{pmatrix} \frac{\rho^0}{\sqrt{2}} + \frac{\phi^{(8)}}{\sqrt{6}} & \rho^+ & K^{*+} \\ \rho^- & -\frac{\rho^0}{\sqrt{2}} + \frac{\phi^{(8)}}{\sqrt{6}} & K^{*0} \\ K^{*-} & \bar{K}^{*0} & -\frac{2}{\sqrt{6}}\phi^{(8)} \end{pmatrix}_\mu , \quad S_\mu = \phi^{(0)}_\mu . \tag{1.76}$$

Introducing these fields and the corresponding bare masses $M_{V,b}$ and $M_{S,b}$ we can write down the free Lagrangian for the octet and singlet vector fields

$$\mathscr{L}_{V,\text{free}} = -\frac{1}{4}\langle V_{\mu\nu}V^{\mu\nu}\rangle + \frac{1}{2}\left\langle M^2_{V,b}V_\mu V^\mu\right\rangle - \frac{1}{4}\langle S_{\mu\nu}S^{\mu\nu}\rangle + \frac{1}{2}M^2_{S,b}S_\mu S^\mu, \tag{1.77}$$

where we again have employed the definition of the covariant derivative eq. (1.56) in $V_{\mu\nu} = D_\mu V_\nu - D_\nu V_\mu$. Again we are interested in the interaction between the lowest-lying vector meson octet and the pseudoscalar mesons, which is modeled in the standard interaction Lagrangian:

$$\begin{aligned} \mathscr{L}_{V,\text{int}} = &-\frac{ig_V}{\sqrt{2}}\langle [u_\mu, u_\nu]\, V^{\mu\nu}\rangle + \frac{g^V_A}{2}\epsilon^{\mu\nu\rho\sigma}\langle \{D_\mu V_\nu, V_\rho\}u_\sigma\rangle \\ &+ g^{VS}_A\epsilon^{\mu\nu\rho\sigma}\langle (D_\mu V_\nu)\, S_\rho u_\sigma\rangle + \dots . \end{aligned} \tag{1.78}$$

In principle, we could construct interaction terms that have more than one derivative acting on the vector meson fields V_μ, S_μ, but we will not consider these in our study of vector meson masses. We also neglect all terms that lead to higher order tadpole contributions to the masses.
Just as in BChPT, the appearance of a non-vanishing mass scale leads to power

counting violating terms, and, similar to the baryon case, a heavy vector meson approach was designed [47, 48], while later on also manifestly covariant regularization schemes have been devised [49–52]. All of these regularization schemes have to face the fact that these vector mesons are not stable particles but rather resonances and hence at a certain mass threshold they will decay into other, lighter particles. Take the $\rho(770)$ as an example: at the threshold $M_\rho^2 > 4M_\pi^2$ it will with a probability of nearly 100% decay into two pions, which, per definition, cannot both have 'soft' momenta and hence, the imaginary part of the loop diagram that generates the decay width will not scale as expected from naïve power counting. Absorbing this imaginary part in one of the low energy counterterms, as discussed in [52, 53], would spoil perturbative unitarity if this process were not considered to happen way above the decay threshold, i.e. $M_\rho^2 \gg 4M_\pi^2$. It should be mentioned that this imaginary part contains valuable information about the vector mesons [50, 52], in this case the decay width of the particle.

1.6 Lattice QCD

As already mentioned in sec. 1.1 there is another approach to obtaining low energy results for QCD, namely lattice QCD, which started with K. Wilson's seminal paper [4]. He showed how to quantize a gauge field theory on an Euclidean space-time lattice without giving up gauge invariance, and thus, rendering the Euclidean path integral finite. Such a four dimensional hypercube both serves as an ultraviolet (finite lattice spacing) and an infrared (finite volume) regulator.
In quantum field theories, we calculate the expectation value of a given operator $\hat{\mathcal{O}}$ via the path integral

$$\left\langle \hat{\mathcal{O}} \right\rangle = \frac{1}{\mathscr{Z}} \int [d\bar{\psi}][d\psi][dA_\mu] \mathcal{O}[\bar{\psi}, \psi, A_\mu] e^{-iS[\bar{\psi},\psi,A_\mu]}, \tag{1.79}$$

where $\mathscr{Z}$ is a normalization constant and is defined as

$$\mathscr{Z} = \int [d\bar{\psi}][d\psi][dA_\mu] e^{-iS[\bar{\psi},\psi,A_\mu]}. \tag{1.80}$$

$\mathcal{O}[\bar{\psi}, \psi, A_\mu]$ is the functional associated to the operator $\hat{\mathcal{O}}$ and S is the desired action in Minkowski space, e.g. in the case of QCD we have

$$S_{\text{QCD}}[\bar{\psi}, \psi, A_\mu] = \int d^4x \mathscr{L}_{\text{QCD}}[\bar{\psi}, \psi, A_\mu]. \tag{1.81}$$

If we discretize the Euclidean version of our quantum field theory and put it in a finite hypercube, we render the evaluation of path-integrals possible: the dimensionality decreases from infinity to a finite number, which still is of $\mathcal{O}(10^7)$. The calculational effort is still enormous, so we need powerful supercomputers and Monte Carlo methods to obtain the desired results.
Let us start from eq. (1.1) again with $\theta = 0$, and first we will take a look at the purely

gluonic part of the theory. We define a parallel transporter along a link connecting the lattice site x and a next neighbour site $x + e_\mu$ (we will call the distance between two sites the lattice spacing a):

$$U(x, \mu) = \mathrm{P} \exp\left(i \int_{x+e_\mu}^{x} A_\nu(z) dz_\nu \right). \tag{1.82}$$

If we consider a local gauge transformation $g(x) \in G$ where G is the gauge group, then the link U transforms in the following way:

$$U'(x, \mu) = g(x) U(x, \mu) g^{-1}(x + e_\mu). \tag{1.83}$$

This is obviously not gauge-invariant, but one finds that the trace of a closed path of these gauge-links is gauge invariant. Let us consider the simplest closed loop, the so-called plaquette, shown in fig. 1.1:

$$U_{\mu\nu}(x) = U(x, \mu) U(x + e_\mu, \nu) U^\dagger(x + e_\nu, \mu) U^\dagger(x, \nu). \tag{1.84}$$

By summing over all plaquettes, Wilson constructed the $SU(N)$ gauge action, which

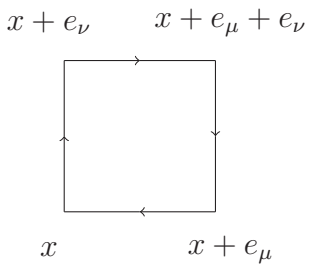

Figure 1.1: The smallest Wilson loop (the plaquette term)

takes the following form:

$$S[U] = \beta \sum_x \sum_{\mu<\nu} \left[1 - \frac{1}{N} \mathrm{Re} \left(\mathrm{tr} \left\{ U_{\mu\nu}(x) \right\} \right) \right], \tag{1.85}$$

where we have introduced $\beta = 2N/g^2$ and g being the coupling constant. In the continuum limit $a \to 0$ one finds that this expression reduces to

$$\lim_{a \to 0} S[U] = \frac{1}{2g} \int d^4x \sum_{\mu,\nu} \mathrm{tr} \left\{ F_{\mu\nu}^2(x) \right\}, \tag{1.86}$$

which reproduces the gluonic term of the Euclidean action. At a first glance, the fermionic action is more straightforward than its gluonic counterpart, since only the

differentiation has to be discretized

$$S_F[\bar{\psi},\psi] = a^4 \sum_x \bar{\psi}(x) \left[\sum_{\mu=1}^{4} \gamma_\mu \frac{1}{2a} \Big(\psi(x+e_\mu) - \psi(x-e_\mu) \Big) + m\psi(x) \right], \tag{1.87}$$

where m stands for the quark mass and the γ_μ are the Euclidean gamma matrices. From this action we can derive the free fermion propagator on the lattice in momentum space, which takes the following form

$$G(p) = \frac{m - \frac{i}{a} \sum_\mu \sin(ap_\mu)}{m^2 + \frac{1}{a^2} \sum_\mu \sin^2(ap_\mu)}. \tag{1.88}$$

We find that $\sin(ap_\mu)$ does not only vanish for $p_\mu = 0$, but also for $p_\mu = \frac{\pi}{4}$, which means the continuum limit $\lim_{a\to 0} G(p)$ does not only produce the correct result at $p = (0,0,0,0)$, but also at 15 other lattice sites. Thus, we do not have the description of a single fermion but rather one for sixteen fermions with mass m. This is the famous doubler problem for naive lattice fermions [54, 55]. The solution presented by Wilson constitutes of adding a term that gives masses proportional to $1/a$ to the doubler fermions so that they decouple in the continuum limit. In the Euclidean action this so called Wilson term takes the form

$$S_{F,\text{Wilson}}[\bar{\psi},\psi] = -a^4 \sum_x \bar{\psi}(x) a \sum_\mu \frac{r}{2a^2} \Big[\psi(x+e_\mu) + \psi(x-e_\mu) - 2\psi(x) \Big], \tag{1.89}$$

where $0 < r \leq 1$. If we look at the gauge transformation properties of the fermion fields

$$\psi'(x) = g(x)\psi(x), \quad \bar{\psi}'(x) = \bar{\psi}(x) g^{-1}(x), \tag{1.90}$$

and combine this with the transformation rules for the gauge links eq. (1.83) we can write down the full, gauge invariant, unimproved, discretized version of the QCD action:

$$\begin{aligned} S[\bar{\psi},\psi,U] = a^4 \sum_x \bar{\psi}(x) \Bigg[& \sum_\mu \frac{\gamma_\mu}{2a} \Big(U(x,\mu)\psi(x+e_\mu) - U^\dagger(x-e_\mu,\mu)\psi(x-e_\mu) \Big) \\ & + m\psi(x) - \frac{r}{2a} \sum_\mu \Big(U(x,\mu)\psi(x+e_\mu) + U^\dagger(x-e_\mu,\mu)\psi(x-e_\mu) \\ & - 2\psi(x) \Big) \Bigg]. \end{aligned} \tag{1.91}$$

This is one way to write down a discretized version of the QCD action in Euclidean spacetime, lattice QCD with Wilson fermions [4]. In principle we can add as many terms as we want as long as they disappear in the continuum limit and are gauge invariant. The process of doing this is called improving and it has to be done for

both the action and the operators considered. There are various different ways how to discretize the fermionic action, e.g. domain-wall fermions [58, 59], Kogut-Susskind-fermions [54, 55, 60], overlap fermions [61, 62] and several more. All of these formulations come with certain difficulties, be it of physical or calculational nature: Wilson fermions explicitly break chiral symmetry, the action for Kogut-Susskind-fermions produces taste doublers.
These discretized actions are then simulated on supercomputers using the Hybrid Monte Carlo (HMC) algorithm [63, 64]. There are several important details to these simulations that have to be mentioned here: first of all, the simulations are usually carried out for quark masses larger than the values we know from experiment, which brings into focus an interplay between lattice QCD and ChPT, where the pseudo-Goldstone boson masses are mere parameters. Thus we can use ChPT formulae to extrapolate lattice data down to the experimentally known realm, whilst determining the low-energy constants which serve as fit parameters in this scenario. Secondly, as explained before, all lattice QCD simulations are confined to the hypercube, i.e. to a finite simulation volume. Hence for small volumes we find that all simulation data in the end suffer from finite volume errors, which in principle have to be removed for the data to yield the correct extrapolation results. To estimate these effects, one can also use ChPT formulae which do not introduce additional fit parameters [65–67]. Lastly, one has to take care of the continuum limit, i.e. take the limit $a \to 0$. For simulations with periodic boundary conditions there exists a natural lower limit for the lattice spacing a so one can still obtain relevant data. There are several remedies for that: one can again employ a special version of ChPT, called Symanzik's effective theory [68, 69], that sets up a proper power counting for the quantity a and allows for a simultaneous extrapolation in both the pseudo-Goldstone boson masses and the lattice spacing. On the simulation side one can nowadays carry out simulations on a hypercubic lattice with open boundary conditions in temporal direction, which allows for a correct sampling at low a without the auto-correlation time going to infinity [70, 71], and thus the continuum limit can be approached. To understand all the techniques and subtleties involved in LQCD simulations, we refer the reader to several good reviews and books to the topic of lattice QCD [5, 72–74].
In this work we will make use of data supplied by the QCDSF collaboration [75]. This data is obtained in a particular way: all simulations are carried out along a trajectory starting at the $SU(3)_f$ symmetric point, i.e. $m_u = m_d = m_s$, while keeping the average quark mass $\bar{m} = \frac{1}{3}(m_u + m_d + m_s)$ fixed. This way m_s and ultimately the K and η masses in the simulations are always lower than the physical K and η masses. This is very advantageous when we apply ChPT formulae to the lattice data in question, since it is known that these formulae show severe convergence problems at the physical point due to the large pseudo-Goldstone boson masses [76–85].
The aim of this work is to try to determine the LECs for several observables to rather high accuracy using the lattice data supplied by the QCDSF collaboration. We calculate the extrapolation formulae for the first moments of the parton distribution functions (PDFs) for nucleons and hyperons (ch. 2), the baryon octet masses (ch. 3) and the vector meson masses (ch. 4). For the vector mesons we also present the

one loop corrections to the $\phi(1020) - \omega(782)$ mixing amplitude. We then employ these formulae to carry out the mass extrapolation for the vector meson masses and the baryon octet masses. We do not concern ourselves with either the continuum extrapolation or the finite volume extrapolation, but we will comment on their neccessity when carrying out the mass extrapolation.

2 First PDF moments from BChPT

In this chapter we concern ourselves with the calculation of the extrapolation formulae for the first moments of the parton distribution functions (PDFs) in the framework of covariant $N_f = 2 + 1$ BChPT. Furthermore, we discuss convergence by investigating higher-order effects for the formulae presented here. This work was published in the European Physics Journal A under the title 'The first PDF moments for three dynamical flavors in BChPT' [86].

2.1 Introduction

Successfully probing and understanding the inner structure of baryons is one of the major branches of research within the hadron physics community: obtaining information about the form factors, about angular momentum carried by the quarks and gluons, about the moments of parton distribution functions etc. by experiment is imperative for that understanding. But just as important is the theoretical description of these seemingly unconnected structure observables, which can be brought together under the concept of generalized parton distributions (GPDs) [87–89]. We will give a brief introduction here. For a very extensive review on the subject matter, we refer the reader to [90].
From a BChPT standpoint, we are interested in investigating matrix elements of the form

$$\langle B', s', p' \,|\mathcal{O}^{\mu\mu_1\cdots\mu_N}|\, B, s, p\rangle \,, \tag{2.1}$$

where the operator $\mathcal{O}^{\mu\mu_1\cdots\mu_N}$ will be defined later, B', B are outgoing/incoming baryons of spin s', s and momentum p', p. Let us start with the definition of the prominent kinematic variables

$$\bar{p} = \frac{p + p'}{2}, \qquad \Delta = p' - p, \qquad t = \Delta^2. \tag{2.2}$$

We also need the definition of light cone coordinates

$$v^{\pm} = \frac{1}{\sqrt{2}}\left(v^0 \pm v^3\right), \tag{2.3}$$

where v is an arbitrary four vector. Using these definitions one can define the parity even generalized parton distributions

$$\begin{aligned} F^q &= \frac{1}{2}\int \frac{d\lambda}{2\pi} e^{ix(\bar{p}z)} \left\langle p' \left| \bar{q}\left(-\frac{1}{2}z\right) \not{n}_- q\left(\frac{1}{2}z\right) \right| p \right\rangle_{z=\lambda n_-} \\ &= \frac{1}{2(\bar{p}n_-)} \left[H^q(x,\xi,t)\bar{u}(p')\not{n}_- u(p) + E^q(x,\xi,t)\bar{u}(p')\frac{i\sigma^{\alpha\beta}(n_-)_\alpha \Delta_\beta}{2m} u(p) \right], \end{aligned} \tag{2.4}$$

where we have introduced the kinematical parameters skewness ξ and momentum fraction x. Note that since we chose $z = \lambda n_-$, n_- can be an arbitrary light-like vector. We then find that the skewness ξ can be expressed as $\xi = -(\Delta n_-)/(2\bar{p}n_-)$. Also note that this definition is only valid in the light-cone gauge, i.e. $A^+ = 0$, otherwise the above expression is not gauge invariant and has to have a Wilson line $\mathscr{W}$ inserted, connecting the two fields at positions $-z/2$ and $z/2$:

$$\mathscr{W}\left[-\frac{1}{2}z^-, \frac{1}{2}z^-\right] = \mathrm{P}\exp\left(ig \int_{\frac{1}{2}z^-}^{-\frac{1}{2}z^-} dx^- A^+(x^- n_-) \right). \tag{2.5}$$

These generalized parton distribution functions and the Mellin moments thereof encode information about baryon structure, e.g., we obtain the Pauli and Dirac form factors from the zeroth moments of H^q and E^q:

$$\int_{-1}^{1} dx\, x^0 H^q(x,\xi,t) = F_1^q(t), \quad \int_{-1}^{1} dx\, x^0 E^q(x,\xi,t) = F_2^q(t), \tag{2.6}$$

where we have used the standard decomposition for the matrix element

$$\langle p' | \bar{q}(0)\gamma^\mu q(0) | p \rangle = \bar{u}(p') \left[\gamma^\mu F_1^q(t) + \frac{i\sigma^{\mu\nu}\Delta_\nu}{2m} F_2^q(t) \right] u(p). \tag{2.7}$$

We also find that for $p = p'$ and equal helicities for ingoing and outgoing hadrons, the GPD H^q reduces to the well known parton distributions

$$H^q(x,0,0) = \begin{cases} q(x) & \text{for } x > 0 \\ -\bar{q}(-x) & \text{for } x < 0 \end{cases}, \tag{2.8}$$

where $q(x)$ and $\bar{q}(x)$ are the quark and antiquark distribution functions. We are especially interested in the Mellin moments of the GPDs, i.e.

$$\int_{-1}^{1} dx\, x^n H^q(x,\xi,t) = \sum_{\substack{i=0 \\ \text{even}}}^{n} (2\xi)^i A^q_{n+1,i}(t) + \mathrm{mod}(n,2)(2\xi)^{n+1} C^q_{n+1}(t), \tag{2.9}$$

$$\int_{-1}^{1} dx\, x^n E^q(x,\xi,t) = \sum_{\substack{i=0 \\ \text{even}}}^{n} (2\xi)^i B^q_{n+1,i}(t) - \text{mod}(n,2)(2\xi)^{n+1} C^q_{n+1}(t), \tag{2.10}$$

where we have introduced the modulus function, which finds the remainder of division of an integer and another integer, in our case n and 2. The functions $A^q(t)$, $B^q(t)$ and $C^q(t)$ are called generalized form factors and they are connected to the matrix elements of local twist two operators

$$\mathcal{O}^q_{\mu\mu_1\ldots\mu_n} = \bar{q}\gamma_{\{\mu} i\overleftrightarrow{D}_{\mu_1} \ldots i\overleftrightarrow{D}_{\mu_n\}} q, \tag{2.11}$$

where we define the operator

$$\overleftrightarrow{D} = \frac{1}{2}(\overrightarrow{D} - \overleftarrow{D}), \tag{2.12}$$

and the operation $_{\{\ldots\}}$ as completely symmetrizing the indices and subtracting the traces. The nucleon matrix elements of these operators are connected to the generalized form factors defined above:

$$\begin{aligned}\left\langle p' \left| \mathcal{O}^q_{\mu\mu_1\ldots\mu_n} \right| p \right\rangle = {} & \bar{u}(p')\gamma_{\{\mu} \sum_{\substack{i=0 \\ \text{even}}}^{n} A^q_{n+1,i}(t)\Delta_{\mu_1}\ldots\Delta_{\mu_i}\bar{p}_{\mu_{i+1}}\ldots\bar{p}_{\mu_n\}} u(p) \\ & - i\bar{u}(p')\frac{\Delta^\alpha \sigma_{\alpha\{\mu}}{2m} \sum_{\substack{i=0 \\ \text{even}}}^{n} B^q_{n+1,i}(t)\Delta_{\mu_1}\ldots\Delta_{\mu_i}\bar{p}_{\mu_{i+1}}\ldots\bar{p}_{\mu_n\}} u(p) \\ & + \bar{u}(p')\frac{1}{m}\text{mod}(n,2) C^q_{n+1}(t)\Delta_{\{\mu}\Delta_{\mu_1}\ldots\Delta_{\mu_n\}} u(p).\end{aligned} \tag{2.13}$$

These matrix elements can be obtained using LQCD methods and can then be analysed using covariant BChPT, as has been done in the two-flavor case [91, 92]. Our work aims at generalizing the BChPT formulae obtained and published in [93] to the three-flavor case.

2.2 First GPD moments

Our work will focus on the first moments, so from now on we set $n = 1$ and thus, we find that the symmetrization operation reduces to the expression

$$A_{\{\mu}B_{\nu\}} = \frac{1}{2}\left(g_{\alpha\mu}g_{\beta\nu} + g_{\beta\mu}g_{\alpha\nu} - \frac{2}{d}g_{\alpha\beta}g_{\mu\nu}\right) A^\alpha B^\beta, \tag{2.14}$$

where d represents the space-time dimension. We are interested in both the flavor-singlet and flavor-octet combinations, that means the relevant operators for our analysis take the form

$$\mathcal{O}^s_{\mu\nu} = i\bar{q}\mathbb{1}\gamma_{\{\mu}\overleftrightarrow{D}_{\nu\}} q, \quad \mathcal{O}^{v,i}_{\mu\nu} = i\bar{q}\lambda^i\gamma_{\{\mu}\overleftrightarrow{D}_{\nu\}} q, \tag{2.15}$$

where λ^a, $a = 1, \ldots, 8$ are again the well-known Gell-Mann matrices. First we look at the decomposition of the matrix elements

$$\mathcal{M}^{s}_{B'B} = \left\langle B', s', \mathbf{p}' \left| \mathcal{O}^{s}_{\mu\nu} \right| B, s, \mathbf{p} \right\rangle, \quad \mathcal{M}^{v,i}_{B'B} \left\langle B', s', \mathbf{p}' \left| \mathcal{O}^{v,i}_{\mu\nu} \right| B, s, \mathbf{p} \right\rangle. \tag{2.16}$$

We find that most generally, these two matrix elements can be decomposed into five different generalized form factors, i.e.

$$\begin{aligned} \mathcal{M}^{s,v}_{B'B} = \bar{u}(p') \Bigg[& A^{s,v}_{B'B}(t) \gamma_{\{\mu} \bar{p}_{\nu\}} - i \frac{B^{s,v}_{B'B}(t)}{2\bar{m}} \Delta^{\alpha} \sigma_{\alpha\{\mu} \bar{p}_{\nu\}} \\ & + \frac{C^{s,v}_{B'B}(t)}{\bar{m}} \Delta_{\{\mu} \Delta_{\nu\}} + \frac{D^{s,v}_{B'B}(t)}{2\bar{m}} \bar{p}_{\{\mu} \Delta_{\nu\}} + E^{s,v}_{B'B}(t) \gamma_{\{\mu} \Delta_{\nu\}} \Bigg] u(p), \end{aligned} \tag{2.17}$$

where we have introduced the average baryon mass $\bar{m} = (m_B + m_{B'})/2$ and the bold font represents the three-components of the four momenta p and p'. To determine the properties of the generalized form factors we look at a Hermitian operator $\mathcal{P}$ and an anti-Hermitian operator $\mathcal{T}$ acting on the matrix elements $\mathcal{M}^{s,v}_{B'B}$ as follows:

$$\left\langle B', s', \mathbf{p}' \left| \mathcal{O}^{s,v}_{\mu\nu} \right| B, s, \mathbf{p} \right\rangle = \left\langle B', s', -\mathbf{p}' \left| \mathcal{P} \mathcal{O}^{s,v}_{\mu\nu} \mathcal{P}^{\dagger} \right| B, s, -\mathbf{p} \right\rangle, \tag{2.18}$$

$$\left\langle B', s', \mathbf{p}' \left| \mathcal{O}^{s,v}_{\mu\nu} \right| B, s, \mathbf{p} \right\rangle = ss' \left\langle B, s, -\mathbf{p} \left| \mathcal{T} (\mathcal{O}^{s,v}_{\mu\nu})^{\dagger} \mathcal{T}^{\dagger} \right| B', s', -\mathbf{p}' \right\rangle, \tag{2.19}$$

where we have considered spin-dependent phases $s, s' = \pm 1$ depending whether baryon spin is $+1/2$ or $-1/2$ [94]. We neglect any other phases since they can be absorbed into a redefinition of the baryon fields. Since the operator we are considering here is Hermitian, we find

$$\mathcal{P} \mathcal{O}^{v,i}_{\mu\nu} \mathcal{P}^{\dagger} = \mathcal{O}^{v,i,\mu\nu}, \quad \mathcal{T} (\mathcal{O}^{v,i}_{\mu\nu})^{\dagger} \mathcal{T}^{\dagger} = i \bar{q} (\lambda^i)^* \gamma^{\{\mu} \overleftrightarrow{D}^{\nu\}} q. \tag{2.20}$$

Using Dirac spinors normalized to $\bar{u}(p,s)u(p,s) = 2m$ we find that $u(-\mathbf{p}, s) = \gamma^0 u(\mathbf{p}, s)$ and $u(-\mathbf{p}, -s) = s\gamma^1\gamma^3 u(\mathbf{p}, s)$. Using these relations and the standard properties of the gamma matrices one finds that under parity transformations the matrix elements have the correct transformation behavior. If we transform the matrix element under $\mathcal{T}$ we expect that

$$\mathcal{M}^{v,i}_{B'B} \equiv ss' \left\langle B', -s', -\mathbf{p}' \left| i \bar{q} (\lambda^i)^* \gamma^{\{\mu} \overleftrightarrow{D}^{\nu\}} q \right| B, -s, -\mathbf{p} \right\rangle^*. \tag{2.21}$$

From this equation we can read off the properties of the generalized form factors:

$$\left[(A, B, C, D, E)^{v,1,3,4,6,8}_{B'B} \right]^* = +(A, B, C, D, E)^{v,1,3,4,6,8}_{B'B}, \tag{2.22}$$

$$\left[(A, B, C, D, E)^{v,2,5,7}_{B'B} \right]^* = -(A, B, C, D, E)^{v,2,5,7}_{B'B}. \tag{2.23}$$

On the other hand, due to the Hermitian nature of the operator considered here we expect to find

$$\mathcal{M}^{v,i}_{B'B} \equiv \left\langle B, s, \mathbf{p} \left| \mathcal{O}^{v,i}_{\mu\nu} \right| B', s', \mathbf{p}' \right\rangle, \tag{2.24}$$

and thus we find that the matrices A, B, C are Hermitian 8×8-matrices whereas D, E are anti-Hermitian. All of these form factors are directly accessible via covariant BChPT and they carry information about the first moments of parton distributions, as mentioned in the previous section, e.g. for the isovector moment we find that

$$A^{v,3}_{pp}(t=0) = \frac{1}{2}\Big(\langle x \rangle_u - \langle x \rangle_d\Big) \equiv \frac{1}{2}\langle x \rangle_{u-d}, \tag{2.25}$$

where we have used the definition

$$\langle x \rangle_q = \int_0^1 dx\, x[q(x) + \bar{q}(x)]. \tag{2.26}$$

2.3 Effective Lagrangians

The effective meson-baryon Lagrangian we have already presented in ch. 1 has to be extended to include interactions with tensorfields in order to describe the matrix elements we are investigating. This was first done in [93] for the $SU(2)_f$ case and we have extended it to the case of three dynamical fermions. We employ traceless tensorfields of definite parity $\tilde{v}_{\{\mu\nu\}}$ for the flavor singlet and $v^i_{\{\mu\nu\}}$ for the flavor octet sector. For the construction of the Lagrangian however we use the following tensor structures

$$V^{\pm}_{\mu\nu} = \frac{1}{2}\left(u^\dagger \lambda^i v^i_{\{\mu\nu\}} u \pm u \lambda^i v^i_{\{\mu\nu\}} u^\dagger\right), \qquad V^0_{\mu\nu} = \frac{\mathbb{1}}{2}\tilde{v}_{\{\mu\nu\}}. \tag{2.27}$$

We do not assign a chiral power to the tensor structures presented above, so when we consider chiral power counting, we have to remind ourselves that now loop-contributions start at chiral order $D = 2$ instead of $D = 3$, as would be expected in standard BChPT:

$$D = 2L + 1 + \sum_{n=2}^{\infty}(n-2)V^{\mathrm{MM}}_n + \sum_{n=\mathbf{0}}^{\infty}(n-1)V^{\mathrm{MB}}_n. \tag{2.28}$$

Using the structures above we can write down the lowest order Lagrangian compatible with the symmetries of QCD and Lorentz covariance:

$$\begin{aligned}\mathscr{L}^{(0)}_{\mathrm{MB},t} &= i\frac{a_D}{4}\left\langle \bar{B}\gamma^\mu\{V^+_{\mu\nu}, D^\nu B\}\right\rangle + i\frac{\Delta a_D}{4}\left\langle \bar{B}\gamma^\mu\gamma_5\{V^-_{\mu\nu}, D^\nu B\}\right\rangle \\ &+ i\frac{a_F}{4}\left\langle \bar{B}\gamma^\mu[V^+_{\mu\nu}, D^\nu B]\right\rangle + i\frac{\Delta a_F}{4}\left\langle \bar{B}\gamma^\mu\gamma_5[V^-_{\mu\nu}, D^\nu B]\right\rangle \\ &+ i\frac{a_s}{2}\left\langle \bar{B}\gamma^\mu V^0_{\mu\nu} D^\nu B\right\rangle + \text{h.c. of all terms.}\end{aligned} \tag{2.29}$$

$(\Delta)a_{D/F}$ have been named accordingly to the appearance of D and F in the lowest order meson baryon Lagrangian, i.e. D appears with the anticommutator while F is associated with the commutator. Additionally to these zeroth order terms, we need the $\mathcal{O}(q^2)$ Lagrangian for the calculation of the contact terms. We again construct all Lorentz covariant terms compatible with the symmetries of QCD:

$$\begin{aligned}\mathscr{L}^{(2)}_{\mathrm{MB},t} &= t_1\left\langle \bar{B}i\gamma^\mu\{V^+_{\mu\nu}, D^\nu B\}\right\rangle\langle\chi_+\rangle + t_2\left\langle \bar{B}i\gamma^\mu[V^+_{\mu\nu}, D^\nu B]\right\rangle\langle\chi_+\rangle \\ &+ t_3\left\langle \bar{B}i\gamma^\mu\{\{V^+_{\mu\nu}, \tilde{\chi}_+\}, D^\nu B\}\right\rangle + t_4\left\langle \bar{B}i\gamma^\mu[\{V^+_{\mu\nu}, \tilde{\chi}_+\}, D^\nu B]\right\rangle \\ &+ t_5\left\langle \bar{B}i\gamma^\mu\{[V^+_{\mu\nu}, \tilde{\chi}_+], D^\nu B\}\right\rangle + t_6\left\langle \bar{B}i\gamma^\mu[[V^+_{\mu\nu}, \tilde{\chi}_+], D^\nu B]\right\rangle \\ &+ t_7\left\langle \bar{B}i\gamma^\mu\{V^+_{\mu\nu}, \{\tilde{\chi}_+, D^\nu B\}\}\right\rangle + t_8\left\langle \bar{B}i\gamma^\mu[V^+_{\mu\nu}, \{\tilde{\chi}_+, D^\nu B\}]\right\rangle \\ &+ t_9\left\langle \bar{B}i\gamma^\mu D^\nu B\right\rangle\left\langle V^+_{\mu\nu}\tilde{\chi}_+\right\rangle + t_{10}\left\langle \bar{B}i\gamma^\mu V^+_{\mu\nu}\right\rangle\langle\tilde{\chi}_+ D^\nu B\rangle \\ &+ t_{11}\left\langle \bar{B}i\gamma^\mu\{V^0_{\mu\nu}, D^\nu B\}\right\rangle\langle\chi_+\rangle + t_{12}\left\langle \bar{B}i\gamma^\mu\{\{V^0_{\mu\nu}, \tilde{\chi}_+\}, D^\nu B\}\right\rangle \\ &+ t_{13}\left\langle \bar{B}i\gamma^\mu[\{V^0_{\mu\nu}, \tilde{\chi}_+\}, D^\nu B]\right\rangle + \text{h.c. of all terms.}\end{aligned} \tag{2.30}$$

Here we have introduced $\tilde{\chi}_+ = \chi_+ - \langle\chi_+\rangle/N_f$. The LEC t_{10} multiplies a non-Hermitian structure, hence it is in general a complex number. The term associated with this LEC also yields a contribution to the generalized form factor E. The full effective Lagrangian we need for our leading one-loop calculation of the generalized form factors at $t = 0$ takes the form

$$\mathscr{L}_{\mathrm{eff}} = \mathscr{L}^{(0)}_{\mathrm{MB},t} + \mathscr{L}^{(1)}_{\mathrm{MB}} + \mathscr{L}^{(2)}_{\mathrm{MB}} + \mathscr{L}^{(2)}_{\mathrm{MB},t}, \tag{2.31}$$

with $\mathscr{L}^{(1)}_{\mathrm{MB}}$ taken from eq. (1.60) and $\mathscr{L}^{(2)}_{\mathrm{MB}}$ from eq. (1.62).

2.4 Extrapolation formulae

All leading one-loop graphs are of chiral order $\mathcal{O}(q^2)$, the hadrons involved are those in the ground state baryon and meson octet. The η' and hence also $\eta - \eta'$ mixing [95] is not included in the calculation. Fig. 2.1 shows the graphs that contribute to the leading one-loop result.
Let us comment on how the power counting formula works for graphs 2.1(a) and

2.1(b) in particular. For both graphs we of course find that the number of loops is equal to one ($L = 1$), we have one ($V^{\mathrm{MB}}_{n=0} = 1$) baryon-meson-tensor-baryon-vertex from $\mathscr{L}^{(0)}_{\mathrm{MB},t}$ and one ($V^{\mathrm{MB}}_{n=1} = 1$) baryon-meson-vertex from $\mathscr{L}^{(1)}_{\mathrm{MB}}$. Thus, according to the power counting formula (2.28), we find the chiral dimension $D = 2+1-1+0 = 2$ as desired.

In this chapter we only present the generalized form factor $A^{s,v}_{B'B}$ for $t = 0$ for the nucleon-to-nucleon case, for all other baryon-baryon combinations we refer the reader to the arXiv.org supplement of [86]. We also present the matching formulae from the $SU(3)_f$ LECs a_F, a_D, a_s and $t_i^{(r)}$ used here to the $SU(2)_f$ LECs $a^{v,s}_{2,0}$ and $c^{(r)}_{8,9}$ used in [93]. These matching relations are obtained through expanding the $SU(3)_f$ result in the strange quark mass m_s and then comparing the leading order to the corresponding $SU(2)_f$ expressions. The matching relations for the meson sector have been worked out in [96, 97] and for the baryon sector in [33]. Let us start with these relations:

$$\begin{aligned} a^v_{2,0} = a_D + a_F + 16B_0 m_s \left(t_1 + t_2 - \frac{1}{3}(2(t_3+t_4) - t_7 - t_8)\right) \\ + \frac{M_K^2}{48\pi^2 F_0^2}\Big[a_F\left(D^2 - 6DF - 3F^2\right) \\ + a_D\left(-7D^2 + 2DF - 3F^2\right) \\ - 3\Big(a_D\left(1 + 7D^2 - 2DF + 3F^2\right) \\ + a_F\left(1 - D^2 + 6DF + 3F^2\right)\Big)\log\left(\frac{M_K}{m_0}\right)\Big] + \mathcal{O}(M_K^3), \end{aligned} \tag{2.32}$$

$$a^s_{2,0} = a_s + \frac{16}{3}B_0 m_s(3t_{11} + t_{12} - 3t_{13}) + \mathcal{O}(M_K^3), \tag{2.33}$$

$$c^r_8(\mu = m_0) = m_0^2\left(4(t_1+t_2) + \frac{2}{3}(2(t_3+t_4) - t_7 - t_8)\right) + \mathcal{O}(M_K^2), \tag{2.34}$$

$$c_9 = \frac{2}{3}m_0^2(6t_{11} - t_{12} + 3t_{13}) + \mathcal{O}(M_K^2). \tag{2.35}$$

We have cut off all the higher order effects for the matching relations. We present the extrapolation formulae without inserting the full expressions for the standard integrals $I_{\mathrm{M}}(M)$, $I_{\mathrm{MB}}(M)$ and $I_{\mathrm{MBB}}(t = 0, M)$ due to concerns about readability. We present the full form of these integrals in app. A. Since all the extrapolation formulae are very lengthy we refer the reader to app. B. Note that the singlet sector does not contain any loop contributions at leading one-loop order. We also find the following relations that relate different form factors $A^{v,i}_{N'N}(0)$:

$$A^{v,1}_{np} = A^{v,3}_{pp}, \quad A^{v,2}_{np} = iA^{v,3}_{pp}, \quad A^{v,3}_{nn} = -A^{v,3}_{pp}, \quad A^{v,8}_{nn} = A^{v,8}_{pp}. \tag{2.36}$$

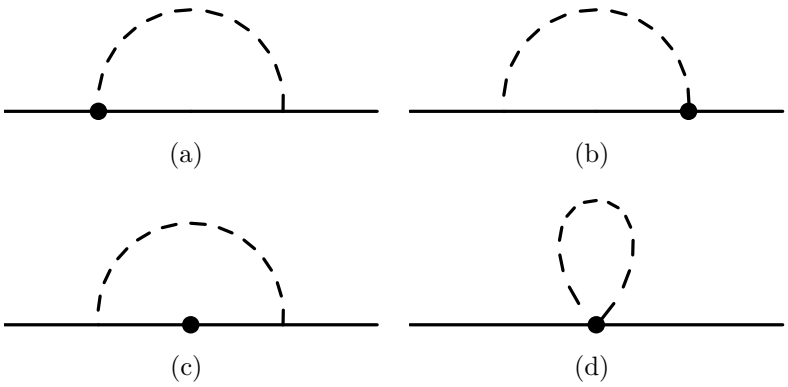

Figure 2.1: Feynman loop-diagrams contributing to the $\mathcal{O}(q^2)$ calculation: the solid line represents members of the lowest-lying baryon octet, the dashed line denotes members of the pseudoscalar meson octet and the dot represents an external tensor field coupling to the baryons and pseudoscalar mesons.

2.5 Results and discussion

In app. B we present the nonvanishing generalized form factors $A^{s,v}_{N'N}$ that we have obtained from our chosen framework of covariant BChPT. In our calculation we have included only the lowest-lying pseudoscalar mesons and the lowest-lying baryon octet. All the other, heavier baryons, e.g. the decuplet, are so far encoded in the values of our low energy constants. This is usually done in a calculation that serves as a first step towards a full description.
The next step usually consists in including the baryon decuplet. Presently in our three-flavor calculations we include e.g. a ΣK state with a threshold energy of about 1685 MeV but we explicitly exclude e.g. the $\Delta\pi$ state with an energy of 1370 MeV. The decuplet can be incorporated in studies employing three-flavor BChPT using both infrared regularization [98] and the heavy baryon formalism [26, 99]. The additional small expansion parameter arising in this extension is the octet-decuplet mass splitting $m_{0,8} - m_{0,10}$, and there are a host of new, undetermined low energy constants appearing when we extend the theory by explicitly including the baryon decuplet. Since this leading one-loop calculation already contains several undetermined LECs, including the baryon-decuplet does not render the theory or our extrapolation formulae more effective. It will, however, be inevitable to include the baryon-decuplet for the study of finite volume effects or for the study of the momentum dependence of the generalized form factors. Thus, it is important that after finishing a full one-loop calculation the decuplet is also included.
In general it is doubtful that a leading one-loop calculation can adequately extrapolate lattice data to the physical point, since here the result is only exact to $\mathcal{O}(q^2)$ and we have found that the truncated expressions deviate noticably from the full expressions for meson masses above 300 MeV. As an example for this we present the nucleon one-loop wave function renormalization factor $Z_N(M_\pi = M_K = M_\eta = M_{\text{symm}})$ in

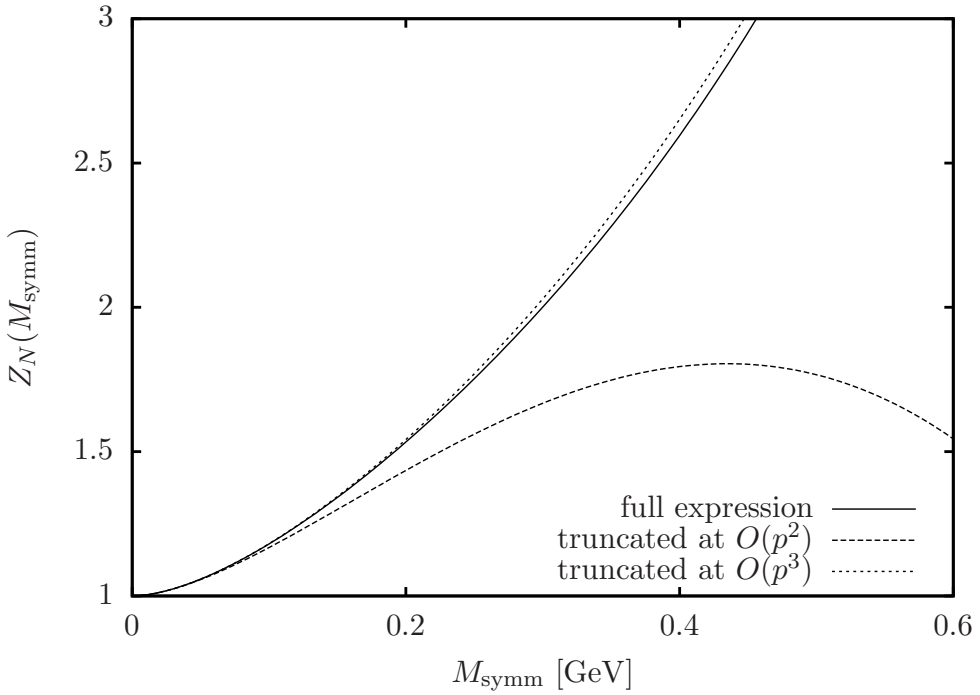

Figure 2.2: One-loop nucleon wave function renormalization for $M_\pi = M_K = M_\eta = M_{\rm symm}$: full result (solid line) and truncated results (dashed and dotted lines).

fig. 2.2. The quantity $M_{\rm symm}$ is called the symmetric meson mass and is defined as $M^2_{\rm symm} = (2M_K^2 + M_\pi^2)/3$. What we find is that these higher-order terms, in this case especially the non-analytic terms proportional to M^3, are numerically important. This is the case for the wave function renormalization constant (fig. 2.2) as well as for the other parts of the one-loop extrapolation formulae.

We employ the extrapolation formulae to analyze lattice QCD data obtained by the QCDSF collaboration. QCDSF uses a simulation strategy where the singlet quark mass is kept fixed and one starts at the $SU(3)_f$ symmetric point. There, the strange quark mass is smaller than it is at the physical point and hence, both the K and η masses are smaller than at the physical point, hence we expect improved convergence behavior at this point. At the symmetric point we have $M_\pi^2 = M_K^2 = M_\eta^2 = (412\,\text{MeV})^2$. In [75] it is argued that for the baryon masses, an expansion in $(M^2_{\rm symm} - M_\pi^2)$ to first order is enough to accurately extrapolate the baryon mass data to the physical point. For the quantities considered here, the situation is more problematic, since here, we already find chiral logarithms appearing at quadratic order, whereas for the baryon masses they appear at $\mathcal{O}(q^4)$, so we expect that an extrapolation linear in $(M^2_{\rm symm} - M_\pi^2)$ will not be sufficient.

We want to investigate how large the higher-order contributions to our results roughly are, hence we take a closer look at the contributions of graph 2.1(a) and 2.1(b). They only start contributing at $\mathcal{O}(q^3)$ and have tunable parameters $\Delta a_{D/F}$, which we will vary within the region $\Delta a_{D/F} \in [-0.3, 0.5]$. At the symmetric point, only t_1, t_2 and

t_{11} are relevant, all the other couplings parametrize $SU(3)_f$ breaking effects. Hence for our study we set all t_i equal to zero and for $a_{D/F}$ we set $a_D = a_F = 0.1$. From [93] we know that $a^v_{2,0} \approx 0.2$. For the other parameters we employ typical values that have also been used for the $SU(2)_f$ analysis, i.e. $m_0 = 1\,\text{GeV}$, $F_0 = 0.09\,\text{GeV}$, $D = 0.8$, $F = 0.5$.

The generated grey band in fig. 2.3 gives a realistic impression of the size of higher-order contributions. Figure 2.3(a) shows the form factor $A^{v,3}_{pp}(0, M_{\text{symm}})$ for varying M_{symm} while fig. 2.3(b) shows a ratio of form factors where we have kept the singlet quark mass fixed and the pion mass is varied, analogously to the simulation strategy presented in [75]. We will refer to curves like the one in fig. 2.3(b) as 'fanplots'. We find that although we have varied $\Delta a_{D/F}$ in a very generous range we still find that the higher-order contributions are under control and hence an extrapolation using this strategy shows improved stability.

Since we already have so many low energy constants in our leading one-loop order calculation, we would need an enormous amount of lattice data to pin them down. Pushing the calculation to higher orders will introduce another host of undetermined parameters, thus it is important that a thorough leading one-loop order analysis of the lattice data to come is carried out before going to full one-loop order.

In the next chapter we will carry out a full one-loop analysis of the baryon-octet masses using the lattice data published in [75] and we will try to pin down a large number of LECs to a rather high accuracy. We will also present a more detailed study of convergence of the BChPT expansion and we will comment on an attempt to extract the nucleon sigma term from the lattice data available so far.

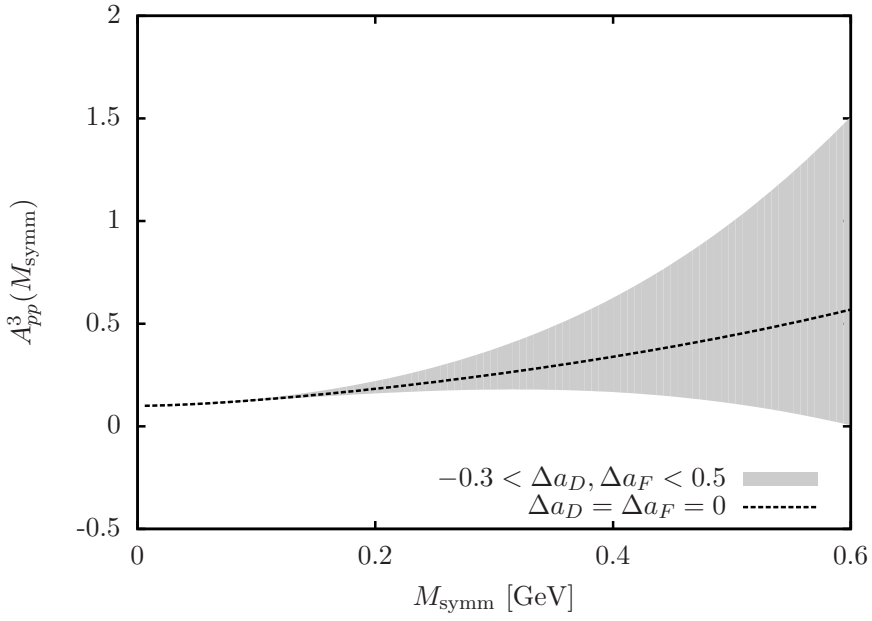

(a)

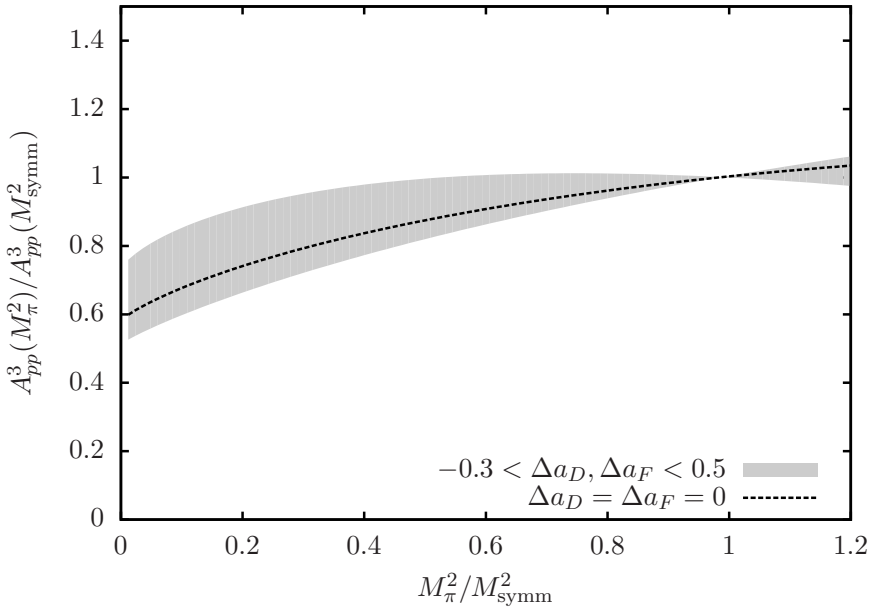

(b)

Figure 2.3: The form factors $A^3_{pp}(0, M_{\rm symm})$ and the ratio of form factors $A^3_{pp}(0, M^2_\pi)/A^3_{pp}(0, M^2_{\rm symm})$ for various values of $\Delta a_{D/F}$. The grey band shows the enveloppe of all possible curves, hence visualizing the size of higher order effects, while the dotted line represents the case $\Delta a_D = \Delta a_F = 0$.

3 Chiral extrapolation of baryon mass ratios

In this chapter we will present a thorough $\mathcal{O}(p^4)$, i.e. full one-loop, analysis of the baryon mass ratios obtained from lattice data presented in [75]. We will also investigate questions of convergence of the chiral expansion, as well as the possibility to extract the nucleon sigma term from these ratios. We present all the LECs or combinations thereof that can be determined by analyzing said lattice data. This work was published in Physical Review D under the title 'Chiral extrapolation of baryon mass ratios' [35].

3.1 Prelude: Meson masses, decay constants and numerical input from lattice QCD

As mentioned before, the simulation trajectory in [75] is such that the average quark mass, i.e. $\bar{m} = (m_u + m_d + m_s)/3 \equiv (2m_\ell + m_s)/3$ is fixed. Here we have assumed isospin symmetry in the light (ℓ) sector. What is effectively varied is the quantity $\delta m_\ell = m_\ell - \bar{m}$ and this trajectory connects the symmetric point ($\delta m_\ell = 0$) with the physical point where the strange quark mass attains the experimentally known value, see tab. 1.1. It is useful to rewrite the leading order GMOR relations eqs. (1.31)-(1.35) in terms of these quantities, i.e.

$$\dot{M}_\pi^2 = 2B_0\bar{m} + 2B_0\delta m_\ell, \tag{3.1}$$

$$\dot{M}_K^2 = 2B_0\bar{m} - B_0\delta m_\ell, \tag{3.2}$$

$$\dot{M}_\eta^2 = 2B_0\bar{m} - 2B_0\delta m_\ell. \tag{3.3}$$

Here, the dot denotes the fact that we are talking about the masses at leading-order in the quark mass expansion. We thus find that the pseudoscalar Goldstone-boson mass at the symmetric point $\dot{M}_\star^2$ to leading order takes the form

$$\dot{M}_\star^2 = 2B_0\bar{m}. \tag{3.4}$$

We in general denote quantities at the symmetric point with a $\star$, while we use 0 to denote quantities in the chiral limit, as is usual in ChPT. There are three relevant linear combinations of masses for this study that are used throughout [75] due to the fact that they show remarkable stability along the chosen trajectory:

$$X_N = \frac{1}{3}(m_N + m_\Sigma + m_\Xi) \approx 1150\,\text{MeV}, \tag{3.5}$$

$$X_\pi^2 = \frac{1}{3}(2M_K^2 + M_\pi^2) \approx (412\,\text{MeV})^2, \tag{3.6}$$

$$X_\eta^2 = \frac{1}{2}(M_\eta^2 + M_\pi^2) \approx (400\,\text{MeV})^2. \tag{3.7}$$

Here, we already presented the values of these quantities at the physical point. Since we want to carry out a full $\mathcal{O}(p^4)$ analysis, we need the GMOR relations to next-to-leading, i.e. one-loop, order and we again can expand said expressions that can be found in [7] in terms of δm_ℓ to quadratic order:

$$\begin{aligned} M_\pi^2 = M_\star^2 &+ (2B_0\delta m_\ell)\left[1 + \frac{2B_0\bar{m}}{(4\pi F_0)^2}\left(\frac{2}{3} + 2\log\left(\frac{\sqrt{2B_0\bar{m}}}{\mu}\right)\right.\right. \\ &\left.\left. -128\pi^2\left(3L_4 + 2L_5 - 6L_6 - 4L_8\right)\right)\right] \\ &+ (B_0\delta m_\ell)^2\left[\frac{5 + 8\log\left(\frac{\sqrt{2B_0\bar{m}}}{\mu}\right) - 768\pi^2(L_5 - 2L_8)}{24\pi^2F_0^2}\right], \end{aligned} \tag{3.8}$$

$$\begin{aligned} M_K^2 = M_\star^2 &- \frac{1}{2}(2B_0\delta m_\ell)\left[1 + \frac{2B_0\bar{m}}{(4\pi F_0)^2}\left(\frac{2}{3} + 2\log\left(\frac{\sqrt{2B_0\bar{m}}}{\mu}\right)\right.\right. \\ &\left.\left. -128\pi^2\left(3L_4 + 2L_5 - 6L_6 - 4L_8\right)\right)\right] \\ &+ (B_0\delta m_\ell)^2\left[\frac{1 + \log\left(\frac{\sqrt{2B_0\bar{m}}}{\mu}\right) - 96\pi^2(L_5 - 2L_8)}{12\pi^2F_0^2}\right], \end{aligned} \tag{3.9}$$

$$\begin{aligned} M_\eta^2 = M_\star^2 &- (2B_0\delta m_\ell)\left[1 + \frac{2B_0\bar{m}}{(4\pi F_0)^2}\left(\frac{2}{3} + 2\log\left(\frac{\sqrt{2B_0\bar{m}}}{\mu}\right)\right.\right. \\ &\left.\left. -128\pi^2\left(3L_4 + 2L_5 - 6L_6 - 4L_8\right)\right)\right] \\ &- (B_0\delta m_\ell)^2\left[\frac{2 + 3\log\left(\frac{\sqrt{2B_0\bar{m}}}{\mu}\right) + 192\pi^2(L_5 - 12L_7 - 6L_8)}{6\pi^2F_0^2}\right]. \end{aligned} \tag{3.10}$$

Here we have introduced the pseudoscalar Goldstone-boson mass to one-loop accuracy which is given by the expression

$$\begin{aligned} M_\star^2 = 2B_0\bar{m}\Bigg[1 + \frac{2B_0\bar{m}}{(4\pi F_0)^2}\Bigg(128\pi^2(-3L_4 - L_5 + 6L_6 + 2L_8) \\ + \frac{2}{3}\log\left(\frac{\sqrt{2B_0\bar{m}}}{\mu}\right)\Bigg)\Bigg]. \end{aligned} \tag{3.11}$$

Inserting these relations into the definitions of X_π and X_η, eqs. (3.6), (3.7), we find the corresponding one loop expressions

$$\begin{aligned} X_\pi^2 &= \frac{1}{3}(2M_K^2 + M_\pi^2) \\ &= M_\star^2 + \frac{(B_0\delta m_\ell)^2}{24\pi^2 F_0^2}\left[3 + 4\log\left(\frac{\sqrt{2B_0\bar{m}}}{\mu}\right) - 384\pi^2(L_5 - 2L_8)\right], \end{aligned} \tag{3.12}$$

$$\begin{aligned} X_\eta^2 &= \frac{1}{2}(M_\eta^2 + M_\pi^2) \\ &= M_\star^2 - \frac{(B_0\delta m_\ell)^2}{48\pi^2 F_0^2}\left[3 + 4\log\left(\frac{\sqrt{2B_0\bar{m}}}{\mu}\right) + 1536\pi^2(L_5 - 6L_7 - 4L_8)\right]. \end{aligned} \tag{3.13}$$

All the low energy constants used here are the renormalized ones presented in [7]. As we have done before, we have omitted the superscript $^{(r)}$ that usually signifies that we are talking about renormalized constants. To follow the notation also used in [75], we introduce a quantity that measures $SU(3)_f$ symmetry-breaking

$$\begin{aligned} \nu &= \frac{M_\pi^2 - X_\pi^2}{X_\pi^2} \\ &= \frac{2B_0\delta m_\ell}{M_\star^2}\Bigg[1 + \frac{2B_0\bar{m}}{24\pi^2 F_0^2}\Bigg(1 + 3\log\left(\frac{\sqrt{2B_0\bar{m}}}{\mu}\right) \\ &\quad - 192\pi^2(3L_4 + 2L_5 - 6L_6 - 4L_8)\Bigg)\Bigg] \\ &\quad + \frac{(2B_0\delta m_\ell)^2}{48\pi^2 F_0^2 M_\star^2}\left[1 + 2\log\left(\frac{\sqrt{2B_0\bar{m}}}{\mu}\right) - 192\pi^2(L_5 - 2L_8)\right] \\ &\quad + \mathcal{O}(\bar{m}^2\delta m_\ell, \bar{m}(\delta m_\ell)^2, (\delta m_\ell)^3). \end{aligned} \tag{3.14}$$

This relation can be inverted and re-expanded to second order in the original variable δm_ℓ, and so we can for further reference always use ν as the variable parametrizing

symmetry-breaking:

$$\begin{aligned} 2B_0\delta m_\ell = \nu M_\star^2 \Bigg[1 - \frac{2B_0\bar{m}}{24\pi^2 F_0^2} \Bigg(1 + 3\log\left(\frac{\sqrt{2B_0\bar{m}}}{\mu}\right) \\ - 192\pi^2(3L_4 + 2L_5 - 6L_6 - 4L_8) \Bigg) \Bigg] \\ - \frac{(\nu M_\star^2)^2}{48\pi^2 F_0^2} \left[1 + 2\log\left(\frac{\sqrt{2B_0\bar{m}}}{\mu}\right) - 192\pi^2(L_5 - 2L_8) \right]. \end{aligned} \tag{3.15}$$

Since we aim at carrying out an expansion around the symmetric point, it is reasonable to express the appearing quantities like decay-constants etc. as quantities at the symmetric point plus corrections in the symmetry-breaking. Basically, there are 26 a priori unknown parameters in the final extrapolation formulae for the masses, so we will need input for some of these LECs e.g. from lattice QCD, meson-baryon-scattering or other sources available. For the low energy constants originating from the purely mesonic sector, i.e. L_i, F_0, we have chosen the following strategy: we take three different sets of LECs that are collected in [100] and we will choose the set that according to the FLAG report fulfills most of their quality criteria. We will then present a sample fanplot for the meson decay constants F_π and F_K and see how well the LECs describe the situation at the physical point. The other sets we will use for estimating the errors on our results. First we write down the one-loop expressions for the meson decay constants and expand them in the expansion parameters $\bar{m}$ and δm_ℓ:

$$F_\pi = F_\star - (B_0\delta m_\ell)\left[\frac{3 + 6\log\left(\frac{\sqrt{2B_0\bar{m}}}{\mu}\right) - 256\pi^2 L_5}{32\pi^2 F_0}\right] + \mathcal{O}((\delta m_\ell)^2), \tag{3.16}$$

$$F_K = F_\star + (B_0\delta m_\ell)\left[\frac{3 + 6\log\left(\frac{\sqrt{2B_0\bar{m}}}{\mu}\right) - 256\pi^2 L_5}{64\pi^2 F_0}\right] + \mathcal{O}((\delta m_\ell)^2), \tag{3.17}$$

$$F_\eta = F_\star + (B_0\delta m_\ell)\left[\frac{3 + 6\log\left(\frac{\sqrt{2B_0\bar{m}}}{\mu}\right) - 256\pi^2 L_5}{32\pi^2 F_0}\right] + \mathcal{O}((\delta m_\ell)^2). \tag{3.18}$$

Here we have again introduced a quantity we call the meson decay constant at the symmetric point, $F_\star$, which is given by

$$F_\star = F_0\left[1 + \frac{2B_0\bar{m}}{(4\pi F_0)^2}\left(64\pi^2(3L_4 + L_5) - 3\log\left(\frac{\sqrt{2B_0\bar{m}}}{\mu}\right)\right)\right] + \mathcal{O}(\bar{m}^2)\,. \tag{3.19}$$

The linear combination of decay constants $F_X = (2F_K + F_\pi)/3$ is, to one-loop order, constant in the whole region of δm_ℓ. In tab. 3.1 we present the three different input sets we consider for our analysis. According to the authors of the report, none of these sets are what they consider as perfect, but the MILC [101, 102] data points seem to be reliable because of the effort that has been put into the continuum extrapolation

Table 3.1: Three parameter sets for the low-energy coefficients F_0, L_i.

F_0 (MeV)	$10^3 L_4$	$10^3 L_5$	$10^3 L_6$	$10^3 L_8$	Ref.
80.3 ± 6.0	-0.08 ± 0.60	0.98 ± 0.40	-0.02 ± 0.40	0.42 ± 0.30	[101]
78.3 ± 3.2	0.04 ± 0.14	0.84 ± 0.38	0.07 ± 0.11	0.36 ± 0.09	[102]
83.8 ± 6.4	-0.06 ± 0.10	1.45 ± 0.07	0.02 ± 0.05	0.62 ± 0.04	[103]

and the renormalization. We added the PACS-CS [103] set solely because they were the only group producing data points at pion masses below 250 MeV. All these low energy constants are given at a renormalization scale $\mu = 770$ MeV. In fig. 3.1 we present the fan plot for the MILC2010 data. We have varied the LEC L_5, which is basically determining the slope at the symmetric point, to obtain the shaded bands. To indicate how good these one-loop formulae describe reality when using these LECs as input, we have indicated the values at the physical point with black dots. Since we have now chosen a set of input parameters we can give numerical values

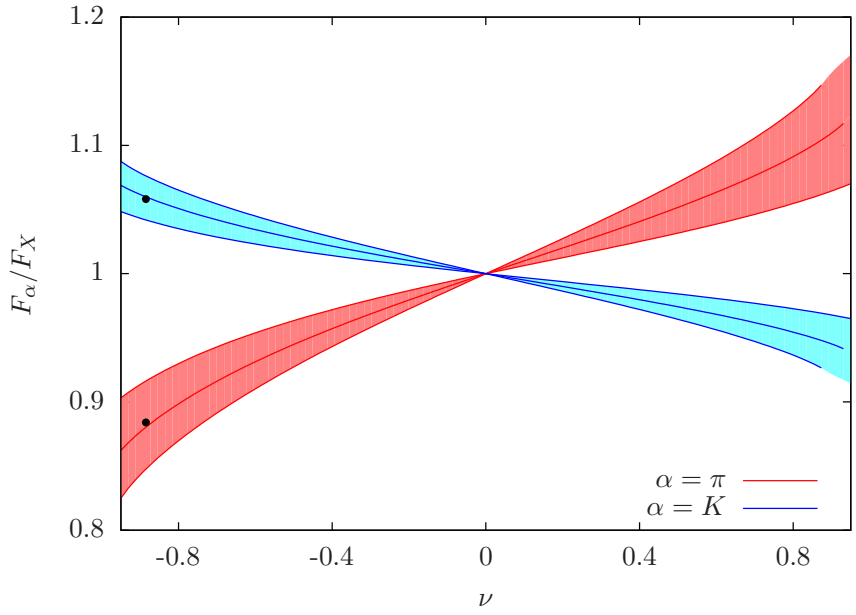

Figure 3.1: The fan plot for the ratios $F_{\pi,K}/F_X$ for the LECs taken from [101]. The shaded bands correspond to the variation of the error assigned to the LEC L_5. We have indicated the values at the physical point by black dots.

for all the quantities that will enter our analysis. We start with the observation in [75], that if X_π is used to set the scale, X_π is very stable over the whole simulation trajectory. We will determine the parameter $2B_0\bar{m}$ from the fact that $M_\star$ is equal to

X_π^{phys}, i.e.

$$\dot{M}_\star \equiv \sqrt{2B_0\bar{m}} = (420 \pm 40)\,\text{MeV}, \tag{3.20}$$

where we have used the other LEC sets for determining the error of this quantity. Furthermore we have made use of the chiral counting scheme: Since the corrections in eq. (3.11) containing F_0 are already of $\mathcal{O}(p^4)$, we can simply replace F_0 by $F_\star$ since this merely amounts to higher order corrections which our calculation is not sensitive to. In this way we also obtain the numerical value for $F_\star$,

$$F_\star = (112 \pm 15)\,\text{MeV}. \tag{3.21}$$

Alternatively we can take the direct route and insert the MILC2010 value for F_0 in eq. (3.11), which leads to $\dot{M}_\star = 428\,\text{MeV}$ and $F_\star = 112.5\,\text{MeV}$. We also find that X_π seems to be very stable over the whole range for ν, which means that

$$3 + 4\log\left(\frac{420}{770}\right) - 384\pi^2(L_5 - 2L_8) \approx 0. \tag{3.22}$$

Indeed, using the central values from the MILC2010 set, we find that the above expression amounts to a numerical value of 0.05 and hence the terms proportional to $(\delta m_\ell)^2$ are heavily supressed.
There is another quantity we have so far not investigated, namely $M_{\bar{s}s}^2 \equiv 2B_0 m_s$ which also naturally arises in $SU(3)_f$ calculations. We will give an $\mathcal{O}(p^4)$ expansion of this quantity, since it, when kept fixed, can be used to express the light quark-mass dependence through the pion mass dependence:

$$\begin{aligned} M_{\bar{s}s}^2 &= 2\dot{M}_K^2 - \dot{M}_\pi^2 \\ &= 2M_K^2 - M_\pi^2 + \frac{1}{48\pi^2 F_0^2}\Bigg[384\pi^2\Big(M_K^4(4L_4 + 2L_5 - 8L_6 - 4L_8) \\ &\quad - M_\pi^4(L_4 + L_5 - 2L_6 - 2L_8)\Big) \\ &\quad + 3M_\pi^4\log\left(\frac{M_\pi}{\mu}\right) - (3M_\eta^4 + 2M_\eta^2 M_\pi^2)\log\left(\frac{M_\eta}{\mu}\right)\Bigg] + \mathcal{O}(M^6). \end{aligned} \tag{3.23}$$

$$\begin{aligned} 2B_0 m_\ell = M_\pi^2\Bigg[1 + \frac{1}{144\pi^2 F_0^2}\Bigg(1152\pi^2\Big(M_\pi^2(2L_4 + L_5 - 4L_6 - 2L_8) \\ + M_{\bar{s}s}^2(L_4 - 2L_6)\Big) + (M_\pi^2 + 2M_{\bar{s}s}^2)\log\left(\sqrt{\frac{M_\pi^2 + 2M_{\bar{s}s}^2}{3\mu^2}}\right) \\ - 9M_\pi^2\log\left(\frac{M_\pi}{\mu}\right)\Bigg)\Bigg] + \mathcal{O}(M^6)\,. \end{aligned} \tag{3.24}$$

If we again use the central values of MILC2010 and furthermore insert the experimentally known pion and kaon masses, we arrive at

$$M_{\bar{s}s} = (715 \pm 100)\,\text{MeV}. \tag{3.25}$$

All the errors that have been quoted above result from varying the input parameters amongst the three sets presented in tab. 3.1. As one can see, there is a clear hierarchy between possible expansion parameters, i.e.

$$M_\pi \approx \sqrt{2B_0 m_\ell} < \sqrt{2B_0 \bar{m}} < \sqrt{2B_0 m_s} = M_{\bar{s}s}, \tag{3.26}$$

and looking at the numerical values eqs. (3.20), (3.25), we can already deduce that an expansion in $M_{\bar{s}s}$ over a typical hadronic scale of 1 GeV will be futile while an expansion in $M_\star$ is expected to work much better.

3.2 Pre-analysis: Baryon masses to leading one-loop order

Before we perform the full $\mathcal{O}(p^4)$ analysis we carry out a short pre-analysis employing the leading one-loop extrapolation formulae originating from the Feynman graph shown in fig. 3.2. One finds the extrapolation formulae that have also been published in e.g. [33], which take the following form:

$$m_N = m_0 - 4b_D\phi_N + 4b_F\varepsilon_N - 2b_0\delta + \frac{1}{96\pi F_0^2}\left[6DF\alpha_N - 9F^2\beta_N - D^2\gamma_N\right], \tag{3.27}$$

$$m_\Lambda = m_0 + \frac{4}{3}b_D\phi_\Lambda - 2b_0\delta - \frac{1}{24\pi F_0^2}\left[9F^2\beta_\Lambda + D^2\gamma_\Lambda\right], \tag{3.28}$$

$$m_\Sigma = m_0 - 4b_D\phi_\Sigma - 2b_0\delta - \frac{1}{24\pi F_0^2}\left[3F^2\beta_\Sigma + D^2\gamma_\Sigma\right], \tag{3.29}$$

$$m_\Xi = m_0 - 4b_D\phi_N - 4b_F\varepsilon_N - 2b_0\delta - \frac{1}{96\pi F_0^2}\left[6DF\alpha_N + 9F^2\beta_N + D^2\gamma_N\right], \tag{3.30}$$

where we have introduced a host of abbreviations:

$$\begin{aligned}
\alpha_N &= \dot{M}_\eta^3 + 2\dot{M}_K^3 - 3\dot{M}_\pi^3, & \beta_\Lambda &= \dot{M}_K^3,\\
\beta_N &= \dot{M}_\eta^3 + 2\dot{M}_K^3 + \dot{M}_\pi^3, & \gamma_\Lambda &= \dot{M}_\eta^3 + \dot{M}_K^3 + 3\dot{M}_\pi^3,\\
\gamma_N &= \dot{M}_\eta^3 + 10\dot{M}_K^3 + 9\dot{M}_\pi^3, & \phi_\Lambda &= -4\dot{M}_K^2 + \dot{M}_\pi^2,\\
\varepsilon_N &= \dot{M}_K^2 - \dot{M}_\pi^2, & \beta_\Sigma &= \dot{M}_K^3 + 2\dot{M}_\pi^3,\\
\phi_N &= \dot{M}_K^2, & \gamma_\Sigma &= \dot{M}_\eta^3 + 3\dot{M}_K^3 + \dot{M}_\pi^3,\\
\delta &= 2\dot{M}_K^2 + \dot{M}_\pi^2, & \phi_\Sigma &= \dot{M}_\pi^2
\end{aligned} \tag{3.31}$$

If one wishes to do so, one can eliminate the η mass via the Gell-Mann-Okubo

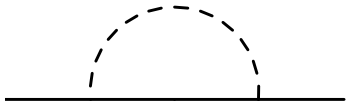

Figure 3.2: Loop graph containing two vertices from the leading order Lagrangian $\mathscr{L}^{(1)}_{\rm MB}$ which produces the leading non-analytic quark-mass corrections. The dashed line represents the pseudoscalar mesons while the solid line again stands for the baryon-octet.

relation [104, 105], at least to the order in which we are working here:

$$3\dot{M}_\eta^2 = 4\dot{M}_K^2 - \dot{M}_\pi^2. \tag{3.32}$$

For all our numerical studies we set the axial couplings D and F to the values $D = 0.75$ and $F = 0.5$, which is to a large extent consistent with other determinations or analyses [22, 24, 106, 107]. There are two more references we would like to add at this point: in [108], large N_c arguments have been employed to fit certain mass combinations where the singlet piece drops out. Their result comes very close to the expectations from phenomenology. A similar result has been published in [109].
This section aims at pre-analyzing the low energy constants appearing at $\mathcal{O}(p^3)$ to get a feeling for the stability of the fits and to have a first look into the convergence pattern of the leading one-loop result. We start by investigating two mass combinations: one that we will call Δ_{DF}, which is only interesting for the numerical values for D and F chosen above, and the other one is the well-known Gell-Mann-Okubo mass difference Δ_{GMO} [104, 105]:

$$\begin{aligned} \Delta_{DF} &= \frac{1}{4}\left(12m_\Sigma - 4m_\Lambda - 5m_N - 3m_\Xi\right) \\ &= \frac{2}{3}\left(20b_D - 3b_F\right)\left(\dot{M}_K^2 - \dot{M}_\pi^2\right) + \mathcal{O}(p^4), \end{aligned} \tag{3.33}$$

$$\begin{aligned} \Delta_{GMO} &= \frac{1}{4}\left(m_\Sigma + 3m_\Lambda - 2m_N - 2m_\Xi\right) \\ &= \frac{D^2 - 3F^2}{96\pi F_0^2}\left(4\dot{M}_K^3 - \dot{M}_\pi^3 - 3\dot{M}_\eta^3\right) + \mathcal{O}(p^4). \end{aligned} \tag{3.34}$$

Let us first analyze Δ_{DF}: after plugging in the baryon masses, again averaged over isospin multiplets,

$$m_N^{\rm phys} = 939\,\text{MeV}, \qquad m_\Lambda^{\rm phys} = 1116\,\text{MeV}, \tag{3.35}$$

$$m_\Sigma^{\rm phys} = 1190\,\text{MeV}, \qquad m_\Xi^{\rm phys} = 1318\,\text{MeV}, \tag{3.36}$$

we find that $\Delta_{DF}^{\rm phys} \approx 292\,\text{MeV}$. If we assume that our values for D and F are roughly correct and that the contributions from $\mathcal{O}(p^4)$ are small, this directly translates into a rough value for the linear combination $(20/3)b_D - b_F \approx 0.65\,\text{GeV}^{-1}$. But since we know that the BChPT expansion already is problematic at the physical point due to

Table 3.2: The leading one-loop fit results: $m_0^{\text{eff}} = m_0 - 6b_0X_\pi^2$ is an effective fit parameter that emerges since this combination appears equally in all baryon octet mass formulae.

F_0 (MeV)	m_0^{eff} (GeV)	b_D (GeV^{-1})	b_F (GeV^{-1})
70	2.279	-0.039	-0.912
80	2.024	-0.015	-0.747
112	1.617	0.024	-0.484
140	1.465	0.038	-0.386

much enhanced non-analytic loop corrections originating from large K and η masses, we have to assume at least a 50% error on this linear combination of LECs, which leaves us with the rough estimate

$$0.3\,\text{GeV}^{-1} \lesssim \left(\frac{20}{3}b_D - b_F\right) \lesssim 1\,\text{GeV}^{-1}. \tag{3.37}$$

We will later crosscheck this with the results from our leading one-loop fits. Let us now turn to Δ_{GMO} by inserting the approximate values $\dot{M}_\pi = 140\,\text{MeV}$, $\dot{M}_K = 495\,\text{MeV}$, $\dot{M}_\eta = 566\,\text{MeV}$ (which is the result if we use eq. (3.32) to calculate the η mass) and the central value for the decay constant in the chiral limit $F_0 = 80.3\,\text{MeV}$. If we now evaluate both sides, we find that

$$\Delta_{GMO}^{\text{phys}} = 5.9\,\text{MeV} + \mathcal{O}(p^4) \equiv 6.0\,\text{MeV}, \tag{3.38}$$

which leads to the conclusion that higher order contributions have to be heavily suppressed while the leading one-loop part makes up almost the entire contribution. This numerical smallness could be traced back to the fact that if one expands Δ_{GMO} in terms of δm_ℓ one finds no terms linear in the symmetry-breaking – it starts at quadratic order.

We use only the experimental values for the baryon masses as input for our fit procedure and present four different fit sets for this pre-analysis, which correspond to different values for the input parameter F_0. To the order we are working here the precise value of F_0 should not be of too much importance to the stability of the fits. As we can see from tab. 3.2, this is not the case and furthermore we find that the convergence of the BChPT expansion is very poor, e.g. we find that for the lowest value of F_0, the leading one-loop correction to the tree-level result at the physical point amounts to -423 MeV, which is very large even if we merely assume a generic suppression factor of $M_K/\Lambda_{\text{had}} \approx 0.5$. This leads to the conclusion that a reliable determination of the low energy constants is not possible at the physical point, due to the aforementioned large K- and η-loop contributions.

However, we can also interpret these fit results as rough estimates for these parameters

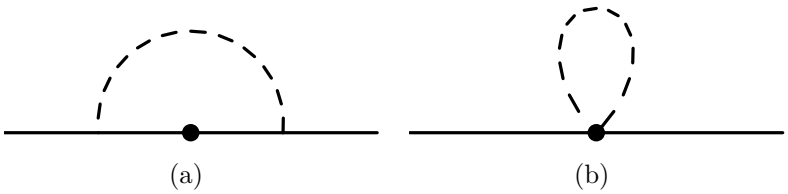

Figure 3.3: Feynman loop-diagrams contributing to the $\mathcal{O}(p^4)$ calculation: the solid line represents members of the lowest lying baryon octet, the dashed line denotes members of the pseudoscalar meson octet and the black dot represents mass insertions or BMMB vertices originating from $\mathscr{L}^{(2)}_{\mathrm{MB}}$.

which should be compatible with a next-to-leading loop analysis of the baryon masses. Let us formulate three properties an $\mathcal{O}(p^4)$ analysis should reproduce:

1. $1\,\mathrm{GeV} \lesssim m_0^{\mathrm{eff}} \lesssim 3\,\mathrm{GeV}$,
2. b_F is negative and lies roughly between $-1\,\mathrm{GeV}^{-1} \lesssim b_F \lesssim 0\,\mathrm{GeV}^{-1}$,
3. b_D is of significantly smaller magnitude than b_F.

3.3 Next-to-leading one-loop contributions

In order to obtain all contributions to the baryon masses at $\mathcal{O}(p^4)$, we have to calculate the additional loop graphs presented in fig. 3.3. The graph 3.3(a) has the same topology as the graph of fig. 3.2 with an additional quark-mass insertion proportional to the $\mathcal{O}(p^2)$ LECs $b_{D,F,0}$. The tadpole-type graph 3.3(b) introduces a whole host of new LECs into the baryon mass formulae, i.e. $b_{1-4,8-11}$. Additionally to those loop contributions, there are seven new contact-terms proportional to the parameters d_{1-7} which absorb the divergences of the regularized loop integrals. We will present the absorption prescriptions later. Before we present the tree-level results of $\mathcal{O}(p^4)$, let us comment on how to obtain the baryon mass shifts $\Delta m_B^{(n)}$ order to order from the baryon self energy $\Sigma^{(n)}(\not{p})$ [33]:

$$\Delta m_B^{(1)} = 0, \tag{3.39}$$

$$\Delta m_B^{(2)} = \Sigma^{(2)}, \tag{3.40}$$

$$\Delta m_B^{(3)} = \Sigma^{(3)}(\not{p} = m_0), \tag{3.41}$$

$$\Delta m_B^{(4)} = \Sigma^{(4)}(\not{p} = m_0) + \Sigma^{(2)} \frac{\partial \Sigma^{(3)}(\not{p})}{\partial \not{p}}\bigg|_{\not{p}=m_0}. \tag{3.42}$$

Graph 3.3(a) does not introduce new parameters hence we will not comment on the calculation of this graph at this point. We rather refer the interested reader to [33]. Since there are plenty new parameters appearing at $\mathcal{O}(p^4)$, it will be important to

fix many of the input parameters, because given the modest amount of data we have, we are not able to determine all of the LECs. An analysis using various available data for the determination of these b_i is presented in [112].
First, let us use eq. (1.63) to calculate all the contact-term contributions to the $\mathcal{O}(p^4)$ mass formulae:

$$\begin{aligned} m_N^{(\mathrm{ct})} &= m_\star^{(\mathrm{ct})} + B_0\delta m_\ell\Big(4(b_D-3b_F) - 16B_0\bar{m}(6d_2-4d_3+9d_5)\Big) \\ &\quad - 16(B_0\delta m_\ell)^2\,(9d_1-3d_2+d_3+6d_7)\,, \end{aligned} \tag{3.43}$$

$$m_\Lambda^{(\mathrm{ct})} = m_\star^{(\mathrm{ct})} + 8B_0\delta m_\ell\,(b_D+16B_0\bar{m}d_3) - 96(B_0\delta m_\ell)^2\,(2d_3+d_4+d_7)\,, \tag{3.44}$$

$$m_\Sigma^{(\mathrm{ct})} = m_\star^{(\mathrm{ct})} - 8B_0\delta m_\ell\,(b_D+16B_0\bar{m}d_3) - 16(B_0\delta m_\ell)^2\,(4d_3+6d_7)\,, \tag{3.45}$$

$$\begin{aligned} m_\Xi^{(\mathrm{ct})} &= m_\star^{(\mathrm{ct})} + B_0\delta m_\ell\Big(4(b_D+3b_F) + 16B_0\bar{m}(6d_2+4d_3+9d_5)\Big) \\ &\quad - 16(B_0\delta m_\ell)^2\,(9d_1+3d_2+d_3+6d_7)\,, \end{aligned} \tag{3.46}$$

where we again have introduced the contact-term contribution to the baryon mass at the symmetric point

$$m_\star^{(\mathrm{ct})} = -4B_0\bar{m}\,(3b_0+2b_D) - 16(B_0\bar{m})^2\,(4d_3+9d_6+3d_7)\,. \tag{3.47}$$

Using eqs. (3.43)-(3.46) we can write down the contact-term contribution to X_N, which is free of terms linear in the symmetry-breaking:

$$X_N^{(\mathrm{ct})} = m_\star^{(\mathrm{ct})} - 32(B_0\delta m_\ell)^2\,(3d_1+d_3+3d_7)\,. \tag{3.48}$$

We also find from eqs. (3.43)-(3.46) that, linearly in the symmetry-breaking, only the linear combinations $\tilde{b}_D \equiv b_D + 16B_0\bar{m}d_3$ and $\tilde{b}_F \equiv b_F + 4B_0\bar{m}(2d_2+3d_5)$ enter the contact-term contributions. Note that d_5 only enters in this combination, hence it cannot be determined from the fan plots, since the tadpole contribution proportional to b_F is already of $\mathcal{O}(p^4)$. Furthermore, the parameters b_0 and d_6 only appear in the combination

$$m_\star = m_0 - 12B_0\bar{m}\,(b_0+12B_0\bar{m}d_6) + \ldots\,, \tag{3.49}$$

which means that these two LECs also cannot be determined from the fan plot data alone, since again a shift in b_F would be of $\mathcal{O}(p^6)$ in the corresponding tadpole graph. The tadpole contributions are derived from the Lagrangian in eq. (1.62). These contributions contain 8 new a priori unknown constants that we will fix by using the results presented in [110, 111]. These parameters have a model-dependent uncertainty due to the approach that was chosen to derive the chiral potential, hence we will use all three different input sets, which are presented in tab. 3.3. Notice that we also added a parameter set where all the $b_{1-4,8-11}$ vanish. By using these four different input sets we try to get control over the uncertainties introduced by taking these values as input, as well as being able to give a proper error estimate on the other low energy constants we will determine from fitting our formulae to lattice data.

Table 3.3: Four parameter sets for the low-energy coefficients $b_{1-4,8-11}$. All parameters are given in units of GeV^{-1}.

set	b_1	b_2	b_3	b_4	b_8	b_9	b_{10}	b_{11}	Ref.
1	-0.082	-0.118	-1.890	-0.215	0.609	-0.633	1.920	-0.919	[110]
2	-0.126	-0.139	-2.227	-0.288	0.610	-0.677	2.027	-0.847	[111]
3	-0.014	-0.207	-1.063	-1.312	0.272	-0.483	1.054	0.328	[111]
4	0	0	0	0	0	0	0	0	-

As mentioned already in sec. 1.4 the infrared renormalized loop integrals still contain divergences as the dimension $d \to 4$, which have to be absorbed by the low energy constants. In this case the $\mathcal{O}(p^4)$ tree-level constants d_i absorb the divergencies originating from the $\mathcal{O}(p^4)$ loop graphs. At order p^3, there are neither counterterms, nor are there divergencies. There is a universal description how to systematically split off the finite, scale dependent part of the LECs from the divergent part, i.e.

$$d_i = \gamma_i^{\mathrm{IR}} L + d_i^{(r)}(\mu), \tag{3.50}$$

where the γ_i^{IR} are presented in app. C. We can then define scale independent quantities $\bar{d}_i$

$$d_i^{(r)}(\mu) = \bar{d}_i + \frac{\gamma_i^{\mathrm{IR}}}{16\pi^2} \log\left(\frac{m_0}{\mu}\right). \tag{3.51}$$

3.4 Chiral analysis of baryon mass ratios

We want to analyze the fan plot data presented in tab. 22 and fig. 20 of [75], which means we have to investigate the chiral behavior of the mass ratios

$$f_B \equiv \frac{m_B}{X_N}, \tag{3.52}$$

for the members of the baryon octet, i.e. $B = N, \Lambda, \Sigma, \Xi$. We present the lattice data for the reader's convenience in tab. 3.4. From the definition, we find that at the symmetric point $f_B = 1$ and $X_\pi = M_\star = 412\,\mathrm{MeV}$. From this point, the lattice simulations move towards the physical point by gradually changing δm_ℓ for fixed $\bar{m}$. In the same table we also see the lowest value for $M_\pi \approx 229\,\mathrm{MeV}$, which means $M_K \approx 477\,\mathrm{MeV}$ and via eq. (3.32) $M_\eta \approx 535\,\mathrm{MeV}$. As one can clearly see, all meson masses are below the physical η mass of $M_\eta^{\mathrm{phys}} = 548\,\mathrm{MeV}$. This is in contrast to the usual way of simulating three quark flavors on the lattice, where the strange quark

Table 3.4: The lattice data taken from [75], a collection of tabs. 20 and 29. We have used X_π to determine the lattice spacing a, see footnote 5 in the same reference.

$N_S^3 \times N_T$	ν	f_N	f_Λ	f_Σ	f_Ξ
$24^3 \times 48$	0.181	1.033(2)	1.009(6)	0.9949(13)	0.9717(26)
$24^3 \times 48$	0	1.0	1.0	1.0	1.0
$24^3 \times 48$	−0.128	0.9769(33)	0.9887(84)	1.005(1)	1.018(3)
$24^3 \times 48$	−0.275	0.9546(32)	0.9885(77)	1.008(2)	1.038(3)
$32^3 \times 64$	−0.404	0.9229(47)	0.9999(28)	1.039(7)	1.078(9)
$32^3 \times 64$	−0.558	0.9426(120)	1.012(10)	1.062(19)	1.115(24)
$32^3 \times 64$	−0.692	0.9185(145)	1.010(13)	1.090(23)	1.163(29)

is set to $m_s(\mu_{\text{QCD}})$ and the light quark mass is varied, rendering all meson masses larger than at the physical point. Thus we believe that using the formulae provided by three-flavor BChPT will show better convergence behavior when applied to the data set presented in 3.4, although meson masses larger than $\approx 400\,\text{MeV}$ are most likely still too high to ensure proper convergence behavior. In [108], Walker-Loud and collaborators use large-N_c arguments to trace the bad convergence behavior back to the flavor-singlet sector. They explicitly show that with their lattice data, BChPT does not yield a controlled expansion for the mass relation R_1. This suggests that it might be a good idea to factor out flavor-singlet combinations, like is done for our baryon mass ratios with X_N.

In [75] it is argued that finite-volume effects tend to cancel in the ratios considered here. Still, we are of the opinion that these finite-volume effects generated by the chiral loops are non-negligible for the data obtained in their work and should be investigated, especially for vector meson masses, see ch. 4.

What one finds when carrying out the analysis of these ratios is that some LECs and combinations thereof, the ones that parametrize the leading symmetry-breaking contributions, can already be obtained in a quite reliable fashion from the fan plot data. This is an important step towards applying BChPT formulae in a theoretically sound and controlled fashion to lattice QCD data. The other LECs, especially the ones parametrizing the singlet contributions to the baryon masses, are more difficult to determine, also due to a lack of information from the lattice, hence we can only give rough estimates for these constants and combinations thereof.

3.4.1 Expansion of mass ratios f_B and X_N

To the order we are working here, we find that we are only sensitive to terms $(\delta m_\ell)^k \bar{m}^{2-k}$, since all other terms are of higher order and will be modified by two-

loop contributions. We write down this double expansion, chiral expansion plus expansion in $(\delta m_\ell)^k \bar{m}^{2-k}$, in the following form:

$$f_B = 1 + (B_0 \delta m_\ell) f_B^{(1)} + (B_0 \delta m_\ell)^2 f_B^{(2)} + \mathcal{O}((\delta m_\ell)^3). \tag{3.53}$$

We then find that these coefficients $f_B^{(n)}$ are functions of $\bar{m}$:

$$\begin{aligned} f_N^{(1)} &= \frac{4(b_D - 3b_F)}{m_0} - \sqrt{2B_0\bar{m}}\frac{3(D^2 + 10DF - 3F^2)}{32 m_0 \pi F_0^2} \\ &\quad + (16 B_0 \bar{m}) \left(\frac{(3b_0 + 2b_D)(b_D - 3b_F)}{m_0^2} - \frac{6d_2 - 4d_3 + 9d_5}{m_0} + \dots \right) \\ &\quad + \mathcal{O}(\bar{m}^{3/2}), \end{aligned} \tag{3.54}$$

$$\begin{aligned} f_\Lambda^{(1)} &= \frac{8 b_D}{m_0} - \sqrt{2B_0\bar{m}}\frac{3(D^2 - 3F^2)}{16 m_0 \pi F_0^2} \\ &\quad + (16 B_0 \bar{m}) \left(\frac{2(3b_0 + 2b_D) b_D}{m_0^2} + \frac{8 d_3}{m_0} + \dots \right) + \mathcal{O}(\bar{m}^{3/2}), \end{aligned} \tag{3.55}$$

$$\begin{aligned} f_\Sigma^{(1)} &= -\frac{8 b_D}{m_0} + \sqrt{2B_0\bar{m}}\frac{3(D^2 - 3F^2)}{16 m_0 \pi F_0^2} \\ &\quad - (16 B_0 \bar{m}) \left(\frac{2(3b_0 + 2b_D) b_D}{m_0^2} + \frac{8 d_3}{m_0} + \dots \right) + \mathcal{O}(\bar{m}^{3/2}), \end{aligned} \tag{3.56}$$

$$\begin{aligned} f_\Xi^{(1)} &= \frac{4(b_D + 3b_F)}{m_0} - \sqrt{2B_0\bar{m}}\frac{3(D^2 - 10DF - 3F^2)}{32 m_0 \pi F_0^2} \\ &\quad + (16 B_0 \bar{m}) \left(\frac{(3b_0 + 2b_D)(b_D + 3b_F)}{m_0^2} + \frac{6d_2 + 4d_3 + 9d_5}{m_0} + \dots \right) \\ &\quad + \mathcal{O}(\bar{m}^{3/2}), \end{aligned} \tag{3.57}$$

and the coefficients for the terms quadratic in δm_ℓ read

$$f_N^{(2)} = -\frac{D^2 + 18DF - 3F^2}{128\sqrt{2B_0\bar{m}} m_0 \pi F_0^2} - 16\frac{3d_1 - 3d_2 - d_3}{m_0} + \dots + \mathcal{O}(\bar{m}^{1/2}), \tag{3.58}$$

$$f_\Lambda^{(2)} = -\frac{10(D^2 - 3F^2)}{128\sqrt{2B_0\bar{m}} m_0 \pi F_0^2} + 32\frac{3d_1 - 5d_3 - 3d_4}{m_0} + \dots + \mathcal{O}(\bar{m}^{1/2}), \tag{3.59}$$

$$f_\Sigma^{(2)} = \frac{2(D^2 - 3F^2)}{128\sqrt{2B_0\bar{m}} m_0 \pi F_0^2} + 32\frac{3d_1 - d_3}{m_0} + \dots + \mathcal{O}(\bar{m}^{1/2}), \tag{3.60}$$

$$f_\Xi^{(2)} = -\frac{D^2 - 18DF - 3F^2}{128\sqrt{2B_0\bar{m}} m_0 \pi F_0^2} - 16\frac{3d_1 + 3d_2 - d_3}{m_0} + \dots + \mathcal{O}(\bar{m}^{1/2}). \tag{3.61}$$

Here, the ellipses denote contributions from loop graphs of fourth order, which are too lengthy to be presented here. Let us focus on the contact-term contributions first. We find that $f_\Sigma^{(1)} = -f_\Lambda^{(1)}$ and also that the linear combination $f_N^{(n)} + f_\Sigma^{(n)} + f_\Xi^{(n)} = 0$. Furthermore, the baryon mass in the chiral limit only appears in combination with

other LECs, i.e. $D/\sqrt{m_0}$, $F/\sqrt{m_0}$, b_i/m_0 and d_i/m_0. And most prominently, the LEC d_7 does not appear at all to this order of the double expansion of the ratios. So, determining d_7 only from fan plot type data would be very hard, since terms proportional $(\delta m_\ell)^3$ should be vanishingly small (the lattice data suggests a rather linear dependence). Since we also want to use D and F as well as $b_{1-4,8-11}$ as input for our analysis, it is unfortunate that m_0 is not accurately known. But what is rather accurately known is the baryon mass at the symmetric point

$$m_\star = m_0 - 4B_0\bar{m}(3b_0 + 2b_D) + \mathcal{O}(\bar{m}^{3/2}), \tag{3.62}$$

due to the additional lattice data available for $m_\star(M_\star)$, which we will also use for our analysis. Thus, we can eliminate m_0 in favor of $m_\star$ and additionally replace F_0 by $F_\star$, since at the order we are working this is valid according to the chiral counting scheme. We can now rewrite the expressions above in terms of the modified LECs $\tilde{b}_{D/F}$, $m_\star$ and $F_\star$:

$$\begin{aligned}
f_N^{(1)} = {} & \frac{4(\tilde{b}_D - 3\tilde{b}_F)}{m_\star} - \sqrt{2B_0\bar{m}}\frac{3(D^2 + 10DF - 3F^2)}{32m_\star\pi F_\star^2} \\
& - \frac{4B_0\bar{m}}{(4\pi F_\star)^2}\left[\frac{\tilde{b}_D - 3\tilde{b}_F}{m_\star}\left(\frac{5}{3} + 8\log\left(\frac{\sqrt{2B_0\bar{m}}}{\mu}\right)\right)\right. \\
& + \frac{2\tilde{b}_D}{m_\star}(13D^2 - 30DF + 9F^2)\left(\frac{1}{3} + \log\left(\frac{\sqrt{2B_0\bar{m}}}{\mu}\right)\right) \\
& - \frac{6\tilde{b}_F}{m_\star}(5D^2 - 6DF + 9F^2)\left(\frac{1}{3} + \log\left(\frac{\sqrt{2B_0\bar{m}}}{\mu}\right)\right) \\
& \left. + \frac{D^2 + 10DF - 3F^2}{m_\star^2}\left(\frac{3}{4} + \log\left(\frac{\sqrt{2B_0\bar{m}}}{\mu}\right)\right)\right] + \mathcal{T}_N^{(1)} + \mathcal{O}(\bar{m}^{3/2}),
\end{aligned} \tag{3.63}$$

$$\begin{aligned}
f_\Lambda^{(1)} = {} & \frac{8\tilde{b}_D}{m_\star} - \sqrt{2B_0\bar{m}}\frac{3(D^2 - 3F^2)}{16m_\star\pi F_\star^2} - \frac{4B_0\bar{m}}{(4\pi F_\star)^2}\left[\frac{2\tilde{b}_D}{m_\star}\left(\frac{5}{3} + 8\log\left(\frac{\sqrt{2B_0\bar{m}}}{\mu}\right)\right)\right. \\
& + \frac{4\tilde{b}_D}{m_\star}(13D^2 + 9F^2)\left(\frac{1}{3} + \log\left(\frac{\sqrt{2B_0\bar{m}}}{\mu}\right)\right) \\
& + \frac{72\tilde{b}_F}{m_\star}DF\left(\frac{1}{3} + \log\left(\frac{\sqrt{2B_0\bar{m}}}{\mu}\right)\right) \\
& \left. + \frac{2(D^2 - 3F^2)}{m_\star^2}\left(\frac{3}{4} + \log\left(\frac{\sqrt{2B_0\bar{m}}}{\mu}\right)\right)\right] + \mathcal{T}_\Lambda^{(1)} + \mathcal{O}(\bar{m}^{3/2}).
\end{aligned} \tag{3.64}$$

Furthermore, $f_\Sigma^{(1)}$ and $f_\Xi^{(1)}$ can be obtained by using the relations given in the text above. The formulae for the coefficients of $(\delta m_\ell)^2$ are only changed by replacing $(m_0, F_0) \to (m_\star, F_\star)$. The abbreviations $\mathcal{T}_B^{(1)}$ stand for all the tadpole contributions

proportional to $b_{1-4,8-11}$:

$$\begin{aligned}\mathcal{T}_N^{(1)} &= \frac{4B_0\bar{m}}{3(4\pi F_\star)^2}\left[\frac{9b_1-15b_2+b_3}{m_\star}\left(1+4\log\left(\frac{\sqrt{2B_0\bar{m}}}{\mu}\right)\right)\right.\\ &\quad\left.+\frac{9b_8-15b_9+b_{10}}{m_\star}\log\left(\frac{\sqrt{2B_0\bar{m}}}{\mu}\right)\right],\\ \mathcal{T}_\Lambda^{(1)} &= \frac{8B_0\bar{m}}{3(4\pi F_\star)^2}\left[\frac{9b_1+b_3}{m_\star}\left(1+4\log\left(\frac{\sqrt{2B_0\bar{m}}}{\mu}\right)\right)\right.\\ &\quad\left.+\frac{9b_8+b_{10}}{m_\star}\log\left(\frac{\sqrt{2B_0\bar{m}}}{\mu}\right)\right],\end{aligned} \tag{3.65}$$

We find that $b_{2,9}$ appear only for $B = N, \Xi$, while the linear combinations $9b_1 + b_3$ and $9b_8 + b_{10}$ enter for all baryons. Due to the symmetry constraints given earlier in the text, we can only derive the parameter combinations $\tilde{b}_{D/F}$ from a derivative of the ratios at the symmetric point.

Since all of the above ratios have been normalized to the linear combination of baryon masses X_N, it is instructive to take a closer look at the chiral expansion of this quantity. In the lattice simulations [75], it is shown to be practically constant along the whole simulation trajectory, which lead to it being used to set the scale for the lattice simulations. When employing the BChPT formulae we derived here, we find that this flat behavior of X_N is not automatically guaranteed. We will rather impose it as a constraint when we carry out the fits to fan plot data. Let us take a look at the chiral expansion of X_N:

$$X_N = m_\star + (B_0\delta m_\ell)^2 X_N^{(2)} + \mathcal{O}((\delta m_\ell)^3), \tag{3.66}$$

where we find the expressions

$$\begin{aligned}m_\star &= m_0 - 4B_0\bar{m}(3b_0+2b_D) - (2B_0\bar{m})^{3/2}\frac{(5D^2+9F^2)}{24\pi F_\star^2}\\ &\quad+\frac{(2B_0\bar{m})^2}{3(4\pi F_\star)^2}\left[32(3b_0+2b_D)\log\left(\frac{\sqrt{2B_0\bar{m}}}{\mu}\right)\right.\\ &\quad-8(9b_1+7b_3+12b_4)\log\left(\frac{\sqrt{2B_0\bar{m}}}{\mu}\right)\\ &\quad-2(9b_8+7b_{10}+12b_{11})\left(\log\left(\frac{\sqrt{2B_0\bar{m}}}{\mu}\right)-\frac{1}{4}\right)\\ &\quad-12(4\pi F_\star)^2(4d_3+9d_6+3d_7)\\ &\quad\left.-\frac{(5D^2+9F^2)}{m_0}\left(1+2\log\left(\frac{\sqrt{2B_0\bar{m}}}{\mu}\right)\right)\right]+\mathcal{O}(\bar{m}^{5/2}),\end{aligned} \tag{3.67}$$

and for the coefficient of $(\delta m_\ell)^2$ we find

$$\begin{aligned} X_N^{(2)} = &-\frac{3(D^2+2F^2)}{16\pi F_\star^2\sqrt{2B_0\bar{m}}} - 32\,(3d_1+d_3+3d_7) + \frac{5b_0}{\pi^2 F_\star^2}\left(\frac{3}{4}+\log\left(\frac{\sqrt{2B_0\bar{m}}}{\mu}\right)\right) \\ &+ \frac{b_D}{6\pi^2 F_\star^2}\left(2D^2\left(5+6\log\left(\frac{\sqrt{2B_0\bar{m}}}{\mu}\right)\right)+15+20\log\left(\frac{\sqrt{2B_0\bar{m}}}{\mu}\right)\right) \\ &- \frac{12b_1+8b_3+15b_4}{12\pi^2 F_\star^2}\left(3+4\log\left(\frac{\sqrt{2B_0\bar{m}}}{\mu}\right)\right) \\ &- \frac{12b_8+8b_{10}+15b_{11}}{24\pi^2 F_\star^2}\left(1+2\log\left(\frac{\sqrt{2B_0\bar{m}}}{\mu}\right)\right) \\ &- \frac{D^2+2F^2}{2m_0\pi^2 F_\star^2}\left(\frac{5}{4}+\log\left(\frac{\sqrt{2B_0\bar{m}}}{\mu}\right)\right) + \mathcal{O}(\bar{m}^{1/2}). \end{aligned} \tag{3.68}$$

As is evident from eqs. (3.67), (3.68), the LEC d_7 shows up both at orders $\bar{m}$ and $(\delta m_\ell)^2$. Hence the baryon mass in the chiral limit m_0 and the combinations of LECs appearing in this expansion will be determined from the behavior of $m_\star(\bar{m})$ since the data presented in [75] contains a few data points in the region $300\,\text{MeV} < M_\star < 500\,\text{MeV}$. Again, we discard any data points available for $M_\star > 500\,\text{MeV}$ since we believe that including those data points will introduce a hardly controllable model-dependence.

3.4.2 Linear fits to lattice data

In this subsection we perform preliminary fits to a linearized version of the mass ratios combined with the constraint that X_N does not deviate much from the physical value. As we have already mentioned above, only the combinations of LECs that are proportional to the terms linear in δm_ℓ can be safely determined from such fits. We approximate

$$f_B \approx 1 + \nu f_B^{(1,v)}, \qquad X_N \approx m_\star + \nu^2 X_N^{(2,\nu)}, \tag{3.69}$$

and using eq. (3.15), expanding up to $\mathcal{O}((2B_0\bar{m})^2)$, we find that we can determine the following linear combinations of LECs:

$$\begin{aligned} &\tilde{b}_D = b_D + 16B_0\bar{m}d_3, \qquad &&\tilde{b}_0 = b_0 - 2B_0\bar{m}\left(\frac{8}{3}d_3 - 6d_6 - 2d_7\right), \\ &\tilde{b}_F \equiv b'_F + 8B_0\bar{m}d_2, \qquad &&\tilde{d}_7 = d_1 + \frac{1}{3}d_3 + d_7. \end{aligned} \tag{3.70}$$

Here we have introduced another linear combination called $b'_F = b_F + 12B_0\bar{m}d_5$. All loop functions are evaluated at a renormalization scale $\mu = 1150\,\text{MeV}$. Furthermore we use that $2B_0\bar{m} = (420\,\text{MeV})^2$ in order to assure that the meson mass at the symmetric point is set to $M_\star = 412\,\text{MeV}$ if we use the central values for the set

Table 3.5: Input values $b_{1-4,8-11}$ taken from tab. 3.3, set 1.

$F_\star\,[\mathrm{MeV}]$	$m_0\,[\mathrm{MeV}]$	$\tilde{b}_D\,[\mathrm{GeV}^{-1}]$	$\tilde{b}_F\,[\mathrm{GeV}^{-1}]$	$\tilde{b}_0\,[\mathrm{GeV}^{-1}]$	$\tilde{d}_7\,[\mathrm{GeV}^{-3}]$
140	1000	0.066	−0.306	−0.599	−0.118
112	800	0.078	−0.352	−0.888	−0.158
112	1000	0.078	−0.352	−0.764	−0.168
112	1200	0.078	−0.352	−0.639	−0.180
80	800	0.109	−0.434	−1.158	−0.257
80	1000	0.109	−0.434	−1.067	−0.271
80	1200	0.109	−0.434	−0.974	−0.287

Table 3.6: Input values $b_{1-4,8-11}$ taken from tab. 3.3, set 2.

$F_\star\,[\mathrm{MeV}]$	$m_0\,[\mathrm{MeV}]$	$\tilde{b}_D\,[\mathrm{GeV}^{-1}]$	$\tilde{b}_F\,[\mathrm{GeV}^{-1}]$	$\tilde{b}_0\,[\mathrm{GeV}^{-1}]$	$\tilde{d}_7\,[\mathrm{GeV}^{-3}]$
140	1000	0.054	−0.308	−0.652	−0.130
112	800	0.062	−0.355	−0.961	−0.173
112	1000	0.062	−0.355	−0.838	−0.183
112	1200	0.062	−0.355	−0.713	−0.195
80	800	0.088	−0.437	−1.270	−0.277
80	1000	0.088	−0.437	−1.179	−0.291
80	1200	0.088	−0.437	−1.086	−0.307

of meson LECs presented in tab. 3.1. In the expressions for $f_B^{(1,\nu)}$ we set $m_\star^{\mathrm{num}} = 1150\,\mathrm{MeV}$, effectively eliminating the baryon mass in the chiral limit, m_0, as explained before. To get an estimate for the error for these combinations we vary the decay constant at the symmetric point $F_\star$ in the region $80 - 140\,\mathrm{MeV}$. We have collected the results of these fits in tabs. 3.5-3.8, for input values for m_0 ranging from 800 MeV to 1200 MeV and for all four parameter sets that were presented in tab. 3.3. From these results we can assess certain ranges for the fit parameters that should, even after carrying out the full $\mathcal{O}(p^4)$ analysis, hold true, based on the expectation of higher-order corrections to our approximate fit formulae eq. (3.69). The bounds we impose on the fit parameters are (in the appropriate units we have already given in

Table 3.7: Input values $b_{1-4,8-11}$ taken from tab. 3.3, set 3.

$F_\star$ [MeV]	m_0 [MeV]	$\tilde{b}_D$ [GeV^{-1}]	$\tilde{b}_F$ [GeV^{-1}]	$\tilde{b}_0$ [GeV^{-1}]	$\tilde{d}_7$ [GeV^{-3}]
140	1000	0.069	−0.310	−0.697	−0.136
112	800	0.083	−0.358	−1.024	−0.181
112	1000	0.083	−0.358	−0.900	−0.192
112	1200	0.083	−0.358	−0.775	−0.203
80	800	0.117	−0.443	−1.362	−0.289
80	1000	0.117	−0.443	−1.271	−0.303
80	1200	0.117	−0.443	−1.178	−0.319

Table 3.8: Input values $b_{1-4,8-11}$ taken from tab. 3.3, set 4.

$F_\star$ [MeV]	m_0 [MeV]	$\tilde{b}_D$ [GeV^{-1}]	$\tilde{b}_F$ [GeV^{-1}]	$\tilde{b}_0$ [GeV^{-1}]	$\tilde{d}_7$ [GeV^{-3}]
140	1000	0.063	−0.271	−0.322	−0.068
112	800	0.072	−0.305	−0.504	−0.091
112	1000	0.072	−0.305	−0.380	−0.101
112	1200	0.072	−0.305	−0.255	−0.113
80	800	0.095	−0.365	−0.580	−0.166
80	1000	0.095	−0.365	−0.490	−0.180
80	1200	0.095	−0.365	−0.396	−0.196

tabs. 3.5-3.8):

$$0.05 \leq \tilde{b}_D \leq \quad 0.15\,, \tag{3.71}$$
$$-0.50 \leq \tilde{b}_F \leq -0.25\,, \tag{3.72}$$
$$-1.50 \leq \tilde{b}_0 \leq -0.20\,, \tag{3.73}$$
$$-0.35 \leq \tilde{d}_7 \leq -0.05\,. \tag{3.74}$$

In the full analysis we will use $\tilde{b}_{D/F}$ as input for every set of input parameters while the parameters m_0, b_0, d_{1-7} will be treated as free fit parameters. Afterwards we can use the linear results for $\tilde{b}_0$ and $\tilde{d}_7$ as a consistency check. Note again that these LEC ranges are only valid for this choice of $2B_0\bar{m}$ and μ.

Table 3.9: $m_\star(M_\star)$ data taken from [75], tab. 19. To obtain these values in units of MeV we have used their value for $a = 0.0834(1)\,\mathrm{fm}$ quoted in footnote 5 in sec. 8.3.2 of [75].

$M_\star\,[\mathrm{MeV}]$	307	357	413
$m_\star(M_\star)\,[\mathrm{MeV}]$	1018(28)	1068(18)	1153(7)

3.4.3 Full one-loop analysis of the fan plot data

In this section we will apply the full one-loop formulae to the fan plot data for the baryon octet masses (see again tab. 3.4) and we will fit $m_\star(M_\star)$ to the three data points that fulfill our demand that $M_\star \leq 413\,\mathrm{MeV}$. For the reader's convenience we present these data points in tab. 3.9. Additionally we impose over the whole range of ν that $X_N(\nu)$ does not deviate from its value at the physical point $X_N(-0.885) = 1150\,\mathrm{MeV}$ by more than 10%. In this whole analysis we again eliminate F_0 in favor of $F_\star$, as we did in the last subsection already, since this formally amounts to an $\mathcal{O}(p^5)$ effect. We obtain f_B through insertion of the full one-loop expression for the baryon masses. Note that we do not expand either in ν or $\bar{m}$ this time. We also do not truncate $X_N(\nu)$ at $\mathcal{O}(\nu^2)$ as has been done in the last subsection. We need input both for the fan plot functions and $X_N(\nu)$, so we use what we have specified in eqs. (3.20), (3.21). All meson LECs we again take from the set MILC2010, see tab. 3.1. Plus, we can use $\tilde{b}_{D/F}$ from the last subsection as input for each single set of $b_{1-4,8-11}$ from tab. 3.3. With all that input, we can determine further parameters from the data sets given in tabs. 3.4 and 3.9: First of all, the $(\delta m_\ell)^2$ dependence is determined by four different parameters, i.e.

$$\tilde{d}_1 = d_1 - \frac{1}{3}d_3, \quad d_2, \quad \tilde{d}_4 = d_4 + \frac{4}{3}d_3, \tag{3.75}$$

as well as $\tilde{d}_7$ which we have defined in eq. (3.70). Since we use $\tilde{b}_D$ as an input value, we can also insert

$$b_D = \tilde{b}_D - 8(0.42\,\mathrm{GeV})^2 d_3 \tag{3.76}$$

in eq. (3.67), we find that we can furthermore determine the combinations

$$b_0' = b_0 - \frac{16}{3}(0.42\,\mathrm{GeV})^2 d_3, \tag{3.77}$$

$$\tilde{d}_6 = \frac{4}{9}d_3 + d_6 + \frac{1}{3}d_7. \tag{3.78}$$

Table 3.10: Results for the fit parameters. The set-number refers to tab. 3.3. $\tilde{b}_{D/F}$ are fixed input. m_0 is given in GeV, $b'_0, \tilde{b}_{D/F}$ in GeV^{-1}, and the d_i are given in GeV^{-3} at a scale $\mu = 1150\,\mathrm{MeV}$. Here, the experimental masses are not included in the fit.

set	$\tilde{b}_D$	$\tilde{b}_F$	m_0	b'_0	$\tilde{d}_1$	d_2	$\tilde{d}_4$	$\tilde{d}_6$	$\tilde{d}_7$	$\tilde{b}_0$
1	0.078	−0.352	1.029	−0.364	0.035	0.122	0.020	−0.532	−0.244	−0.927
2	0.062	−0.355	1.051	−0.373	0.040	0.126	0.018	−0.603	−0.272	−1.011
3	0.083	−0.358	1.064	−0.400	0.030	0.121	0.030	−0.641	−0.289	−1.078
4	0.072	−0.305	0.930	−0.271	0.025	0.101	0.042	−0.213	−0.113	−0.497

The running of $X_N(\delta m_\ell = 0)$ also enables us to obtain a value for the baryon mass in the chiral limit m_0. We find that, using the earlier defined $\tilde{b}_0$, we can write it as

$$\tilde{b}_0 = b'_0 + 6(0.42\,\mathrm{GeV})^2 \tilde{d}_6, \tag{3.79}$$

if we also use $\sqrt{2B_0\bar{m}} = 0.42\,\mathrm{GeV}$.
We present the results of our several different fit scenarios in tabs. 3.10-3.14. In tab. 3.10 we have used $\tilde{b}_{D,F}$ as input and have determined all the other parameters, while in tab. 3.13 we have added four additional data points, namely the mass ratios at the physical point. We have assigned an error of 5 MeV due to our neglect of isospin-breaking effects, the physical point is located at $\nu \approx -0.885$. As consistency checks we have included two fit sets where we fit all the LECs and then calculate $\tilde{b}_0$ and $\tilde{b}_F$, once with and once without including the four additional experimentally known data points. Finally, tab. 3.14 contains a stability check where we have used the central value for F_0 from the MILC2010 set instead of $F_\star$ and we have not fixed $\tilde{b}_{D,F}$ but have included the experimentally known mass ratios. We find that all the fits have a χ^2/d.o.f. ≈ 0.2, which has two different reasons: first, the parameters $\tilde{b}_{D,F}$ are mostly determined by the data around the symmetric point, because there the mass ratio formulae prove to be very linear, see fig. 3.5. Secondly we have a host of free parameters, which means that there is enough leeway to describe the behavior of X_N appropriately. We have carried out many different fits to assess the general error that comes from various assumptions, i.e. the uncertainties we have from the various input values for b_i, the higher-order corrections we neglect due to shifting $F_0 \to F_\star$, using parameters gained from fitting the linear approximations of our full extrapolation functions as input for our full fits etc. Overall we observe a good agreement of the fits; although we vary the input parameters in a rather broad range we end up with very similar results.

3.5 Discussion of results

In this section we will first discuss the convergence of the expansion of $m_\star$ and then we will take a closer look at the parameters that parametrize symmetry-breaking.

Table 3.11: Results for the fit parameters, this time including the experimentally known baryon masses.

set	$\tilde{b}_D$	$\tilde{b}_F$	m_0	b'_0	$\tilde{d}_1$	d_2	$\tilde{d}_4$	$\tilde{d}_6$	$\tilde{d}_7$	$\tilde{b}_0$
1	0.078	−0.352	1.026	−0.370	0.035	0.046	0.044	−0.525	−0.257	−0.926
2	0.062	−0.355	1.046	−0.381	0.041	0.050	0.041	−0.594	−0.287	−1.010
3	0.083	−0.358	1.058	−0.411	0.030	0.047	0.054	−0.630	−0.306	−1.077
4	0.072	−0.305	0.936	−0.262	0.024	0.017	0.063	−0.222	−0.115	−0.496

Table 3.12: Consistency check. Here, the combinations $\tilde{b}_{D,F}$ are not fixed, and the experimental masses are not included in the fit. The values for $\tilde{b}_0$, $\tilde{b}_F$ are computed for each set of fit results.

set	m_0	b'_0	$\tilde{b}_D$	b'_F	$\tilde{d}_1$	d_2	$\tilde{d}_4$	$\tilde{d}_6$	$\tilde{d}_7$	$\tilde{b}_0$	$\tilde{b}_F$
1	1.028	−0.372	0.087	−0.405	0.043	0.119	0.039	−0.531	−0.244	−0.933	−0.321
2	1.050	−0.381	0.072	−0.409	0.048	0.122	0.036	−0.602	−0.273	−1.017	−0.323
3	1.063	−0.407	0.092	−0.412	0.040	0.121	0.051	−0.640	−0.289	−1.084	−0.327
4	0.929	−0.278	0.079	−0.346	0.033	0.095	0.059	−0.211	−0.114	−0.501	−0.280

For the discussion of convergence let us take a closer look at $m_\star$, eq. (3.67), using the fit results from tab. 3.10 as input parameters. Naively we would expect the suppression factor to be of the order

$$\frac{\sqrt{2B_0\bar{m}}}{4\pi F_\star} \sim \frac{420}{4\pi \cdot 112} \sim 0.3, \tag{3.80}$$

while we already know that the leading non-analytic loop correction of $\mathcal{O}(p^3)$ is much enhanced with respect to the value quoted above. We find, that

$$m_\star = m_0 - 4B_0\bar{m}(3b_0 + 2b_D) - (2B_0\bar{m})^{3/2}\frac{(5D^2+9F^2)}{24\pi F_\star^2} + \frac{(2B_0\bar{m})^2}{3(4\pi F_\star)^2}\Big[\,...\,\Big] \tag{3.81}$$

$$\to (1029 + 330 - 397 + 186)\,\text{MeV} = 1148\,\text{MeV} \text{ for set 1 from tab. 3.10,} \tag{3.82}$$

$$\to (1051 + 351 - 397 + 143)\,\text{MeV} = 1148\,\text{MeV} \text{ for set 2 from tab. 3.10,} \tag{3.83}$$

$$\to (1064 + 365 - 397 + 115)\,\text{MeV} = 1147\,\text{MeV} \text{ for set 3 from tab. 3.10,} \tag{3.84}$$

$$\to \quad (930 + 236 - 397 + 380)\,\text{MeV} = 1149\,\text{MeV} \text{ for set 4 from tab. 3.10.} \tag{3.85}$$

As we can see, $m_\star \approx m_\star^{\text{num}} = 1150\,\text{MeV}$ for all the different sets as we have used this as a constraint for the fit parameters. The convergence behavior we observe here is inconclusive if investigated order by order. What we can conclude is that the fourth order contribution is roughly in line with a suppression factor of ≈ 0.5. There is the possibility to analyze the convergence behavior by only comparing full orders, i.e. the full tree-level contribution $\mathcal{O}(p)$ and $\mathcal{O}(p^2)$ with the full one-loop

Table 3.13: Consistency check. Here, the fit includes the experimental baryon masses, but the combinations $\tilde{b}_{D,F}$ are not fixed.

set	m_0	b'_0	$\tilde{b}_D$	b'_F	$\tilde{d}_1$	d_2	$\tilde{d}_4$	$\tilde{d}_6$	$\tilde{d}_7$	$\tilde{b}_0$	$\tilde{b}_F$
1	1.021	−0.378	0.077	−0.357	0.039	0.022	0.051	−0.518	−0.257	−0.926	−0.341
2	1.042	−0.389	0.062	−0.361	0.044	0.025	0.048	−0.587	−0.287	−1.010	−0.343
3	1.054	−0.417	0.082	−0.365	0.035	0.025	0.062	−0.624	−0.305	−1.077	−0.347
4	0.930	−0.269	0.069	−0.295	0.027	0.010	0.067	−0.213	−0.115	−0.494	−0.302

Table 3.14: Stability check. Here we use the value from MILC2010 for the meson decay constant as input everywhere, instead of $F_\star$. The fit includes the experimental baryon masses, but the combinations $\tilde{b}_{D,F}$ are not fixed.

set	m_0	b'_0	$\tilde{b}_D$	b'_F	$\tilde{d}_1$	d_2	$\tilde{d}_4$	$\tilde{d}_6$	$\tilde{d}_7$	$\tilde{b}_0$	$\tilde{b}_F$
1	1.116	−0.329	0.118	−0.470	0.075	0.121	0.134	−1.247	−0.524	−1.649	−0.385
2	1.144	−0.337	0.097	−0.476	0.084	0.129	0.123	−1.411	−0.583	−1.831	−0.385
3	1.161	−0.371	0.126	−0.482	0.067	0.127	0.157	−1.500	−0.618	−1.960	−0.392
4	0.993	−0.211	0.098	−0.381	0.048	0.063	0.152	−0.516	−0.250	−0.757	−0.336

contributions $\mathcal{O}(p^3)$ and $\mathcal{O}(p^4)$, which leads us to a suppression factor ranging from 0.15 to 0.2 for sets 1-3. For set four, neither approach gives reasonable results: for the first way of assessing convergence by looking at order-to-order suppression we do not see any suppression at all, while the second approach yields a suppression factor of roughly ≈ 0.02 which is unrealistic for BChPT for $2B_0\bar{m} = (0.42\ textGeV)^2$. In both scenarios our fits with $b_{1-4,8-11} = 0$ seem to be meaningless in a perturbative sense. What we also can clearly see is the enhanced contribution from the leading non-analytic loop corrections $\propto M^3$. This shows that our fits are really sensitive to the LECs b_{1-11}.
We can now shift the average quark mass $2B_0\bar{m}$ from $(0.42\,\mathrm{GeV})^2$ to $(0.3\,\mathrm{GeV})^2$, which results also in a shift $F_\star \to 104\,\mathrm{MeV}$. If we again take a look at the perturbative expansion we find

$$m_\star \to (1029 + 169 - 168 - 10)\,\mathrm{MeV} = 1020\,\mathrm{MeV} \text{ for set 1 from tab. 3.10,} \quad (3.86)$$
$$m_\star \to (1051 + 179 - 168 - 39)\,\mathrm{MeV} = 1023\,\mathrm{MeV} \text{ for set 2 from tab. 3.10,} \quad (3.87)$$
$$m_\star \to (1064 + 186 - 168 - 57)\,\mathrm{MeV} = 1025\,\mathrm{MeV} \text{ for set 3 from tab. 3.10,} \quad (3.88)$$
$$m_\star \to (930 + 120 - 168 + 122)\,\mathrm{MeV} = 1004\,\mathrm{MeV} \text{ for set 4 from tab. 3.10.} \quad (3.89)$$

Again we see that the third order term is of the same magnitude as the second order term, while we also find that the $\mathcal{O}(p^4)$ term is well under control except for set 4. When comparing full loop orders we again find a suppression factor of roughly

0.16 for the sets 1-3 while set 4 again presents itself with an unrealistically small suppression factor of 0.05. This is a hypothetical study since lattice data at such small values for the average quark mass is not yet available. Hence, all the parameters that can mostly be determined from the singlet sector alone will be subject to big uncertainties, i.e. the parameters m_0, b_0' and $\tilde{d}_6$ will come with loose upper and lower bounds.
We can see how drastically the situation changes if we add a data point for the symmetric mass $m_\star(M_\star)$ at $M_\star > 500\,\mathrm{MeV}$ and carry out the same fits. We find that $m_0 \approx 800\,\mathrm{MeV}$, $b_0' \approx -0.9\,\mathrm{GeV}^{-1}$ and $\tilde{d}_6 \approx 0.04\,\mathrm{GeV}^{-3}$, while the other parameters more or less keep their previous values. This constitutes a very serious problem, since m_0 is a LEC that appears in every single three-flavor BChPT calculation, so it is mandatory to pin down especially the baryon mass in the chiral limit. For that, further data points for $m_\star(M_\star)$ have to be collected, preferrably in the region $M_\star < 300\,\mathrm{MeV}$ since the error bands in this region are quite sizable, see fig. 3.4. Up to this point in our analysis, we can only give rough bounds for these singlet parameters, which we base on the results presented in tabs. 3.10-3.14, which are:

$$800\,\mathrm{MeV} \leq m_0 \leq 1200\,\mathrm{MeV}\,, \tag{3.90}$$

$$-1\,\mathrm{GeV}^{-1} \leq b_0' \leq 0\,\mathrm{GeV}^{-1}\,, \tag{3.91}$$

$$-2\,\mathrm{GeV}^{-3} \leq \tilde{d}_6 \leq 0.50\,\mathrm{GeV}^{-3}\,. \tag{3.92}$$

This leads us to revising the previous boundaries we gave for $\tilde{b}_0$, since the above value for b_0' gives us a new lower limit on $\tilde{b}_0$:

$$-2\,\mathrm{GeV}^{-1} \leq \tilde{b}_0 \leq -0.20\,\mathrm{GeV}^{-1}. \tag{3.93}$$

We find that the uncertaintiy of the extrapolation of the symmetric baryon mass grows immensely right below the last data point. Note that the fourth data point, which was not used in our regular analysis, is presented in fig. 3.4 to show that data points $> 500\,\mathrm{MeV}$ are not well described by our extrapolation. Secondly, that data point was used to show that uncontrollable uncertainties are introduced when we add data above the 500 MeV threshold to our analysis. Fig. 3.4 also shows the $\mathcal{O}(p^5)$ effect that stems from eliminating F_0 in favor of $F_\star$. One can clearly see that again above the 500 MeV threshold this effect drastically influences the curves. We can conclude that chiral extrapolations above 500 MeV introduce a hardly controllable model-dependence. Furthermore the finding that chiral extrapolations of lattice data above that threshold cannot be trusted is consistent with the findings of other studies, [81, 113]. In [114], S. Dürr et al. present a study of two-flavor lattice data examining purely mesonic observables and they advocate that only data points below a threshold of 300 MeV yield reliable results when extrapolated to the physical point. After discussing the singlet parameters in length let us now turn to the LECs that parametrize symmetry-breaking. We present the fit curves in fig. 3.5. The first observation one can make about the values of the LECs that parametrize the terms

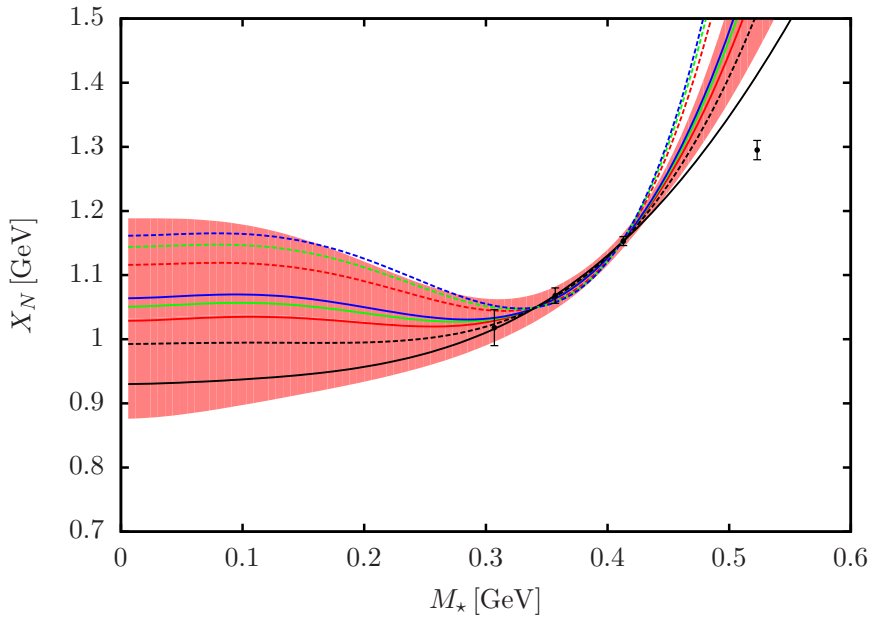

Figure 3.4: The function $m_\star(M_\star)$ for the four parameter sets from tab. 3.10 (solid) and 3.14 (dashed). Furthermore we have used the color code: set 1 (red), set 2 (green), set 3 (blue) and set 4 (black). The band here shows the one-sigma band associated to the solid red curve.

linear in symmetry-breaking for the various different sets of input parameters is that both $\tilde{b}_D$ and $\tilde{b}_F$ are almost the same, no matter whether we use values obtained from linear approximations to the mass ratio extrapolation formulae or whether we treat those parameters as free for our analysis employing the full extrapolation formulae. This hints at a very stable determination of these parameters. If we investigate the bounds we gave in eqs. (3.71) and (3.72) we find that all fit sets produce values within these boundaries. When we investigate the linear combination $(20/3)\tilde{b}_D - \tilde{b}_F$ we find that for all fits from tabs. 3.10-3.13, the linear combination falls in the bounds we have presented in sec. 3.2. For sets 1-3 from tab. 3.14 we find that the values for this particular linear combination lie a little above the given bounds. We find that the LECs parametrizing the linear part of symmetry-breaking can be determined in a very stable manner, which is due to the new impressive lattice data that leads to the fan plots we present here.
Lastly we need to discuss the linear combinations of LECs that parametrize the non-linear part of the symmetry-breaking effects. Since they appear at $\mathcal{O}(p^4)$, which is the order we are working at in our full one-loop calculation, we will not be able to determine them to very high precision. From the results we have gathered, we can extract the following allowed ranges (in units of GeV^{-3}):

$$-0.05 \leq \tilde{d}_1 \leq 0.15, \tag{3.94}$$

$$0.00 \leq d_2 \leq 0.25, \tag{3.95}$$

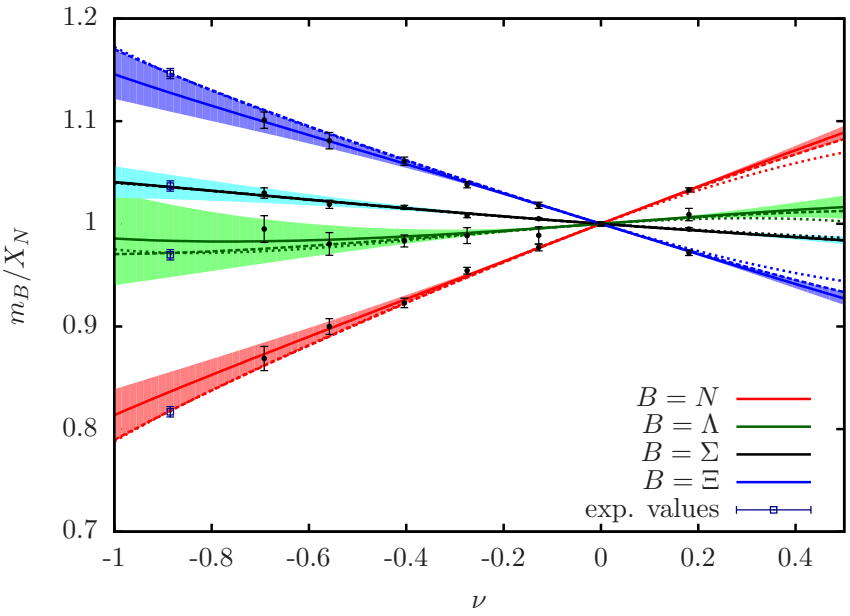

Figure 3.5: Three different fit results for b_{1-11} taken from set 1. The three curves represent the results from tabs. 3.10 (solid), 3.11 (dashed) and 3.13 (dotted). The bands again are the one-sigma bands corresponding to the solid curves. Note that the fit results in tabs. 3.11 and 3.13 contain the experimentally known mass ratios as data points.

$$-0.10 \leq \tilde{d}_4 \leq 0.20, \tag{3.96}$$

$$-0.75 \leq \tilde{d}_7 \leq -0.05. \tag{3.97}$$

All these values have been determined at a renormalization scale $\mu = 1150\,\text{MeV}$ and they can be evolved to other renormalization scales via eqs. (C.3)-(C.9) when infrared regularization is used at a different scale μ.
When we compare eq. (3.97) to eq. (3.74) we see that the linear approximation grossly underestimates the uncertainty in $\tilde{d}_7$. This is mostly due to the fact that the combination $\tilde{d}_7$ has to compensate for the quite sizable $\mathcal{O}(p^3)$ contribution in order to keep the observable $X_N(\nu)$ approximately constant. In fig. 3.6 we present the function $X_N(\nu)$ over the whole range for ν for our four results from tab. 3.10.
As we can see from comparing tab. 3.10 to tab. 3.11, including the experimentally known mass ratios mainly modifies the LEC d_2. We can see the effect on the fit curves in fig. 3.5, when we compare the dotted and dashed lines with the solid lines. We see that the curves that deviate most are the ones for f_N and f_Ξ. These findings lead us to conclude that a truly reliable extrapolation of fan plot data down to the physical point is still to be considered problematic, although a lot of progress towards such an extrapolation has been made in this work for the involved LECs and combinations thereof.
Borasoy and Meißner [76] have estimated d_{1-7} in the framework of HBChPT using

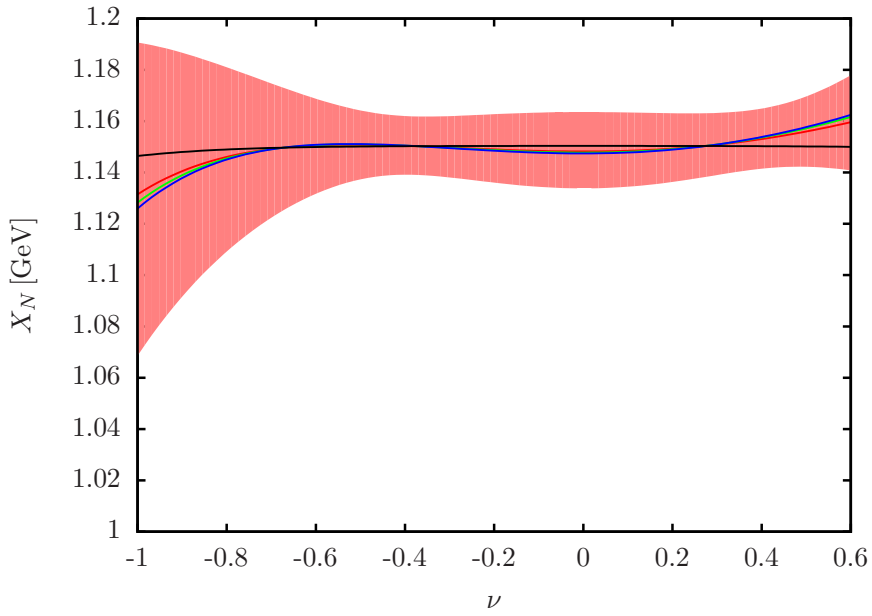

Figure 3.6: The function $X_N(\nu)$ for the four fit sets from tab. 3.10. The color code is, again: set 1 (red), set 2 (green), set 3 (blue) and set 4 (black). We again show the one-sigma band pertaining to the red curve.

the resonance saturation principle and combining it with a fit to experimental baryon masses and sigma terms. We show a direct comparison of their estimates and our results in tab. 3.15. Of course this comparison is of purely qualitative nature, due to the different regularization schemes and even more importantly the fact that the sigma term and the baryon masses at the physical point have been used as input, despite the bad convergence properties at the physical point.
Shortly after [35] was submitted to arXiv.org, two other analyses of the lattice data available at that time were published [112, 115], the latter of which uses a framework similar to the one we employed, so it is reasonable to compare their LECs with ours. The comparison of $\mathcal{O}(p^4)$ LECs is presented in tab. 3.15, while the comparison of several fit values for the bayon mass in the chiral limit m_0 can be found in tab. 3.16. We find that the d_{1-7} mostly fit into our relatively broad ranges. The same is true for the values for m_0. Only the value quoted in [116] is not in line with our results. In general one has to be cautious here, since all these values were obtained in different regularization schemes at sometimes even different renormalization scales μ. We have checked that the latter however does not have a big influence on our results.
As far as the LEC combinations $\tilde{b}_{D,F,0}$ are concerned, $\tilde{b}_{F,0}$ from [76, 112] are covered by our relatively broad ranges, wheras for $\tilde{b}_D$ our result is not compatible with the results quoted in the two references. In [112], one finds that their LEC b_D jumps from a rather small value at $\mathcal{O}(p^3)$ to a comparatively large value at $\mathcal{O}(p^4)$, i.e. from $\approx 0.05/\text{GeV}$ to $\approx 0.22/\text{GeV}$. Such a large jump could hint at a convergence problem and since almost all of the data analyzed in ref. [112] is at or above the threshold

Table 3.15: Comparison of our results to the estimates obtained from resonance saturation presented in [76] and the fit results published in [112]. As an estimate for the parameter β_R appearing in the publication we use $\beta_R \approx 0$, because the value of the combinations only depends very slightly on β_R, if it is varied in the range $[-0.1, 0.1]\,\mathrm{GeV}^{-1}$ as advocated in their paper. All LECs are given in units of $[\mathrm{GeV}^{-3}]$.

Ref.	$\tilde{d}_1$	d_2	$\tilde{d}_4$	$\tilde{d}_6$	$\tilde{d}_7$
this work	$[-0.05, 0.15]$	$[0.00, 0.25]$	$[-0.10, 0.20]$	$[-2, 0.5]$	$[-0.75, -0.05]$
[76]	-0.015	0.035	0.015	-0.0217	-0.072
[112]	$0.020(23)$	$0.296(53)$	$0.298(76)$	$-0.053(39)$	$-0.059(40)$

Table 3.16: Results for m_0 (in GeV) from refs. [76, 112, 116, 117]. For our estimate, see eq. (3.90).

Ref.	[112], Fit I	[116]	[117]	[76]
m_0	0.880 ± 0.022	0.756 ± 0.032	0.944 ± 0.002	0.767 ± 0.110

where the three-flavor expansions work in a reliable manner, it is important to redo this analysis once more data with small meson masses, i.e. in particular small strange quark masses, is available.

3.6 Pion-nucleon sigma term

The pion-nucleon sigma term is a quantity which measures the contribution of the explicit breaking of chiral symmetry to the nucleon mass. It is defined as

$$\sigma_{\pi N}(t) = m_\ell \left\langle N', p' \left| \bar{u}u + \bar{d}d \right| N, p \right\rangle , \tag{3.98}$$

where $t = (p' - p)^2$. We can extract $\sigma_{\pi N}(0)$ from the nucleon mass formulae via the Feynman-Hellman theorem [118, 119],

$$\sigma_{\pi N}(0) = m_\ell \frac{\partial m_N(m_\ell, m_s)}{\partial m_\ell}. \tag{3.99}$$

From the $\mathcal{O}(p^3)$ mass formula for the nucleon, we find that the $\mathcal{O}(p^3)$ sigma term can be written as

$$\sigma_{\pi N}(0) = -2\dot{M}_\pi^2(2b_0 + b_D + b_F) - \frac{\dot{M}_\pi^2}{64\pi F_0^2}\left(4\alpha_N^\pi \dot{M}_\pi + 2\alpha_N^K \dot{M}_K + \frac{4}{3}\alpha_N^\eta \dot{M}_\eta\right), \tag{3.100}$$

where we find the coefficients α_N^i to be

$$\alpha_N^\pi = \frac{9}{4}(D+F)^2\,, \quad \alpha_N^K = \frac{1}{2}(5D^2 - 6DF + 9F^2)\,, \quad \alpha_N^\eta = \frac{1}{4}(D-3F)^2. \tag{3.101}$$

If we investigate this quantity at this order, we find that the one-loop contribution is of order

$$-\dot{M}_\pi^2\left(\frac{\dot{M}_K}{4\pi F_0}\right)\left(\frac{5.54}{\text{GeV}}\right) \approx -50\,\text{MeV}, \tag{3.102}$$

at the physical point with our particular choice for D and F, see sec. 3.2. So this positive quantity of about 50 MeV acquires a contribution of about -50 MeV at leading one-loop order, which casts strong doubts on the applicability of BChPT at the physical point. From eqs. (3.43)-(3.46) we can derive the contributions of the $\mathcal{O}(p^4)$ contact-terms to the sigma term:

$$\begin{aligned}\sigma_{\pi N}^{(\text{ct})}(0) = -2B_0 m_\ell\Big(& 4b_0 + 2b_D + 2b_F + \frac{32}{3}B_0\bar{m}\,(4d_3 + 9d_6 + 3d_7) \\ &+ \frac{8}{3}B_0\bar{m}\,(6d_2 - 4d_3 + 9d_5) \\ &+ 16(B_0\delta m_\ell)\,(3d_1 + d_2 - d_3 + 3d_5 + 2d_7)\Big).\end{aligned} \tag{3.103}$$

This equation can be rewritten using our previously defined fit parameters, eqs.(3.70) and (3.77), and we obtain the form

$$\begin{aligned}\sigma_{\pi N}^{(\text{ct})}(0) = -2B_0 m_\ell\Big(& 4b_0' + 2\tilde{b}_D + 2\tilde{b}_F + 96B_0\bar{m}\tilde{d}_6 \\ &+ \frac{16}{3}(B_0\delta m_\ell)(3\tilde{d}_1 + 3d_2 - 4d_3 + 9d_5 + 6\tilde{d}_7)\Big)\end{aligned} \tag{3.104}$$

Since we were not able to determine the LECs d_3 and d_5, we can only give a rough estimate for the sigma term. In general, we can write the complete sigma term as a part that is independent of these LECs and a d_3 and d_5 dependent part:

$$\begin{aligned}\sigma_{\pi N}(0) &= \sigma_{\pi N}(0)\Big|_{d_3=d_5=0} + \frac{8}{3}(2B_0\delta m_\ell)(2B_0 m_\ell)(9d_5 - 4d_3) \\ &\approx \sigma_{\pi N}(0)\Big|_{d_3=d_5=0} - \frac{8}{3}M_\pi^2(X_\pi^2 - M_\pi^2)(9d_5 - 4d_3).\end{aligned} \tag{3.105}$$

Let us consider two scenarios for estimating the combination $d_5 - (4/9)d_3$: we take the results of fit sets 1 and 4 from tab. 3.10 as input and calculate $\sigma_{\pi N}(0)|_{d_3=d_5=0}$, which results in 67 MeV and 47 MeV respectively. Then we impose a consistency condition on d_3 and d_5 by requiring that these two LECs do not yield more than a 100% correction to the linear combinations of LECs we defined as b'_F and $\tilde{b}_D$. This gives us the following bounds on the LECs and the linear combination thereof:

$$-0.07\,\mathrm{GeV}^{-3} \leq d_3 \leq 0.07\,\mathrm{GeV}^{-3}, \tag{3.106}$$

$$-0.38\,\mathrm{GeV}^{-3} \leq d_5 \leq 0.38\,\mathrm{GeV}^{-3}, \tag{3.107}$$

$$-0.41\,\mathrm{GeV}^{-3} \leq \left(d_5 - \frac{4}{9}d_3\right) \leq 0.41\,\mathrm{GeV}^{-3}. \tag{3.108}$$

The above bounds lead to two ranges for the sigma terms, dependent on the input value for $\sigma_{\pi N}(0)|_{d_3=d_5=0}$, i.e.

$$39\,\mathrm{MeV} \leq \sigma_{\pi N}(0) \leq 95\,\mathrm{MeV} \text{ for set 1}, \tag{3.109}$$

$$19\,\mathrm{MeV} \leq \sigma_{\pi N}(0) \leq 75\,\mathrm{MeV} \text{ for set 4}. \tag{3.110}$$

The values quoted in this work are in perfect agreement with the latest three-flavor lattice determinations of the sigma term [120, 121]. The estimates we give here for d_3 and d_5 are also in tune with the fit results presented in [112]. Convergence for the sigma term at the physical point is still very questionable, so one should see these results only as what they were intended to be, i.e. rough bounds on the pion-nucleon sigma term. For a reliable determination one needs data points at smaller average quark masses and in general one would need the whole fan plot data at different values for $M_\star$, so that a relieable determination of d_3 and d_5 is also possible.
In general, we advocate to determine the sigma term employing $N_f = 2$ lattice data combined with $SU(2)_f$ BChPT, as is done in [122]. There is also the possibility to extract the pion-nucleon sigma term from πN-scattering by using the chiral symmetry of the strong interactions at the unphysical Cheng-Dashen point [123]. This has been done several times and usually favors a somewhat larger sigma term [124], while lattice determinations favor a lower value [120–122].

4 Chiral behavior of vector meson self-energies

In this chapter we concern ourselves with extrapolating the vector meson mass data presented in [75]. We calculate the vector meson octet masses to one-loop accuracy, while our representation of the vector meson self-energy also allows us to discuss the one-loop corrections to the $\phi(1020) - \omega(782)$ mixing amplitude. This work has been published in Physical Review D under the title 'Chiral behavior of vector meson self-energies' [125].

4.1 Generalities

In this chapter we concern ourself with calculating the vector meson self-energy to leading one-loop order within the framework of ChPT. Let us start with investigating the free vector field propagator in momentum space, which can be derived from the Lagrangian presented in eq. (1.77):

$$(\mathbf{D}_0^{-1})_{\mu\nu}(k) = -i\frac{\left(g_{\mu\nu} - \frac{k_\mu k_\nu}{M_{V,b}^2}\right)}{s - M_{V,b}^2} = -i\frac{\left(g_{\mu\nu} - \frac{k_\mu k_\nu}{s}\right)}{s - M_{V,b}^2} + i\frac{k_\mu k_\nu}{sM_{V,b}^2}. \tag{4.1}$$

In the above expression we have again introduced the abbreviation $s = k^2$. We assume $M_{V,b}$ to be real, so the width of the vector mesons is generated dynamically, via dressing by meson loops. In fig. 4.1 we schematically show the vector meson self-energy $\Pi_{\mu\nu}(k)$, which we can formally write in terms of a transversal and a

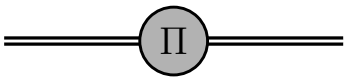

Figure 4.1: The vector meson self-energy $\Pi_{\mu\nu}(k)$. The double line represents incoming/outgoing vector mesons.

longitudinal part:

$$\Pi_{\mu\nu}(k) = \left(g_{\mu\nu} - \frac{k_\mu k_\nu}{k^2}\right)\Pi_T(s) + \frac{k_\mu k_\nu}{k^2}\Pi_L(s). \tag{4.2}$$

Let us resum the geometric series of irreducible two-point graphs

$$(\mathbf{D}^{-1})_{\mu\nu} = (\mathbf{D}_0^{-1})_{\mu\nu} + (\mathbf{D}_0^{-1})_{\mu\alpha}(i\Pi)^{\alpha\beta}(\mathbf{D}_0^{-1})_{\beta\nu} + \ldots = (\mathbf{D}_0 - i\mathbf{\Pi})^{-1}_{\mu\nu}\,, \tag{4.3}$$

where we find $(\mathbf{D}_0)_{\mu\nu} = i((k^2 - M_{V,b}^2)g_{\mu\nu} - k_\mu k_\nu)$. Next, we can invert the matrix presented in eq. (4.3) and we obtain

$$(\mathbf{D}^{-1})_{\mu\nu}(k) = \frac{(-i)\left(g_{\mu\nu} - \frac{k_\mu k_\nu}{s}\right)}{s - M_{V,b}^2 - \Pi_T(s)} + \frac{ik_\mu k_\nu}{s(M_{V,b}^2 + \Pi_L(s))}. \tag{4.4}$$

The first term resembles the transversal part of the free spin one propagator, with the pole position perturbatively shifted from $M_{V,b}^2$ to $M_{V,b}^2 + \Pi_T$, whereas the second term in eq. (4.4) does not have a pole in the vicinity of $M_{V,b}^2$, assuming that perturbation theory is applicable. When sandwiched between vertices derived from eq. (1.78), we find that the second term vanishes due to the transversal nature of the vertices. Hence we only need to concern ourselves with the calculation of Π_T, but for general interactions one should make sure that $\Pi_T(0) = \Pi_L(0)$ so that the self-energy does not develop a pole at $s = 0$. We also are only interested in the mesonic contributions to Π_T and hence we will assume that all other hadronic contributions have already been absorbed in all the parameters that occur in our framework, which is common practice within an effective field theory treatment describing low-energy interactions. In the chiral limit case where we send the quark mass matrix $\mathscr{M} \to 0$, the denominator of the transversal part of the full propagator takes the form

$$s - M_{V,b}^2 - \mathring{\Pi}_T^{\mathrm{PGB}}(s) = s - M_{V,b}^2 - \mathring{\Pi}_{T,\mathrm{loop}}^{\mathrm{PGB}}(s) - \sum_{n=0}^{N} \mathring{c}_n s^n, \tag{4.5}$$

where the circle denotes quantities in the chiral limit and the superscript PGB denotes that these are solely contributions from the interactions between vector mesons and the pseudoscalar bosons. The terms proportional to $\mathring{c}_n$ are counterterms that absorb the divergencies from the loop part of the self-energy, where N depends on the degree of divergence of the loop graphs under consideration. We will not need the explicit form of such counterterms here, although their construction is straight forward, see e.g. [43, 126].

Without loss of generality, we set the longitudinal part of the self-energy $\mathring{\Pi}_L^{\mathrm{PGB}}(s) = 0$, which due to the pole situation at $s = 0$ leads to $\mathring{\Pi}_T^{\mathrm{PGB}}(0) = 0$. In principle, the longitudinal components that would appear in our calculation are only due to the parametrization we chose for the vector fields and can be removed by a field redefinition that only affects the spin zero component of the vector fields (for a

discussion see e.g. [42], eq. (3.9) and comments on said equation). This leads us directly to the conditions

$$\mathring{c}_0 = 0 \quad \text{and} \quad \mathring{\Pi}^{\mathrm{PGB}}_{T,\mathrm{loop}}(s) \xrightarrow{s\to 0} 0, \tag{4.6}$$

which means that the bare mass $M_{V,b}$ is not renormalized by the loop graphs we evaluate. Let us define two parameters $\mathring{M}_V$ and $\mathring{\Gamma}_V$ to write the pole position of the propagator in the chiral limit,

$$\mathring{s}_{\mathrm{pole}} = \mathring{M}_V^2 - i\mathring{M}_V\mathring{\Gamma}_V, \tag{4.7}$$

so that we have

$$\mathring{s}_{\mathrm{pole}} - M_{V,b}^2 - \left[\mathring{\Pi}^{\mathrm{PGB}}_{T,\mathrm{loop}}(\mathring{s}_{\mathrm{pole}}) + \sum_{n=1}^{N} \mathring{c}_n \mathring{s}^n_{\mathrm{loop}}\right] = 0. \tag{4.8}$$

We treat the corrections that appear in the brackets to one-loop accuracy while simultaneously assuming that the parameter $\mathring{\Gamma}_V$ is sufficiently small compared to $\mathring{M}_V$, i.e. $\mathring{\Gamma}_V \ll \mathring{M}_V$, so that terms of quadratic order in the imaginary part of the pole position can be neglected. For the vector field propagators appearing in loop calculations, we take the free propagators with the pole position shifted to $\mathring{s}_{\mathrm{loop}}$ so that we can immediately relate the imaginary part of the loop integrals occurring in $\mathring{\Pi}^{\mathrm{PGB}}_T(\mathring{M}_V)$, i.e.

$$\mathring{M}_V\mathring{\Gamma}_V = -\operatorname{Im}\left[\mathring{\Pi}^{\mathrm{PGB}}_{T,\mathrm{loop}}(\mathring{s}_{\mathrm{pole}})\right] - \operatorname{Im}\left[\sum_{n=1}^{N} \mathring{c}_n \mathring{s}^n_{\mathrm{pole}}\right] \approx -\operatorname{Im}\left[\mathring{\Pi}^{\mathrm{PGB}}_{T,\mathrm{loop}}(\mathring{M}_V^2)\right]. \tag{4.9}$$

Since the difference between $\mathring{M}_V^2$, $M_{V,b}^2$ and the width $\mathring{\Gamma}_V$ formally amounts to a two-loop effect when we insert it in the loop corrections, we can eliminate the unobservable parameter $M_{V,b}^2$ to one-loop accuracy:

$$\begin{aligned} M_{V,b}^2 &= \mathring{M}_V^2 - \operatorname{Re}\left[\mathring{\Pi}^{\mathrm{PGB}}_{T,\mathrm{loop}}(\mathring{s}_{\mathrm{pole}})\right] - \operatorname{Re}\left[\sum_{n=1}^{N} \mathring{c}_n \mathring{s}^n_{\mathrm{pole}}\right] \\ &\equiv \mathring{M}_V^2 - \operatorname{Re}\left[\mathring{\Pi}^{\mathrm{PGB}}_{T,\mathrm{loop}}(\mathring{s}_{\mathrm{pole}})\right] - \operatorname{Re}\left[\sum_{n=0}^{N} \mathring{d}_n (\mathring{s}_{\mathrm{pole}} - \mathring{M}_V^2)^n\right] \\ &\approx \mathring{M}_V^2 - \operatorname{Re}\left[\mathring{\Pi}^{\mathrm{PGB}}_{T,\mathrm{loop}}(\mathring{s}_{\mathrm{pole}})\right] - \mathring{d}_0, \end{aligned} \tag{4.10}$$

where we have used the approximations that were mentioned above. We make strong use of the applicability of perturbation theory, not however of the convergence of the low-energy expansion in s. Since we are interested in the resonance region itself, it is

reasonable to reorder the series of the counterterms c_n in the following way:

$$\sum_{n=0}^{N} c_n s^n = \sum_{n=0}^{N} d_n (s - \mathring{M}_V^2)^n, \qquad \sum_{n=0}^{N} (-1)^n \mathring{d}_n \mathring{M}_V^{2n} = 0. \tag{4.11}$$

We can now expand the denominator of eq. (4.5) around $\mathring{s}_{\text{pole}}$ and if we employ eqs. (4.9), (4.10) and negelct all terms proportional to $\mathcal{O}((s - \mathring{s}_{\text{pole}})^2)$, we find the following expansion:

$$\begin{aligned} s - M_{V,b}^2 - \mathring{\Pi}_T^{\text{PGB}}(s) \approx \mathring{s}_{\text{pole}} &+ (s - \mathring{s}_{\text{pole}}) \Bigg(1 - \frac{d}{ds} \mathring{\Pi}_{T,\text{loop}}^{\text{PGB}} \Big|_{s=\mathring{s}_{\text{pole}}} \\ &- \sum_{n=1}^{N} n \mathring{d}_n (\mathring{s}_{\text{pole}} - \mathring{M}_V^2)^{n-1} \Bigg) \\ &- \Bigg(\mathring{M}_V^2 + \mathring{\Pi}_{T,\text{loop}}^{\text{PGB}}(\mathring{s}_{\text{pole}}) - \text{Re}\, \mathring{\Pi}_{T,\text{loop}}^{\text{PGB}}(\mathring{s}_{\text{pole}}) \\ &+ i \text{Im} \sum_{n=1}^{N} \mathring{d}_n (\mathring{s}_{\text{pole}} - \mathring{M}_V^2)^n \Bigg) \\ \approx (s - \mathring{s}_{\text{pole}}) &\left(1 - \frac{d}{ds} \mathring{\Pi}_{T,\text{loop}}^{\text{PGB}} \Big|_{s=\mathring{s}_{\text{pole}}} - \mathring{d}_1 + 2i \mathring{d}_2 \mathring{M}_V \mathring{\Gamma}_V \right) \\ &+ \mathring{s}_{\text{pole}} - \left(\mathring{M}_V^2 - i \mathring{M}_V \mathring{\Gamma}_V \right). \end{aligned} \tag{4.12}$$

We also find that in the vicinity of the pole, the transversal part of the propagator takes the form

$$\left(\mathring{\mathbf{D}}^{-1} \right)_{\mu\nu}^{T} (k) = \frac{(-i) \mathring{R} \left(g_{\mu\nu} - \frac{k_\mu k_\nu}{s} \right)}{s - \mathring{s}_{\text{pole}}}, \tag{4.13}$$

where the residue $\mathring{R}$ is easily to be read off from eq. (4.12). As a renormalization condition we require that $\text{Re}\, \mathring{R} = 1$, and we find that at one-loop order that amounts to a condition on $\mathring{d}_1$, i.e.

$$\mathring{d}_1 \equiv -\text{Re} \frac{d}{ds} \mathring{\Pi}_{T,\text{loop}}^{\text{PGB}} \Big|_{s=\mathring{s}_{\text{pole}}}. \tag{4.14}$$

So far we have only treated the chiral limit case, so let us now switch on the quark masses. After going through the same steps as above, we end up with the following result:

$$s - M_{V,b}^2 - \Pi_T^{\text{PGB}}(s) = s - \mathring{M}_V^2 - \bar{\Pi}_{T,\text{loop}}^{\text{PGB}}(s) - e_0 + D_N - \sum_{n=1}^{N} d_n (s - \mathring{M}_V^2)^n, \tag{4.15}$$

$$\bar{\Pi}_{T,\text{loop}}^{\text{PGB}}(s) = \Pi_{T,\text{loop}}^{\text{PGB}}(s) - \text{Re}\, \mathring{\Pi}_{T,\text{loop}}^{\text{PGB}}(\mathring{s}_{\text{pole}}), \tag{4.16}$$

$$D_N = \mathrm{Re}\sum_{n=1}^{N} \mathring{d}_n(\mathring{s}_{\mathrm{pole}} - \mathring{M}_V^2)^n = \mathrm{Re}\sum_{n=2}^{N} \mathring{d}_n(-i\mathring{M}_V\mathring{\Gamma}_V)^n, \tag{4.17}$$

$$e_n = d_n - \mathring{d}_n. \tag{4.18}$$

All the contributions from quark-mass dependent counterterms we have collected in the e_n terms. It is important to note that the parameter $M_{V,b}$ here is the same parameter used in eq. (4.8) since we treat the quark-mass corrections to the bare mass as another perturbation in addition to the PGB loops; at leading order in the expansion around $s = \mathring{M}_V^2$ these are given by e_0. Furthermore, when investigating the constant D_N defined in eq. (4.17) we find that it is of two-loop order, which lies beyond the scope of this work. It is hence neglected from now on.
Let us take a closer look on the pole position s_{pole} of the propagator for non-vanishing quark masses: we find that the relevant non-analytic terms from loop graphs start at $\mathcal{O}(m_q^{3/2}) \sim \mathcal{O}(M_{\mathrm{PGB}}^3)$, whereas the corrections from the mass-dependent counterterms yield even powers of M_{PGB}. Schematically, this results in the following expansions:

$$s_{\mathrm{pole}} = \mathring{s}_{\mathrm{pole}} + x_2 M_{\mathrm{PGB}}^2 + x_3 M_{\mathrm{PGB}}^3 + \mathcal{O}(M_{\mathrm{PGB}}^4 \log M_{\mathrm{PGB}}, M_{\mathrm{PGB}}^4), \tag{4.19}$$

$$e_n = e_n^{(2)} M_{\mathrm{PGB}}^2 + \mathcal{O}(M_{\mathrm{PGB}}^4). \tag{4.20}$$

We can again investigate the expansion in terms of $(s_{\mathrm{pole}} - \mathring{s}_{\mathrm{pole}})$, which leads to

$$\begin{aligned}
0 &= s_{\mathrm{pole}} - \left(\mathring{M}_V^2 + \bar{\Pi}_{T,\mathrm{loop}}^{\mathrm{PGB}}(s_{\mathrm{pole}}) + e_0 + \sum_{n=1}^{N} d_n(s_{\mathrm{pole}} - \mathring{M}_V^2)^n - D_N\right) \\
&= (s_{\mathrm{pole}} - \mathring{s}_{\mathrm{pole}}) - i\mathring{M}_V\mathring{\Gamma}_V - \mathrm{Re}\,\bar{\Pi}_{T,\mathrm{loop}}^{\mathrm{PGB}}(\mathring{s}_{\mathrm{pole}}) - \mathrm{Re}\sum_{n=0}^{N} e_n(\mathring{s}_{\mathrm{pole}} - \mathring{M}_V^2)^n \\
&\quad - i\left(\mathrm{Im}\,\Pi_{T,\mathrm{loop}}^{\mathrm{PGB}}(\mathring{s}_{\mathrm{pole}}) + \mathrm{Im}\sum_{n=1}^{N} d_n(\mathring{s}_{\mathrm{pole}} - \mathring{M}_V^2)^n\right) \\
&\quad - (s_{\mathrm{pole}} - \mathring{s}_{\mathrm{pole}})\left(\frac{d}{ds}\,\Pi_{T,\mathrm{loop}}^{\mathrm{PGB}}\Big|_{s=\mathring{s}_{\mathrm{pole}}} + \sum_{n=1}^{N} n d_n(\mathring{s}_{\mathrm{pole}} - \mathring{M}_V^2)^{n-1}\right) \\
&\quad + \mathcal{O}((s_{\mathrm{pole}} - \mathring{s}_{\mathrm{pole}})^2) \\
&\approx (s_{\mathrm{pole}} - \mathring{s}_{\mathrm{pole}})\left(1 - \frac{d}{ds}\,\Pi_{T,\mathrm{loop}}^{\mathrm{PGB}}\Big|_{s=\mathring{s}_{\mathrm{pole}}} - d_1 + 2id_2\mathring{M}_V\mathring{\Gamma}_V\right) \\
&\quad - \mathrm{Re}\,\bar{\Pi}_{T,\mathrm{loop}}^{\mathrm{PGB}}(\mathring{s}_{\mathrm{pole}}) - e_0 - i\,\mathrm{Im}\left(\Pi_{T,\mathrm{loop}}^{\mathrm{PGB}}(\mathring{M}_V^2) - \mathring{\Pi}_{T,\mathrm{loop}}^{\mathrm{PGB}}(\mathring{M}_V^2)\right).
\end{aligned} \tag{4.21}$$

We can now also employ the conditions eqs. (4.14), (4.19) and (4.20) to end up with the following result:

$$\begin{aligned}
s_{\mathrm{pole}} - \mathring{s}_{\mathrm{pole}} = \mathrm{Re}\,\bar{\Pi}_{T,\mathrm{loop}}^{\mathrm{PGB}}(\mathring{s}_{\mathrm{pole}}) + e_0^{(2)} M_{\mathrm{PGB}}^2 \\
+ i\,\mathrm{Im}\left(\Pi_{T,\mathrm{loop}}^{\mathrm{PGB}}(\mathring{M}_V^2) - \mathring{\Pi}_{T,\mathrm{loop}}^{\mathrm{PGB}}(\mathring{M}_V^2)\right) + \mathcal{O}(\hbar^2) \\
+ \mathcal{O}\left(M_{\mathrm{PGB}}^4 \log M_{\mathrm{PGB}}, M_{\mathrm{PGB}}^4\right).
\end{aligned} \tag{4.22}$$

Here, we have indicated that we have neglected all two-loop contributions, denoted by $\mathcal{O}(\hbar^2)$. Furthermore we can fix the coefficient $e_1^{(2)}$ via the condition that $\mathrm{Re}\, R = 1 + \mathcal{O}(M_{\mathrm{PGB}}^4)$. We can fix e_0 and d_1 up to and including $\mathcal{O}(M_{\mathrm{PGB}})$ from the quark-mass dependence of the vector meson masses and again the renormalization condition mentioned above. We are not aware of a natural or model-independent way to determine the coefficients $\mathring{d}_{n\geq 2}$. In general, the off-shell behavior of an amplitude like $\Pi_T(s)$ will depend on the chosen field parametrization, e.g. [127].
So far we have investigated an expansion around the chiral limit where the quark masses and thus all pseudo-Goldstone boson masses are zero. This expansion is a problematic one, since in our physical world, as mentioned before, the PGB masses are not small compared to the reference scales, in this case the vector meson masses. One finds that $M_K M_{K^*}^{-1} \approx 0.6$ and $M_\eta M_\omega^{-1} \approx 0.7$ due to the large strange quark masses. It is because of that reasoning that we can conclude that the extrapolation from the chiral limit to the physical point is most likely not under sufficient theoretical control, see ch. 3 for a discussion of that problem. Another problem is due to the fact that vector mesons can decay. Thus, the closer we get to the chiral limit, the more important it gets to account for the possibility of the decay into three, four, etc. nearly massless PGBs. Thus, a one-loop calculation is certainly not sufficient to calculate the self-energy near the chiral limit reliably. Finally, we have neglected the effects that are $\mathcal{O}(\mathring{\Gamma}_V^2 \mathring{M}_V^{-2})$, although in some of the intermediate steps of our reasoning they need not be tiny.
As already described in ch. 3, we again want to extrapolate the lattice data presented in [75] and we adapt our extrapolation to their simulation concept. Since this time we only attempt a leading one-loop calculation, we have to modify eq. (3.11) by neglecting all terms of $\mathcal{O}(p^4)$, i.e. we find

$$M_{\mathrm{PGB}}^2(\delta m_\ell = 0) = M_\star^2 = 2B_0 \bar{m} + \mathcal{O}(\bar{m}^2 \log \bar{m}) \approx (412\,\mathrm{MeV})^2, \tag{4.23}$$

for $\bar{m} = \bar{m}^{\mathrm{phys}}$. The value for the octet vector meson mass at the symmetric point is derived from [75] to be $M_V^\star = 855\,\mathrm{MeV}$, which means that at and in the vicinity of the symmetric point the vector mesons are almost stable particles. It is certainly not a disadvantage to choose the symmetric point as a reference point for our calculations and extrapolations. We will only use eqs. (4.15) and (4.22) to analyze the running of $(s_{\mathrm{pole}}^\star - \mathring{s}_{\mathrm{pole}})$ with varying $\bar{m}$. For analyzing the symmetry-breaking effects, we will make use of the symmetric point as a reference point.
To see the mechanism at work, let us return to eq. (4.15) and employ the first line of eq. (4.21) to write

$$s_{\mathrm{pole}}^\star = \mathring{M}_V^2 + \bar{\Pi}_{T,\mathrm{loop}}^{\mathrm{PGB}\star}(s_{\mathrm{pole}}^\star) + e_0^\star + \sum_{n=1}^{N} d_n^\star (s_{\mathrm{pole}}^\star - \mathring{M}_V^2)^n - D_N, \tag{4.24}$$

and following the lines presented above, we find that

$$\begin{aligned} s - M_{V,b}^2 - \Pi_T^{\mathrm{PGB}}(s) = s - s_{\mathrm{pole}}^\star - \left(\Pi_{T,\mathrm{loop}}^{\mathrm{PGB}}(s) - \Pi_{T,\mathrm{loop}}^{\mathrm{PGB}\star}(s_{\mathrm{pole}}^\star) + e_0 - e_0^\star\right) \\ - \left(\sum_{n=1}^{N} \delta d_n (s_{\mathrm{pole}}^\star - \mathring{M}_V^2)^n + \sum_{n=1}^{N} f_n (s - s_{\mathrm{pole}}^\star)^n\right), \end{aligned} \tag{4.25}$$

$$\delta d_n = d_n - d_n^\star, \tag{4.26}$$

$$f_n = \sum_{m=n}^{N} d_m \binom{m}{n} (s_{\mathrm{pole}}^\star - \mathring{M}_V^2)^{m-n}. \tag{4.27}$$

As argued before, at the symmetric point the width is tiny and hence, we can neglect it, setting $\mathrm{Im}\, s_{\mathrm{pole}}^\star = 0$ and $\mathrm{Re}\, s_{\mathrm{pole}}^\star = (M_V^\star)^2$. Furthermore we can absorb the terms proportional to δd_n, which are of order $\mathcal{O}(\delta m_\ell)$, in the term $e_0 - e_0^\star$. They constitute $\bar{m}$ corrections to the symmetry-breaking behavior due to $s_{\mathrm{pole}}^\star - \mathring{M}_V^2 = \mathcal{O}(\bar{m})$. Symbolically, we write

$$\delta e = e_0 - e_0^\star + \sum_{n=1}^{N} \delta d_n (s_{\mathrm{pole}}^\star - \mathring{M}_V^2)^n = \mathcal{O}(\delta m_\ell). \tag{4.28}$$

Hence we can write the denominator of the vector meson propagator in its final form

$$\begin{aligned} s - M_{V,b}^2 - \Pi_T^{\mathrm{PGB}}(s) = s - s_{\mathrm{pole}}^\star - \Bigg(\delta e + \Pi_{T,\mathrm{loop}}^{\mathrm{PGB}}(s) - \Pi_{T,\mathrm{loop}}^{\mathrm{PGB}\star}(s_{\mathrm{pole}}^\star) \\ + \sum_{n=1}^{N} f_n (s - s_{\mathrm{pole}}^\star)^n\Bigg). \end{aligned} \tag{4.29}$$

Since we will set $s_{\mathrm{pole}}^\star = (M_V^\star)^2$ to the value quoted in [75], we have effectively eliminated every reference to the chiral limit mass $\mathring{M}_V$ from eq. (4.29). For a fixed value of $\bar{m}$ we take the propagators appearing in the loop integrals as free propagators with a pole position shifted to $M_V^\star$. We have reordered the original counterterms in such a way that the energy dependence of the self-energy is expanded around $M_V^\star$ instead of $\mathring{M}_V$. Anologously, one expands around $M_S^\star$ in the singlet case. We again require, in analogy to eq. (4.14), that the real part of the residue at the pole position is equal to one, thus fixing the parameter f_1 order by order in δm_ℓ.
In the last part of this section, let us shortly discuss the singlet-octet mixing in the general case that $m_\ell \neq m_s$. We find that the neutral octet isosinglet field not only mixes with MM, VM and SM states, but also with one-particle singlet states. Hence, the one particle propagator in the $\phi^{(0)} - \phi^{(8)}$ sector is non-diagonal [128] and we

have to invert the corresponding matrix, which yields

$$\begin{aligned}\mathbf{D}_{\text{mix}}^{-1} &= i\begin{pmatrix} s - M_S^{\star 2} - \delta\Pi_{00} & -\Pi_{08} \\ -\Pi_{80} & s - M_V^{\star 2} - \delta\Pi_{88} \end{pmatrix}^{-1} \\ &= \frac{i}{\det_{08}}\begin{pmatrix} s - M_V^{\star 2} - \delta\Pi_{88} & \Pi_{08} \\ \Pi_{80} & s - M_S^{\star 2} - \delta\Pi_{00} \end{pmatrix},\end{aligned} \tag{4.30}$$

where we again only consider the transversal part of the self-energies and the expressions have been expanded about the symmetric point. We have introduced the expressions $\delta\Pi_{00/88}$, which stand for $\Pi_{00/88}(s) - \Pi_{00/88}(s^\star_{V/S,\text{pole}})$. Again, we have neglected the tiny widths at the symmetric point. We also write Π_{00} instead of $\Pi_{\phi^{(0)}}$ for better legibility, as we also do for its isoscalar octet counterpart.
Since we are looking for the mass eigenvalues of this sector, we determine the (complex) zeroes of the determinant $\det_{08}$, see ref. [129]. We find that

$$\det_{08} = (s - M_V^{\star 2} - \delta\Pi_{88})(s - M_S^{\star 2} - \delta\Pi_{00}) - \Pi_{08}\Pi_{80}. \tag{4.31}$$

For energy-independent self-energies, this is a simple quadratic equation in s and the two roots are identified with the masses of the $\phi(1020)$ and the $\omega(782)$. This treatment leads to the expressions for masses and the mixing angle Θ_V presented in e.g. [46].

4.2 Extrapolation fomulae

To derive the extrapolation formulae, additionally to the effective Lagrangians of eqs. (1.77), (1.78) we need the chiral Lagrangian that contains the leading quark-mass insertions for the self-energies, see also [46–48, 130]:

$$\mathscr{L}_{V,\chi} = b_0^V \langle V_\mu V^\mu\rangle\langle\chi_+\rangle + b_D^V\langle V_\mu\{\chi_+, V^\mu\}\rangle + b_0^{VS} S_\mu S^\mu\langle\chi_+\rangle + b_{08} S_\mu\langle V^\mu\chi_+\rangle. \tag{4.32}$$

We find that these $\mathcal{O}(p^2)$ mass insertions include the singlet-octet mixing terms and yield the following energy-independent contributions to the self-energies:

$$\Pi_{\rho,\text{ct}} = 8B_0\left(b_0^V(2m_\ell + m_s) + 2b_D^V m_\ell\right), \tag{4.33}$$

$$\Pi_{K^*,\text{ct}} = 8B_0\left(b_0^V(2m_\ell + m_s) + b_D^V(m_\ell + m_s)\right), \tag{4.34}$$

$$\Pi_{\phi^{(8)},\text{ct}} = 8B_0\left(b_0^V(2m_\ell + m_s) + \frac{2}{3}b_D^V(m_\ell + 2m_s)\right), \tag{4.35}$$

$$\Pi_{\phi^{(0)},\text{ct}} = 8B_0 b_0^{VS}\left(2m_\ell + m_s\right), \tag{4.36}$$

$$\Pi_{08,\text{ct}} = 4B_0 b_{08}\sqrt{\frac{2}{3}}(m_\ell - m_s) = \Pi_{80,\text{ct}}. \tag{4.37}$$

One can easily see that the singlet-octet mixing term disappears at the $SU(3)_f$

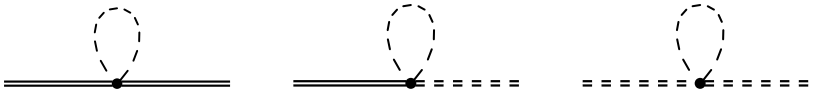

Figure 4.2: The three tadpole graphs we have included in our calculation. The double solid line represents an octet vector meson while the double dashed line stands for the singlet vector meson. The dashed line represents any of our pseudo-Goldstone bosons π, K, η.

symmetric point where $m_\ell = m_s$. From eq. (4.32), we can also derive the contributions from the tadpole graphs presented in fig. 4.2, which again contain an octet-singlet mixing contribution proportional to the LEC b_{08}:

$$\begin{aligned}\Pi_{\rho,\mathrm{tad}} = &-\frac{4B_0 b_0^V}{F_0^2}\left(6m_\ell I_\pi + 4(m_\ell+m_s)I_K + \frac{2}{3}(m_\ell+2m_s)I_\eta\right)\\ &-\frac{4B_0 b_D^V}{F_0^2}\left(6m_\ell I_\pi + 2(m_\ell+m_s)I_K + \frac{2}{3}m_\ell I_\eta\right),\end{aligned} \tag{4.38}$$

$$\begin{aligned}\Pi_{K^\star,\mathrm{tad}} = &-\frac{4B_0 b_0^V}{F_0^2}\left(6m_\ell I_\pi + 4(m_\ell+m_s)I_K + \frac{2}{3}(m_\ell+2m_s)I_\eta\right)\\ &-\frac{4B_0 b_D^V}{F_0^2}\left(3m_\ell I_\pi + 3(m_\ell+m_s)I_K + \frac{1}{3}(m_\ell+4m_s)I_\eta\right),\end{aligned} \tag{4.39}$$

$$\begin{aligned}\Pi_{\phi^{(8)},\mathrm{tad}} = &-\frac{4B_0 b_0^V}{F_0^2}\left(6m_\ell I_\pi + 4(m_\ell+m_s)I_K + \frac{2}{3}(m_\ell+2m_s)I_\eta\right)\\ &-\frac{4B_0 b_D^V}{F_0^2}\left(2m_\ell I_\pi + \frac{10}{3}(m_\ell+m_s)I_K + \frac{2}{9}(m_\ell+8m_s)I_\eta\right),\end{aligned} \tag{4.40}$$

$$\Pi_{\phi^{(0)},\mathrm{tad}} = -\frac{4B_0 b_0^{VS}}{F_0^2}\left(6m_\ell I_\pi + 4(m_\ell+m_s)I_K + \frac{2}{3}(m_\ell+2m_s)I_\eta\right), \tag{4.41}$$

$$\Pi_{08,\mathrm{tad}} = -\frac{B_0 b_{08}}{F_0^2}\sqrt{\frac{2}{3}}\left(6m_\ell I_\pi - 2(m_\ell+m_s)I_K + \frac{2}{3}(m_\ell-4m_s)I_\eta\right), \tag{4.42}$$

where we have defined the appearing loop functions I_M in eq. (A.1). Furthermore we find that $\Pi_{08,\mathrm{tad}} = \Pi_{80,\mathrm{tad}}$ and that this contribution to singlet-octet mixing also vanishes in the $SU(3)_f$ limit as expected. There are several other possible terms that generate tadpole contributions, see e.g. [47]. In said publication the authors use large N_c arguments to constrain the corresponding LECs. Strictly speaking our formulae are only complete at leading one-loop order $\mathcal{O}(p^3)$, but we take the tadpole graphs into account to estimate higher-order effects. We show all leading one-loop order contributions to the vector meson self-energies in fig. 4.3.
The first graph we want to investigate is the bubble-type graph fig. 4.3(a), which exclusively occurs for the octet vector mesons and which follows directly from the first term of the Lagrangian eq. (1.78). This graph is particularly interesting since it has been missed in the so-called 'heavy vector meson' approach from [47], while the contribution due to the intermediate two-PGB states is absent in quenched QCD

[131]. We find that calculating this diagram results in contributions to the masses as well as to the widths. Thus we find the results for the respective octet vector mesons:

$$\Pi_{\rho,\text{bubble}}(s) = -\frac{g_V^2 s^2}{F_0^4}\left(4I_A^{\pi\pi}(s) + 2I_A^{\bar{K}K}(s)\right), \tag{4.43}$$

$$\Pi_{K^\star,\text{bubble}}(s) = -\frac{g_V^2 s^2}{F_0^4}\left(3I_A^{\pi K}(s) + 3I_A^{K\eta}(s)\right), \tag{4.44}$$

$$\Pi_{\phi^{(8)},\text{bubble}}(s) = -\frac{g_V^2 s^2}{F_0^4} 6 I_A^{\bar{K}K}(s). \tag{4.45}$$

We also present the explicit mass corrections that arise from the sunset diagrams figs. 4.3(b)-4.3(d), they take the form

$$\Pi_{\rho,\text{sun}}(s) = -\frac{4(g_A^V)^2 s}{F_0^2}\left(\frac{2}{3}I_A^{\pi V}(s) + 2I_A^{KV}(s) + \frac{2}{3}I_A^{\eta V}(s)\right) - \frac{4(g_A^{VS})^2 s}{F_0^2} I_A^{\pi S}(s), \tag{4.46}$$

$$\Pi_{K^\star,\text{sun}}(s) = -\frac{4(g_A^V)^2 s}{F_0^2}\left(\frac{3}{2}I_A^{\pi V}(s) + \frac{5}{3}I_A^{KV}(s) + \frac{1}{6}I_A^{\eta V}(s)\right) - \frac{4(g_A^{VS})^2 s}{F_0^2} I_A^{KS}(s), \tag{4.47}$$

$$\Pi_{\phi^{(8)},\text{sun}}(s) = -\frac{4(g_A^V)^2 s}{F_0^2}\left(2I_A^{\pi V}(s) + \frac{2}{3}I_A^{KV}(s) + \frac{2}{3}I_A^{\eta V}(s)\right) - \frac{4(g_A^{VS})^2 s}{F_0^2} I_A^{\eta S}(s), \tag{4.48}$$

$$\Pi_{\phi^{(0)},\text{sun}}(s) = -\frac{4(g_A^{VS})^2 s}{F_0^2}\left(3I_A^{\pi V}(s) + 4I_A^{KV}(s) + I_A^{\eta V}(s)\right), \tag{4.49}$$

while the last graph of fig. 4.3 contributes to singlet-octet mixing. The calculation yields

$$\Pi_{08,\text{sun}}(s) = -\frac{4 g_A^V g_A^{VS}}{F_0^2} s\left(\sqrt{6}I_A^{\pi V}(s) - 2\sqrt{\frac{2}{3}}I_A^{KV}(s) - \sqrt{\frac{2}{3}}I_A^{\eta V}(s)\right). \tag{4.50}$$

The above expressions are inserted into eqs. (4.29) and (4.30), where we also employ $s^\star_{V,\text{pole}} = (M_V^\star)^2 = (885\,\text{MeV})^2$ [75] and furthermore $s^\star_{S,\text{pole}} = (M_S^\star)^2$, where the singlet vector meson mass in the chiral limit $M_S^\star$ is an unknown parameter that can be determined from fitting the extrapolation formulae to lattice data. The complex zeroes of eq. (4.29) give the mass and decay width of the corresponding vector meson, i.e. $s_{V,\text{pole}} = M_V^2 - iM_V\Gamma_V$, where V stands for any of the vector mesons under consideration here.

Now that we have presented all these expressions for the loop contributions to the self energy, we have to discuss power counting and regularization of the loop integrals appearing in these expressions. We evaluate all integrals using dimensional regularization and the $\overline{\text{MS}}$ renormalization scheme to take care of the ultraviolet divergencies. We have absorbed a constant part of our loop integrals into $(M_V^\star)^2$ by

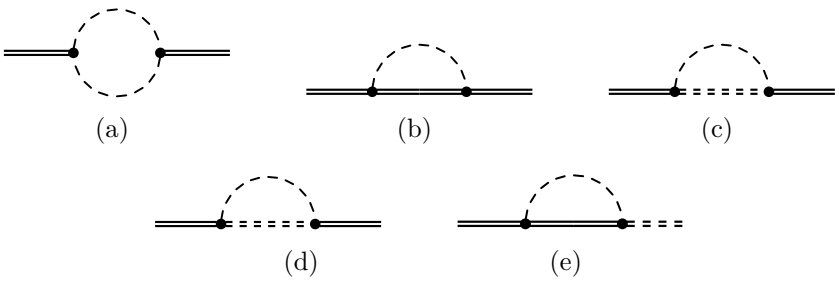

Figure 4.3: The other loop diagrams we include in our calculation. The double solid line represents the octet vector mesons and the double dashed line represents the singlet vector meson. The dashed line stands for any of the pseudo-Goldstone bosons π, K or η.

subtracting $\Pi^\star_{T,\mathrm{loop}}(s^\star_{\mathrm{pole}})$. We also use renormalization conditions as, e.g., $\mathrm{Re}\, R \equiv 1$, hence our renormalized loop contributions start formally at second chiral order, i.e. with terms proportional to $(s-(M_V^\star)^2)^2$ and δm_ℓ. The power-counting for the loop graphs is not straightforward, as has been mentioned in sec. 1.5 and was discussed in detail in [50, 52]. Now and then, we resort to dispersion-theoretic arguments, since in that language, all loop integrals are, in principle, up to a polynomial in s, determined by their branch cuts and threshold singularities. We give an example for the dispersive approach in app. D.2. In [129, 131, 132] the authors have used dispersive techiques to treat the $\pi\pi$ loop.
We also present the counterterms f_1 ocurring in eq. (4.29) up to linear terms in the symmetry breaking variable δm_ℓ, neglecting counterterms of $\mathcal{O}((s-s^\star_{\mathrm{pole}})^2)$ and $\mathcal{O}((s-s^\star_{\mathrm{pole}})\delta m_\ell^2)$:

$$f_1^\rho = f_1^{V\star} - 8B_0 z_D^V \delta m_\ell + \mathcal{O}((\delta m_\ell)^2), \tag{4.51}$$
$$f_1^{K^\star} = f_1^{V\star} + 4B_0 z_D^V \delta m_\ell + \mathcal{O}((\delta m_\ell)^2), \tag{4.52}$$
$$f_1^{\phi^{(8)}} = f_1^{V\star} + 8B_0 z_D^V \delta m_\ell + \mathcal{O}((\delta m_\ell)^2), \tag{4.53}$$
$$f_1^{\phi^{(0)}} = f_1^{S\star} + \mathcal{O}((\delta m_\ell)^2), \tag{4.54}$$
$$f_1^{08} = 0 - 2\sqrt{6}B_0 z_{08}\delta m_\ell + \mathcal{O}((\delta m_\ell)^2). \tag{4.55}$$

Neglecting the energy-dependent terms sets limits on the accuracy in determining the energy-dependence of the self-energies in the resonance region. The above terms can of course be derived from effective Lagrangians, e.g. in the case of the mixing renormalization parameter z_{08}, we find that

$$\mathscr{L}_{\mathrm{mix}} = b'_{08} S_\mu \langle V^\mu \chi_+\rangle - \frac{z_{08}}{4} S_{\mu\nu}\langle V^{\mu\nu}\chi_+\rangle + \dots . \tag{4.56}$$

We can now redefine the coupling constant for a fixed value for $M_V^\star$ as $b'_{08} = b_{08} + z_{08}(M_V^\star)^2$. All the terms that have been omitted from eq. (4.56) would call for more complicated redefinitions eventually involving higher powers of $s-(M_V^\star)^2$.

Analogously, we can derive the z_{DV} counterterm from a Lagrangian of the form

$$\mathscr{L}_{V,\text{counter}} = -\frac{z_{DV}}{4} \langle V_{\mu\nu} \{\chi_+, V^{\mu\nu}\} \rangle + \ldots, \tag{4.57}$$

and so on. In contrary to $f_1^{V,S\star}$ and z_{DV}, which are fixed from the renormalization condition $\mathrm{Re}\, R \equiv 1$, there is no natural way to fix z_{08}. Hence, for now we treat it as a free parameter as to arrive at an unbiased description of the singlet-octet mixing amplitude.

4.3 Fit results and discussion

Since we choose the $SU(3)_f$ symmetric point instead of the chiral limit as the reference point for our analysis, it is reasonable to replace $F_0 \to F_\star$ in the loop contributions to the self-energies, which, as mentioned in ch. 3, amounts to a two-loop effect. The expression for $F_\star$ is presented in eq. (3.19). As a numerical input for analyzing the fanplots and mixing-determinant, we again use $F_\star \approx 112\,\mathrm{MeV}$. When we determine the running of $M_V^\star(\bar{m})$, we use the whole formula eq. (3.19) and again use the MILC2010 set, presented in tab. 3.1, as input. We set the renormalization scale to $\mu = 770\,\mathrm{MeV}$. The parameter g_V appearing as the coefficient of the bubble-type loop graphs we can fix from looking at the ρ decay width $\Gamma[\rho \to \pi\pi]$, which is given by

$$\Gamma[\rho \to \pi\pi] = \frac{g_V^2 M_\rho^2}{48\pi F_\star^4} \left[M_\rho^2 - 4M_\pi^2\right]^{3/2}. \tag{4.58}$$

We obtain the value for g_V by requiring that at the physical point, $\Gamma[\rho \to \pi\pi] \approx 150\,\mathrm{MeV}$, which leads to a g_V value of about 0.125. In order to test the stability of our fits and examine the influence of higher-order effects we use a second set of parameters, where we replace F_0 by the pion decay constant $F_\pi \approx 92.4\,\mathrm{MeV}$, which yields a g_V value of 0.085.

One of the biggest uncertainties in analyzing the data presented in [75] is the input values we choose for the axial type of couplings $g_A^{V/VS}$ that generate the sunset graphs. When we compare the interaction terms presented in eq. (1.77) with the heavy vector meson Lagrangian of [46] we find that $g_1 \equiv g_A^{VS}$ and $g_2 \equiv g_A^V$. Jenkins et al. seem to favor the predictions derived from the non-relativistic chiral quark model, i.e.

$$g_A^V \equiv g_2^{\chi qm} = \frac{3}{4}, \qquad g_A^{VS} \equiv g_1^{\chi qm} = \frac{\sqrt{3}}{2}. \tag{4.59}$$

In [47], the authors employ large N_c arguments to neglect the linear combination $g' \equiv g_A^{VS} - (2/\sqrt{3}) g_A^V$ which leads to a value for $g \equiv g_A^V/2 = 0.375$. In said reference, they quote several other estimates, some of which amount to smaller values, e.g. $g \equiv 0.3$. Combining this with the assumption that $g' \approx 0$, we obtain $g_A^V \approx 0.6$ and $g_A^{VS} \approx 0.7$. We will use several different sets for these axial-type couplings to

Table 4.1: The lattice data taken from [75], a collection of tabs. 20 and 29. We have used X_π to determine the lattice spacing a, see footnote 5 in the same reference.

$N_S^3 \times N_T$	ν	M_ρ/X_ρ	M_{K^*}/X_ρ
$24^3 \times 48$	0.181	1.25(2)	0.9877(12)
$24^3 \times 48$	0	1.0	1.0
$24^3 \times 48$	−0.128	0.9859(22)	1.007(1)
$24^3 \times 48$	−0.275	0.9706(34)	1.015(2)
$32^3 \times 64$	−0.404	0.9488(50)	1.026(3)
$32^3 \times 64$	−0.558	0.9392(63)	1.030(3)
$32^3 \times 64$	−0.692	0.9431(109)	1.028(5)
exp. value	−0.885	0.910(5)	1.046(5)

Table 4.2: $M_V^\star(M_\star)$ data taken from [75], tab. XIX. To obtain these values in units of MeV we have used their value for $a = 0.0771(3)$ fm quoted in footnote 5 in sec. 8.3.2 of [75].

$M_\star$ [MeV]	307	357	413
$M_V^\star(M_\star)$ [MeV]	808(17)	825(7)	855(4)

estimate the theoretical uncertainties involved. It is important to do so since the sunset graphs in most cases yield the dominant corrections to the tree-level result. As already presented in ch. 3, we analyze lattice data presented by the QCDSF collaboration in [75] and given in tabs. 4.1 and 4.2 for the convenience of the reader. The data from tab. 4.2 is used to determine the vector meson mass in the chiral limit $\mathring{M}_V$, which does not appear in any of the other observables, since we have effectively eliminated it, and b_0^V, which we have absorbed in $M_V^\star$ in the other observables, from the running of $M_V^\star(\bar{m})$. As can be seen in tab. 4.1, for this analysis we have added the mass ratios at the physical point. The singlet mass $M_S^\star$ appears both in the symmetric mass $M_V^\star$ and in the mass ratios used, but mostly it is determined from the condition that the singlet-octet mixing determinant, eq. (4.31), has zeroes at $s = M_{\omega,\phi}^2 - iM_{\omega,\phi}\Gamma_{\omega,\phi}$ (we use the numbers at the physical point quoted in [1] as input). We disregard the imaginary part, i.e. $\Gamma_{\omega,\phi} \approx 0$, since it is generated mostly by a two-loop effect where three pions occur in an intermediate state. The LEC b_{08} is determined solely from the zeroes of the determinant and has no direct influence on the masses of the ρ and K^*. If we wanted to determine the subleading z_{08} term,

Table 4.3: Fit results (type A) including tadpole contributions, where g_V, g_A^V and g_A^{VS} have been used as input.

fit	g_V	g_A^V	g_A^{VS}	$\mathring{M}_V$ [GeV]	b_0^V	b_D^V	$M_S^\star$ [GeV]	b_{08}	color
$1A$	0.125	3/4	$\sqrt{3}/2$	0.631	0.056	0.022	1.011	0.218	black
$2A$	0.125	0.6	0.7	0.627	0.054	0.019	1.000	0.237	orange
$3A$	0.125	1/2	1/2	0.625	0.053	0.017	0.988	0.249	blue
$4A$	0.125	0	0	0.618	0.051	0.015	0.979	0.266	red
$5A$	0.085	3/4	$\sqrt{3}/2$	0.693	0.031	0.065	0.958	0.231	black
$6A$	0.085	0.6	0.7	0.683	0.027	0.063	0.949	0.245	orange
$7A$	0.085	1/2	1/2	0.678	0.025	0.062	0.938	0.253	blue
$8A$	0.085	0	0	0.667	0.020	0.062	0.930	0.266	red

we would need detailed information about the energy dependence of the mixing amplitude. In the large N_c limit, the vector mesons form a nonet, which in the matrix notation takes the form $N_\mu = V_\mu + \sqrt{3}^{-1}\mathbb{1}S_\mu$, where additional flavor traces are suppressed, see e.g. [46–48, 130]. When we compare with these types of Lagrangians, we can find relations like

$$b_0^V \approx 0, \qquad b_{08} - \frac{4}{\sqrt{3}} b_D^V \approx 0, \qquad z_{08} - \frac{4}{\sqrt{3}} z_D^V \approx 0. \tag{4.60}$$

We will, in general, not rely on such estimates, but the last relation for z_{08} will be used in the fit set that is denoted with A, where we set $z_{08} \to 4\sqrt{3}^{-1} z_D^V$. In a second set, the fit set B, we simply set $z_{08} \equiv 0$, i.e. neglect this energy-dependent correction. Thus, in set B, the energy dependence of the mixing amplitude is entirely given by the loop graphs.
We have collected all the fit results for various different values of the input parameters $g_A^{V(S)}$ including tadpoles in tabs. 4.3 and 4.4 and without tadpoles in tabs. 4.5 and 4.6. We present the fan plots corresponding to these results in fig. 4.4 and the plot for the vector meson mass at the symmetric point is presented in fig. 4.5. Note that we have used the notation

$$X_\rho = \frac{1}{3}\left(2M_{K^*} + M_\rho\right), \tag{4.61}$$

as has been done in [75]. In the fan plots, one can barely distinguish the different colored lines around the symmetric point ($\delta m_\ell = 0$), which is expected from our expansion formulae, where the calculated corrections to $M_V^\star$ are of $\mathcal{O}(\delta m_\ell)$. It seems that the variation of the input parameters can almost completely be absorbed by shifting the fitted parameters as can be seen from tabs. 4.3-4.6. We can observe a

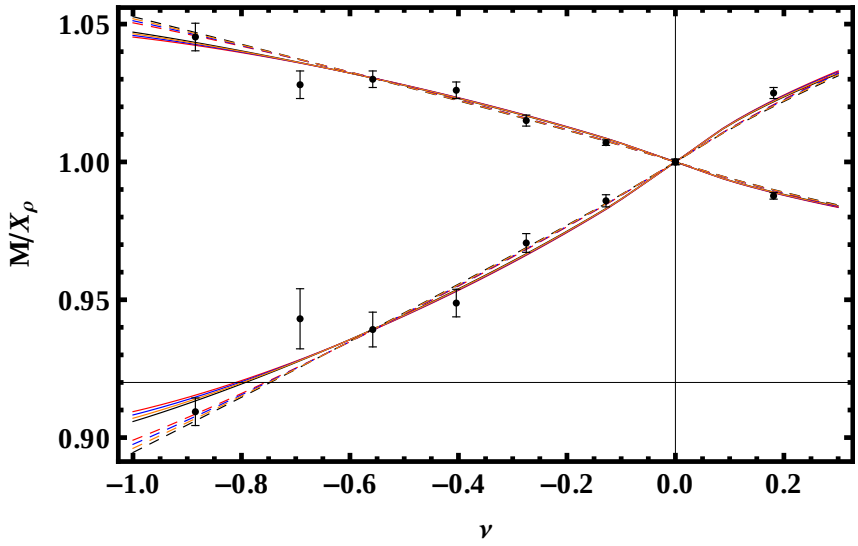

Figure 4.4: The ratios M_ρ/X_ρ and M_{K^*}/X_ρ plotted for all parameter sets from Tab. 4.3. The color code for the different curves is shown in tabs. 4.3-4.6. Full lines: 1A-4A, dashed lines: 5A-8A. X_ρ is defined in [75], see also eq. (4.61).

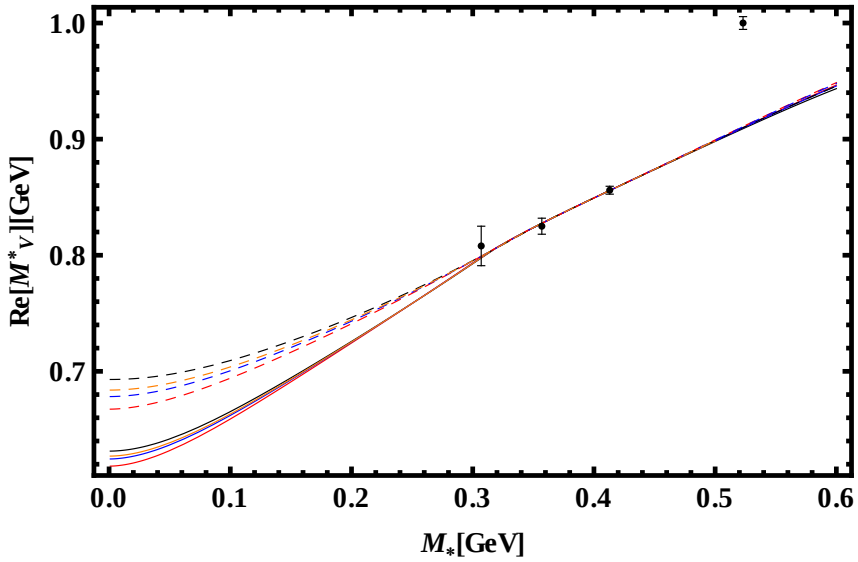

Figure 4.5: The symmetric mass $M_V^\star$ (octet vector meson mass for $\delta m_\ell = 0$) plotted for all parameter sets from Tab. 4.3. The color code for the different curves is shown in tabs. 4.3-4.6. Full lines: 1A-4A, dashed lines: 5A-8A.

Table 4.4: Fit results (type B) including tadpole contributions, where g_V, g_A^V and g_A^{VS} have been used as input.

fit	g_V	g_A^V	g_A^{VS}	$\mathring{M}_V$ [GeV]	b_0^V	b_D^V	$M_S^\star$ [GeV]	b_{08}	color
$1B$	0.125	3/4	$\sqrt{3}/2$	0.636	0.060	0.017	0.935	0.208	black
$2B$	0.125	0.6	0.7	0.630	0.057	0.015	0.924	0.220	orange
$3B$	0.125	1/2	1/2	0.626	0.054	0.015	0.914	0.227	blue
$4B$	0.125	0	0	0.618	0.051	0.015	0.902	$\pm$0.238	red
$5B$	0.085	3/4	$\sqrt{3}/2$	0.696	0.032	0.062	0.924	0.220	black
$6B$	0.085	0.6	0.7	0.685	0.028	0.062	0.914	0.230	orange
$7B$	0.085	1/2	1/2	0.679	0.025	0.061	0.904	0.237	blue
$8B$	0.085	0	0	0.667	0.020	0.062	0.893	$\pm$0.246	red

rather large shift in the parameter b_D^V, which comes from absorbing the contribution $\propto g_V^2/F_\star^4$ from the bubble-type graph. This means that mostly, the functional form of our leading one-loop corrections fixes the shape of the curves, at least in the parameter regions we have used. This also applies to the dependence of $M_V^\star$ on $M_\star$, albeit to a lesser extent, as can be seen in fig. 4.5. Here, we clearly observe that the variation of g_V has an effect on the determination of $\mathring{M}_V$. For a more accurate determination of $M_V^\star(\bar{m})$ in the vicinity of the chiral limit we would need more input from lattice QCD. We also observe that the data point at around 500 MeV which was not included in the fits is missed collectively by all fit curves. As a side remark, we find that a very slight cusp at the $V_\star \to \phi_\star\phi_\star$ decay threshold (at around $M_\star \approx 330$ MeV) is visible in fig. 4.5. This effect, however, does not seem to be of much importance here, which would be different for scalar meson resonances, see [133].

In figs. 4.6 and 4.7 we present the real and imaginary part of the self-energy function for the ρ-meson, for a typical fit result from tab. 4.3. We find that the real part of $\Pi_\rho(s)$ has zero slope at $s = (M_V^\star)^2$, which reflects our chosen renormalization conditions. The energy dependence of $\Pi_{08}(s)$ is presented in fig. 4.8. All the different fit sets can be very well distinguished, but the trend is the same for every set: our fits favor a limited, however non-negligible energy dependence of the mixing amplitude, which can be traced back to the loop graphs as well as to the counterterm coefficient z_{08} in the A type fits. In [47], a strong energy dependence and a possible sign change in the mixing amplitude have been observed between the $\omega(782)$ and the $\phi(1020)$ mass (see their Table II). Furthermore, we present the real part of the determinant $\det_{08}$ for four typical fits in the (s, ν) plane in fig. 4.9. The energy dependence of the zeroes of the determinant can be read off from this figure over the whole ν range examined in this work. We also produced contour plots of the same fit results, showing the position of the zeroes of $\mathrm{Re}[\det_{08}]$ and illustrating the running of the

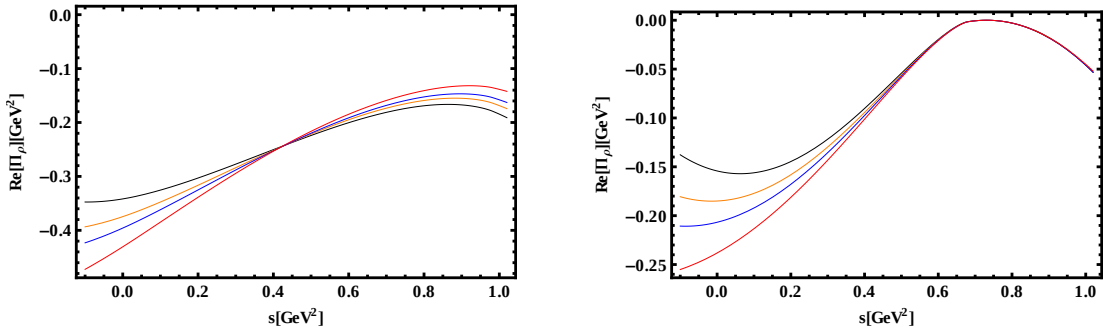

(a) $1A - 4A$, $\nu = -0.885$ (b) $1A - 4A$, $\nu = 0$

Figure 4.6: The energy dependence of the real part of Π_ρ plotted for the parameter sets $1A - 4A$ for $\nu = -0.885$ (left) and $\nu = 0$ (right). The color code for the different curves is shown in the tables above.

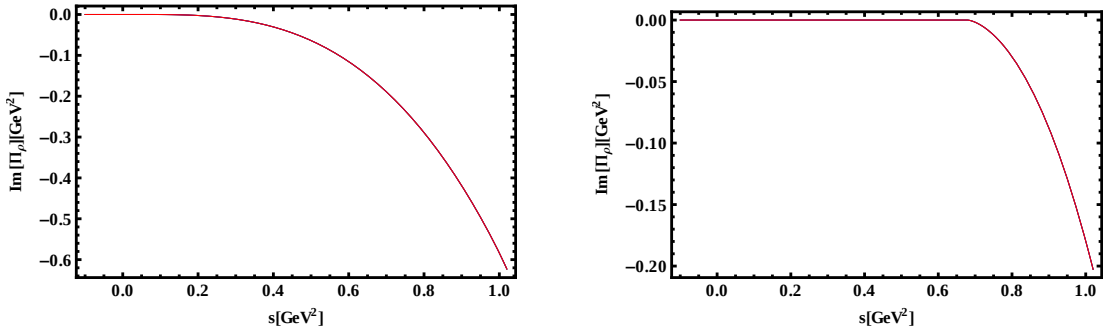

(a) $1A - 4A$, $\nu = -0.885$ (b) $1A - 4A$, $\nu = 0$

Figure 4.7: The energy dependence of the imaginary part of Π_ρ plotted for the parameter sets $1A - 4A$ for $\nu = -0.885$ (left) and $\nu = 0$ (right). The color code for the different curves is shown in the tables above.

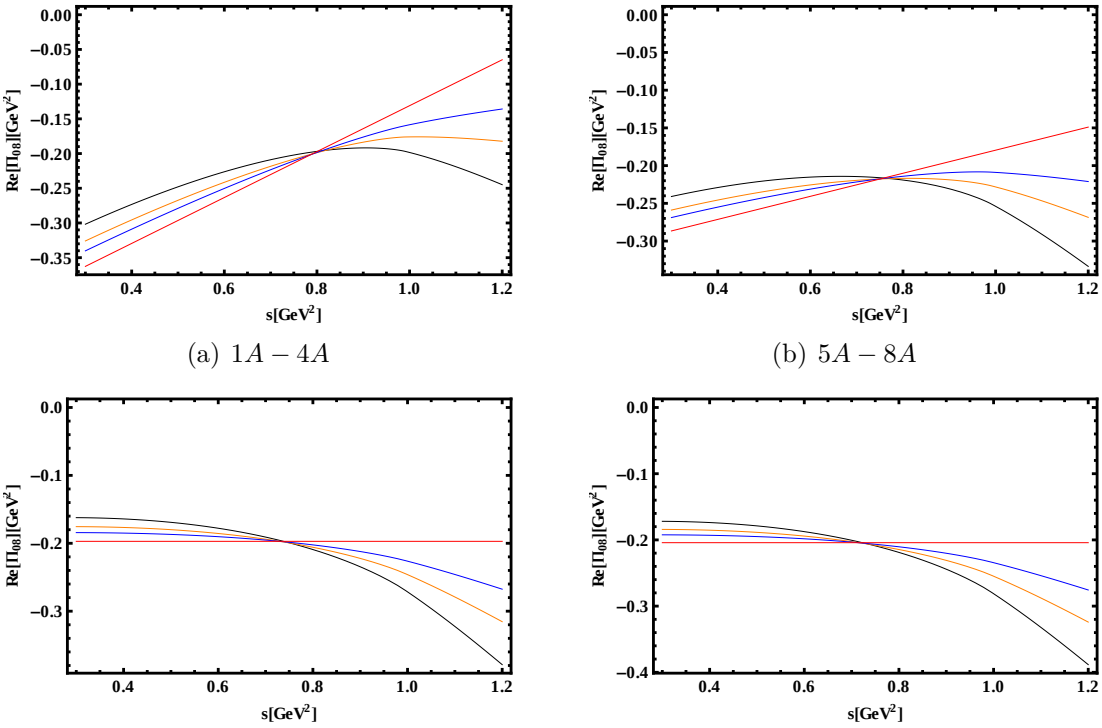

(a) $1A - 4A$ (b) $5A - 8A$

(c) $1B - 4B$ (d) $5B - 8B$

Figure 4.8: The energy dependence of Π_{08} plotted for all parameter sets including tadpoles. The fit sets without tadpoles have been omitted due to their similarity. The color code for the different curves is shown in tabs. 4.3-4.6.

Table 4.5: Fit results (type A) without tadpole contributions, where g_V, g_A^V and g_A^{VS} have been used as input.

fit	g_V	g_A^V	g_A^{VS}	$\mathring{M}_V$ [GeV]	b_0^V	b_D^V	$M_S^\star$ [GeV]	b_{08}
$1A'$	0.125	3/4	$\sqrt{3}/2$	0.630	0.076	0.025	1.010	0.247
$2A'$	0.125	0.6	0.7	0.626	0.073	0.021	0.999	0.268
$3A'$	0.125	1/2	1/2	0.623	0.072	0.019	0.988	0.281
$4A'$	0.125	0	0	0.617	0.068	0.017	0.979	0.300
$5A'$	0.085	3/4	$\sqrt{3}/2$	0.691	0.048	0.073	0.957	0.261
$6A'$	0.085	0.6	0.7	0.682	0.043	0.072	0.947	0.276
$7A'$	0.085	1/2	1/2	0.677	0.040	0.071	0.937	0.285
$8A'$	0.085	0	0	0.666	0.034	0.070	0.929	0.300

real part of the zeroes when tuning the symmetry-breaking variable ν.
In all the results we have collected above we have discarded a second class of fits that produce additional unphysical states in the singlet-octet sector. These appear in the energy region where our present calculation should be applicable. This class of solutions favors rather large axial coupling constants $g_A^{V(S)}$. We show one example of such a fit result in tab. 4.7. Here, we find that b_{08} is considerably smaller than in the earlier fits, while $M_S^\star$ is notably larger and all the other parameters fall into the previously determined range. In fig. 4.11 we plot the typical behavior of the determinant $\det_{08}$ for these two classes of fits. All obtained fits can be grouped into either the standard fits, i.e. the ones presented in tabs. 4.3-4.6, or fits showing spurious states with relatively large $g_A^{V(S)}$ and $M_S^\star$ and smaller b_{08}. We find that the plots for the masses look relatively similar to the 'standard case' fits, but $\det_{08}$ shows a very non-parabolic behavior. For the fit set denoted by $\widetilde{1A}$ we find the parameter z_{08} to be $0.734\,\mathrm{GeV}^{-2}$, whereas for the fits $1A - 4A$ we find an interval of $0.826\text{-}0.900\,\mathrm{GeV}^{-2}$ and for $5A - 8A$ we find $0.374\text{-}0.416\,\mathrm{GeV}^{-2}$.
While our formulas are accurate and model independent to one-loop order and to $\mathcal{O}(p^3)$ in chiral counting, it is important to further study the energy dependence of the two-point amplitudes. In our opinion, this study shows that if the possibility of a sizable variation of the mixing amplitude between $s = M_\omega^2$ and $s = M_\phi^2$ is not taken into account, the whole analysis is not under sufficient theoretical control. The accuracy of this study itself is limited by the lack of lattice data for the variation of the ω and ϕ masses for different values in symmetry-breaking parameter $\delta m_\ell \sim \nu$. This data could be used to check the validity of the mixing scenarios we have outlined here and illustrated in fig. 4.9. The analysis of the mixing that is presented here is of course only of qualitative nature. For a quantitative discussion of the dynamics of $\phi(1020) - \omega(782)$ mixing we would additionally have to consider vector meson decays and include the corresponding relevant final-state-interactions etc. [134–138]. Such

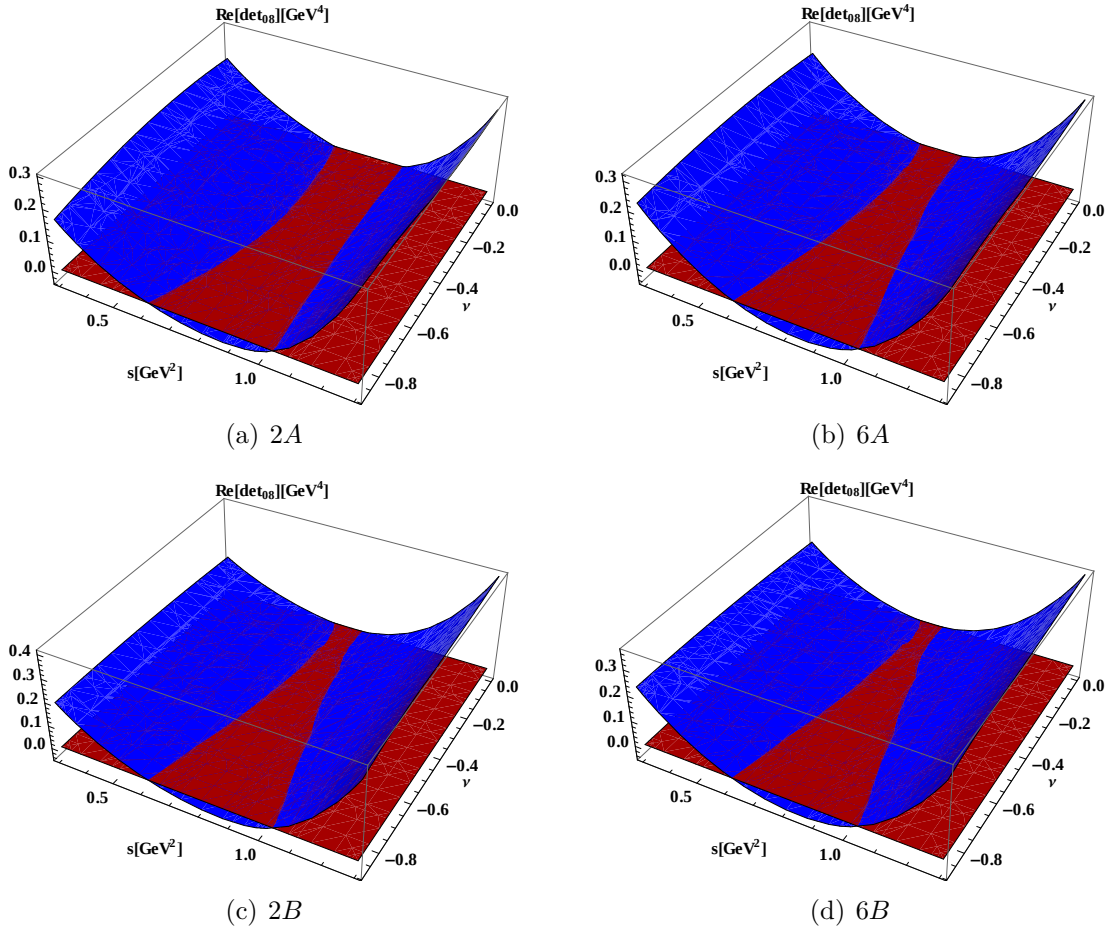

(a) $2A$ (b) $6A$

(c) $2B$ (d) $6B$

Figure 4.9: The real part of $\det_{08}$ plotted in the (s, ν) plane for fits $2A$, $6A$, $2B$, $6B$.

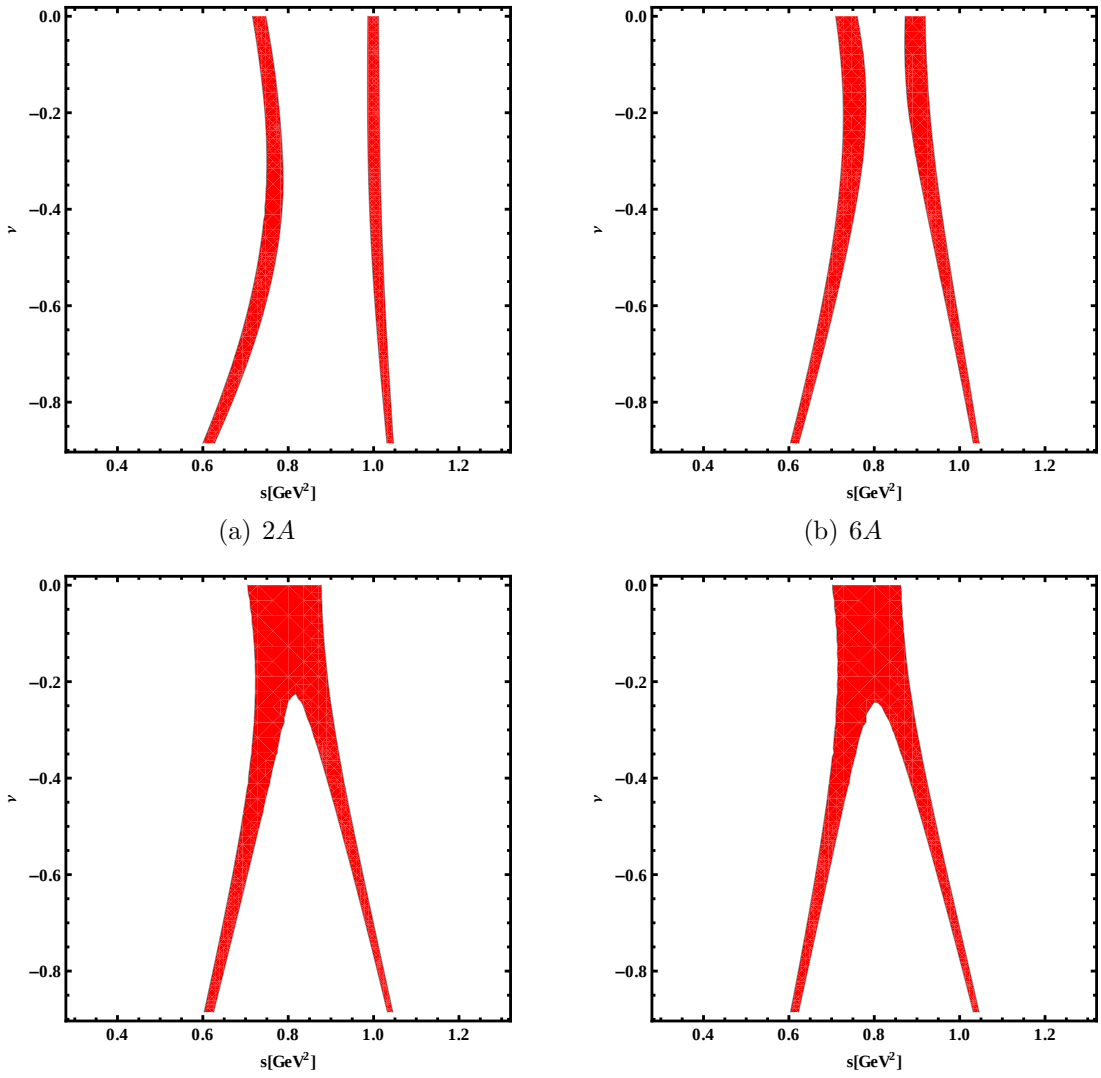

(a) $2A$ (b) $6A$

(c) $2B$ (d) $6B$

Figure 4.10: The plots depict the absolute value of $\mathrm{Re}[\det_{08}]$. The areas where $|\mathrm{Re}[\det_{08}]| < 0.004\,\mathrm{GeV}^4$ holds are colored red.

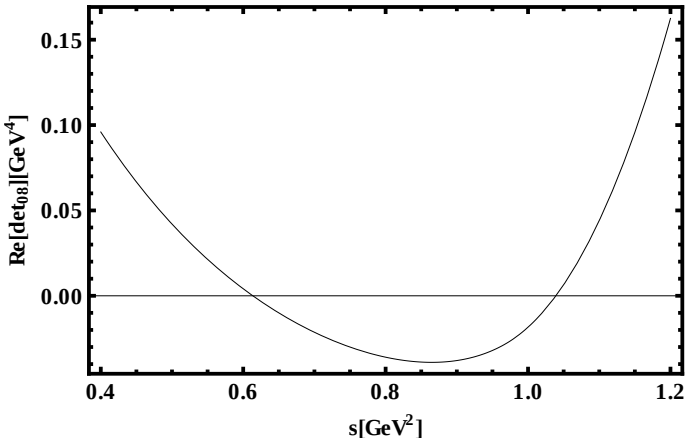

(a) $1A$

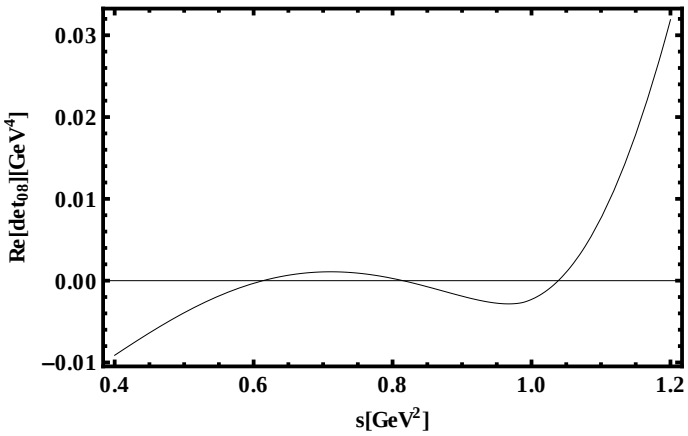

(b) $\widetilde{1A}$

Figure 4.11: Re[$\det_{08}$] at $\nu = -0.885$ for a standard fit (1A of Tab. 4.3) (left) and for the fit of tab. 4.7 showing spurious states (right)

Table 4.6: Fit results (type B) without tadpole contributions, where g_V, g_A^V and g_A^{VS} have been used as input.

fit	g_V	g_A^V	g_A^{VS}	$\mathring{M}_V$ [GeV]	b_0^V	b_D^V	$M_S^\star$ [GeV]	b_{08}
$1B'$	0.125	3/4	$\sqrt{3}/2$	0.635	0.080	0.019	0.934	0.234
$2B'$	0.125	0.6	0.7	0.629	0.076	0.018	0.923	0.247
$3B'$	0.125	1/2	1/2	0.625	0.073	0.017	0.913	0.256
$4B'$	0.125	0	0	0.617	0.068	0.017	0.901	$\pm$0.268
$5B'$	0.085	3/4	$\sqrt{3}/2$	0.694	0.050	0.071	0.923	0.247
$6B'$	0.085	0.6	0.7	0.684	0.044	0.070	0.912	0.259
$7B'$	0.085	1/2	1/2	0.678	0.040	0.070	0.902	0.266
$8B'$	0.085	0	0	0.666	0.034	0.070	0.891	$\pm$0.277

Table 4.7: Result for a fit showing spurious states.

fit	g_V	g_A^V	g_A^{VS}	$\mathring{M}_V$ [GeV]	b_0^V	b_D^V	$M_S^\star$ [GeV]	b_{08}
$\widetilde{1\mathrm{A}}$	0.125	3/4	$\sqrt{3}/2$	0.611	0.046	0.032	1.199	0.001

an extensive analysis is beyond the scope of the investigation we have presented here. Here we want to remark that we do not observe a clear large N_c pattern in our results. The LEC b_0^V is not notably supressed in comparison to b_D^V and the mass splitting $M_S^\star - M_V^\star$ is small but definitely non-negligible. Furthermore, the parameter b_{08} comes out somewhat larger than we would expect from the estimate of eq. (4.60), independently of the chosen scenario to fix z_{08}. We can of course not rule out such a scenario, since our study itself has several theoretical uncertainties which we have discussed in length in the paragraphs above. We want to point out that especially b_0^V is subject to large higher-order corrections, see tabs. 4.3-4.6.

5 Outlook

Using the symmetric point as a starting point for the extrapolation of lattice data to the physical point has proven to be a valuable strategy. We have shown that employing this strategy within the framework of $SU(3)_f$ BChPT yields reliable results in chapters 3 and 4. In order to achieve a further increase in accuracy, these first investigations have to be extended in various directions, which we will shortly outline in this chapter.

5.1 First PDF moments from BChPT

We consider the extrapolation of the first PDF moments as another benchmark of the applicability of $SU(3)_f$ BChPT since the extrapolation of three-point functions in general is more problematic than the extrapolation of two-point functions, see e.g. the extrapolation of the electromagnetic form factors in $SU(2)_f$ BChPT [139] compared to the relatively uncomplicated extrapolation of the nucleon mass [92].
As already mentioned in chapter 2, to pin down the $\mathcal{O}(p^2)$ LECs we would already need a large amount of data. Pushing the calculation to the next order will introduce a host of new undetermined parameters, so that for the time being only a leading one-loop calculation is realistic. Including the baryon decuplet will also be inevitable for a thorough study since some of the appearing intermediate states like $K\Sigma$ have higher mass than e.g. the $\pi\Delta$ threshold. So far, all these effects are encoded in the LECs, but in principle these intermediate decuplet states should be treated explicitly. This will also introduce new LECs, namely the new meson-octet-baryon-decuplet coupling constant and the tensor couplings to the decuplet baryons, hence including the decuplet will without more data not enable us to obtain more accurate results. However, there are ways to increase accuracy without introducing new low energy constants, e.g. by taking finite volume corrections into account, as has been done for the nucleon mass [66] and the electromagnetic form factors [67] (for details of the calculations also see the references therein). It would be reasonable though to include the decuplet before calculating finite volume effects.

5.2 Chiral extrapolation of baryon mass ratios

The accuracy of the extrapolation of baryon mass ratios is mostly affected by two factors: first, the input parameters we chose and second, the lack of lattice data at a larger variety of values of $\bar{m}$. Let us comment on each of these factors separately.
When we are talking about the input parameters used, we mostly have two sources of theoretical uncertainty: the model-dependence that is encoded in the results for the b_i that were obtained via meson-baryon-scattering in [110, 111] as well as our input values for the axial coupling constants D and F. We have tried to eliminate the theoretical uncertainty that is emanating from the b_i by simply considering all three different input sets and checking the convergence of our expansion. In our opinion the result was satisfying, as can also be seen when comparing the b_i we used as input values with the b_i obtained directly from mass fits, see [112]. That leaves the fixed input parameters D and F, which can in principle be determined from lattice studies. In [24] it was pointed out though that a chiral expansion of the parameters was not possible. We propose that a combined fit of both baryon mass ratios and lattice data obtained for the hyperon axial couplings in the same manner as has been presented in [75] and leaving D and F as two additional fit parameters could help to obtain both a higher accuracy for the baryon mass ratio LECs as well as for the axial couplings D and F.
Our discussion of the πN sigma term clearly shows that for a reliable determination of all low energy constants there is a lack of lattice data. We would need fan plot data for different values of $\bar{m}$ to be able to calculate $\sigma_{\pi N}$ from the nucleon mass. Also, fig. 3.4 shows that additional values of X_N for smaller $\bar{m}$ would greatly increase the accuracy of our fit results.

5.3 Chiral behavior of vector meson self-energies

Extending this present calculation to a next-to-leading one-loop calculation without assuming a large N_c scaling meets several difficulties: First, extending the calculation leads to the appearance of an abundance of new tadpole contributions, which means that, to determine the new LECs, one would have to include e.g. $V\phi \to V\phi$ scattering data. Second, just like with the baryon mass ratios, additional fan plot data at different fixed values for the average quark mass $\bar{m}$ would be neccessary to fix the quark-mass insertions appearing at fourth chiral order.
At this order, one could also consider calculating the electromagnetic contributions and the effects of isospin breaking, which we have totally neglected in our calculation, since they are also not included in the lattice study we obtain our data sets from. Numerical estimates of these effects can be found in [47, 140].
For a further study we should also consider calculating the finite size corrections for the lattice data we employed for our analysis, although it is claimed in [75] that the finite size effects cancel to a large extent in the mass ratios.
A rather large uncertainty again results from a lack of information, this time in

the singlet-octet mixing sector. The only information we have there are the masses and decay widths of the $\omega(782)$ and $\phi(1020)$ vector mesons at the physical point. To improve this situation, we need lattice data for $M_\omega(\nu)$ and $M_\phi(\nu)$ to be able to determine the parameters b_{08} and z_{08} instead of having to assume several scenarios for the parameter z_{08}.

A Standard integrals

This chapter contains all standard integrals that appear in the formulae in this thesis. Let us start with the scalar one-point integrals in the IR scheme, which are defined in the following way:

$$I_{\mathrm{M}} = \int_{\mathrm{IR}} \frac{d^d l}{(2\pi)^d} \frac{i}{l^2 - M^2} = 2M^2\lambda + \frac{M^2}{16\pi^2} \log\left(\frac{M^2}{\mu^2}\right) + \mathcal{O}(d-4), \tag{A.1}$$

$$I_{\mathrm{B,V}} = \int_{\mathrm{IR}} \frac{d^d l}{(2\pi)^d} \frac{i}{l^2 - m^2} = 0, \tag{A.2}$$

where m represents non-vanishing masses, e.g. the baryon mass m_B or the vector meson masses M_V, whereas M is to be identified with the mass of a member from the pseudoscalar meson octet, e.g. π, K, η. The parameter λ, defined in eq. (1.48), contains the $(d-4)^{-1}$ pole. From now on we will omit the $\mathcal{O}(d-4)$ terms since they are only relevant for two-loop calculations. If we employ the decomposition

$$I(s) = H(s) - R(s), \tag{A.3}$$

we find the following relations for these easiest scalar integrals:

$$R_{\mathrm{M}} = 0, \quad H_{\mathrm{B,V}} = R_{\mathrm{B,V}} = 2m^2\lambda + \frac{m^2}{16\pi^2} \log\left(\frac{m^2}{\mu^2}\right). \tag{A.4}$$

For our calculations we also need the scalar two-point integral in the IR scheme, $I_{\mathrm{MB,V}}$:

$$I_{\mathrm{MB,V}}(s) = \int_{\mathrm{IR}} \frac{d^d l}{(2\pi)^d} \frac{i}{[(p-l)^2 - m^2]\,[l^2 - M^2]}, \tag{A.5}$$

Here we have used the notation $p^2 = s$. This integral can be evaluated [28] to

$$I_{\mathrm{MB,V}}(s) = \frac{s - m^2 + M^2}{s}\lambda - \frac{1}{16\pi^2}\frac{\alpha(\alpha+\Omega)}{1+2\alpha\Omega+\alpha^2}(2\log\alpha - 1) - \frac{1}{8\pi^2}\frac{\alpha\sqrt{1-\Omega^2}}{1+2\alpha\Omega+\alpha^2}\arccos\left(-\frac{\Omega-\alpha}{\sqrt{1+2\alpha\Omega+\alpha^2}}\right), \tag{A.6}$$

where we have employed the definitions for α and Ω that have been presented in eq. (1.67). Since the IR integral is in general described as the decomposition eq. (A.3) we will also give the general formulae for $H_{\mathrm{MB,V}}$ and $R_{\mathrm{MB,V}}$:

$$H_{\mathrm{MB,V}}(s) = 2\lambda + \frac{1}{16\pi^2}\left[-1 + \log\left(\frac{m^2}{\mu^2}\right) + \frac{s-m^2+M^2}{2s}\log\left(\frac{M^2}{m^2}\right) - \frac{4|\mathbf{q}|}{\sqrt{s}}\operatorname{arctanh}\left(\frac{2|\mathbf{q}|\sqrt{s}}{(m+M)^2-s}\right)\right], \tag{A.7}$$

$$R_{\mathrm{MB,V}}(s) = \frac{s+m^2-M^2}{2s}\left[2\lambda + \frac{1}{16\pi^2}\left(\log\left(\frac{m^2}{\mu^2}\right) - 1\right)\right] + \frac{|\mathbf{q}|}{8\pi^2\sqrt{s}}\operatorname{arctanh}\left(\frac{2|\mathbf{q}|\sqrt{s}}{s+m^2-M^2}\right). \tag{A.8}$$

Here we have introduced the abbreviation

$$|\mathbf{q}| = \frac{\sqrt{(s-(m+M)^2)(s-(m-M)^2)}}{2\sqrt{s}}. \tag{A.9}$$

The last scalar function we have to take a look at is the three-point integral I_{MBB}, which is defined as

$$I_{\mathrm{MBB}}(p'^2, p^2, t) = \int_{\mathrm{IR}} \frac{d^d l}{(2\pi)^d}\frac{i}{[((p'-l)^2-m^2]\,[(p-l)^2-m^2]\,[l^2-M^2]}, \tag{A.10}$$

where we have used the standard definition $t = (p'-p)^2$. In our case, only the forward case of this integral, i.e. $t = 0$ is needed, which takes the form

$$I_{\mathrm{MBB}}(m^2, m^2, 0) = -\frac{\lambda}{m^2} - \frac{1}{16\pi^2 m^2}\left[\log\alpha + \frac{1}{2} - \frac{\alpha}{\sqrt{4-\alpha^2}}\arccos\left(-\frac{\alpha}{2}\right)\right]. \tag{A.11}$$

There is another integral mentioned in the main text, i.e. $I_A^{\mathrm{MB,V}}$, which is given by the following expression:

$$I_A^{\mathrm{MB,V}} = \frac{1}{4s(d-1)}\Big[\Big(4sM^2 - (s+M^2-m^2)^2\Big)I_{\mathrm{MB,V}} + (s+M^2-m^2)I_{\mathrm{M}} + (s-M^2+m^2)I_{\mathrm{V}}\Big]. \tag{A.12}$$

This decomposition is also valid for the non-IR-regularized functions H. Integrals of the type I_A^{MM} can be obtained by replacing m with M in the above expressions.

B Additional material for chapter 2

In this chapter we present the results for the generalized nucleon form factors $A^{s,v}_{N'N}(t=0)$ that have been omitted from chapter 2 due to reasons of legibility. Let us start off with the fairly short expressions for the singlet form factors:

$$A^s_{pp}(0) = \frac{a_s}{2} + \frac{8}{3}M_K^2(3t_{11} + t_{12} - 3t_{13}) + M_\pi^2\left(4t_{11} - \frac{8t_{12}}{3} + 8t_{13}\right), \tag{B.1}$$

$$A^s_{nn}(0) = \frac{a_s}{2} + \frac{8}{3}M_K^2(3t_{11} + t_{12} - 3t_{13}) + M_\pi^2\left(4t_{11} - \frac{8t_{12}}{3} + 8t_{13}\right). \tag{B.2}$$

The form factors $A^{v,3/8}_{pp}(0)$ are fairly more complicated, hence we will not present the the full expressions, we will rather use abbreviations for all the scalar integrals still appearing in the formulae. First, we present the formfactor $A^{v,3}_{pp}(0)$:

$$\begin{aligned} A^{v,3}_{pp}(0) = {} & Z_N\frac{a_D + a_F}{2} + \alpha^{v,3}_{pp} + \frac{I_{\mathrm{M}}(M_\pi)}{24F_0^2m_0^2}\beta^{v,3}_{pp} + \frac{I_{\mathrm{M}}(M_K)}{36F_0^2m_0^2}\gamma^{v,3}_{pp} + \frac{I_{\mathrm{M}}(M_\eta)}{24F_0^2m_0^2}\delta^{v,3}_{pp} \\ & - \frac{I_{\mathrm{MB}}(M_\pi)}{48F_0^2m_0^2}\epsilon^{v,3}_{pp} - \frac{I_{\mathrm{MB}}(M_K)}{36F_0^2m_0^2}\zeta^{v,3}_{pp} + \frac{I_{\mathrm{MB}}(M_\eta)}{48F_0^2m_0^2}\eta^{v,3}_{pp} + \frac{I_{\mathrm{MBB}}(0,M_\pi)}{16F_0^2m_0^2}\theta^{v,3}_{pp} \\ & + \frac{I_{\mathrm{MBB}}(0,M_K)}{12F_0^2m_0^2}\iota^{v,3}_{pp} - \frac{I_{\mathrm{MBB}}(0,M_\eta)}{48F_0^2m_0^2}\kappa^{v,3}_{pp} + \lambda^{v,3}_{pp}. \end{aligned} \tag{B.3}$$

Here, we have introduced a host of abbreviations, which are defined as:

$$\alpha^{v,3}_{pp} = \frac{4}{3}\Big[3(t_1+t_2)(2M_K^2 + M_\pi^2) - 2(2t_3 + 2t_4 - t_7 - t_8)(M_K^2 - M_\pi^2)\Big] \tag{B.4}$$

$$\begin{aligned} \beta^{v,3}_{pp} = {} & \Big[(D+F)\Big(3(a_D+a_F)(D+F) + 8(\Delta a_D + \Delta a_F)\Big)M_\pi^2 \\ & - 3(a_D+a_F)\Big(4 + (D+F)^2\Big)m_0^2\Big] \end{aligned} \tag{B.5}$$

$$\gamma_{pp}^{v,3} = \Big[2\Big(-\Delta a_D(D-3F) - 9a_F(D-F)^2 + 3a_D(D-F)(D+3F) + 3(D+F)\Delta a_F\Big)M_K^2 - 3\Big(3a_F - 6a_F(D-F)^2 + a_D(3+2(D-F)(D+3F))\Big)m_0^2\Big] \tag{B.6}$$

$$\delta_{pp}^{v,3} = (a_D+a_F)(D-3F)^2(m_0^2 - M_\eta^2) \tag{B.7}$$

$$\epsilon_{pp}^{v,3} = (D+F)M_\pi^2\Big[-16(\Delta a_D + \Delta a_F)(4m_0^2 - M_\pi^2) + 3(a_D+a_F)(D+F)(-8m_0^2+5M_\pi^2)\Big] \tag{B.8}$$

$$\zeta_{pp}^{v,3} = M_K^2\Big[2(D(\Delta a_D - 3\Delta a_F) - 3F(\Delta a_D + \Delta a_F))(4m_0^2 - M_K^2) + 3(D-F)((a_D-3a_F)D + 3(a_D+a_F)F)(-8m_0^2+5M_K^2)\Big] \tag{B.9}$$

$$\eta_{pp}^{v,3} = (a_D+a_F)(D-3F)^2M_\eta^2(-8m_0^2+5M_\eta^2) \tag{B.10}$$

$$\theta_{pp}^{v,3} = (a_D+a_F)(D+F)^2M_\pi^2(8m_0^4 - 12m_0^2M_\pi^2 + 3M_\pi^4) \tag{B.11}$$

$$\iota_{pp}^{v,3} = (D-F)((a_D-3a_F)D + 3(a_D+a_F)F)M_K^2 \times (8m_0^4 - 12m_0^2M_K^2 + 3M_K^4) \tag{B.12}$$

$$\kappa_{pp}^{v,3} = (a_D+a_F)(D-3F)^2M_\eta^2(8m_0^4 - 12m_0^2M_\eta^2 + 3M_\eta^4) \tag{B.13}$$

$$\begin{aligned}\lambda_{pp}^{v,3} = &-\frac{(D+F)M_\pi^4}{2304\pi^2F_0^2m_0^4}\Big[9(a_D+a_F)(D+F)(2m_0^2 - M_\pi^2) + 4(\Delta a_D + \Delta a_F)(6m_0^2 - M_\pi^2)\Big] \\ &+ \frac{M_K^4}{3456\pi^2F_0^2m_0^4}\Big[54a_F(D-F)^2(2m_0^2 - M_K^2) - 18a_D(D^2+2DF-3F^2)(2m_0^2 - M_K^2) \\ &+ (D(\Delta a_D - 3\Delta a_F) - 3F(\Delta a_D + \Delta a_F))(6m_0^2 - M_K^2)\Big] \\ &+ \frac{(a_D+a_F)}{768\pi^2F_0^2m_0^4}(D-3F)^2(2m_0^2M_\eta^4 - M_\eta^6)\end{aligned} \tag{B.14}$$

The last result of this chapter is the formfactor $A^{v,8}_{pp}(0)$, which takes a similar form as $A^{v,3}_{pp}(0)$:

$$\begin{aligned} A^{v,8}_{pp}(0) = Z_N \frac{3a_F - a_D}{2\sqrt{3}} - \alpha^{v,8}_{pp} + \frac{I_{\mathrm{M}}(M_\pi)}{8F_0^2 m_0^2}\beta^{v,8}_{pp} + \frac{I_{\mathrm{M}}(M_K)}{12\sqrt{3}F_0^2 m_0^2}\gamma^{v,8}_{pp} - \frac{I_{\mathrm{M}}(M_\eta)}{24\sqrt{3}F_0^2 m_0^2}\delta^{v,8}_{pp} \\ + \frac{I_{\mathrm{MB}}(M_\pi)}{16F_0^2 m_0^2}\epsilon^{v,8}_{pp} + \frac{I_{\mathrm{MB}}(M_K)}{6\sqrt{3}F_0^2 m_0^2}\zeta^{v,8}_{pp} + \frac{I_{\mathrm{MB}}(M_\eta)}{48\sqrt{3}F_0^2 m_0^2}\eta^{v,8}_{pp} + \frac{I_{\mathrm{MBB}}(0,M_\pi)}{16F_0^2 m_0^2}\theta^{v,8}_{pp} \\ - \frac{I_{\mathrm{MBB}}(0,M_K)}{3\sqrt{3}F_0^2 m_0^2}\iota^{v,8}_{pp} + \frac{I_{\mathrm{MBB}}(0,M_\eta)}{48\sqrt{3}F_0^2 m_0^2}\kappa^{v,8}_{pp} + \lambda^{v,8}_{pp}. \end{aligned} \tag{B.15}$$

In order to present the result in a more legible way, we have introduced various abbreviations:

$$\begin{aligned} \alpha^{v,8}_{pp} = \frac{4}{3\sqrt{3}}\Big[& 3(t_1 - 3t_2)(2M_K^2 + M_\pi^2) \\ & + 2(10t_3 - 6t_4 + t_7 - 3t_8 + 6t_9)(M_K^2 - M_\pi^2)\Big], \end{aligned} \tag{B.16}$$

$$\beta^{v,8}_{pp} = \sqrt{3}(a_D - 3a_F)(D+F)^2(-m_0^2 + M_\pi^2), \tag{B.17}$$

$$\begin{aligned} \gamma^{v,8}_{pp} = \Big[& 2(5D\Delta a_D - 4a_D D(D-3F) - 3\Delta a_D F - 3D\Delta a_F + 9F\Delta a_F)M_K^2 \\ & + (-27a_F + a_D(9 + 8D(D-3F)))m_0^2\Big], \end{aligned} \tag{B.18}$$

$$\delta^{v,8}_{pp} = (a_D - 3a_F)(D-3F)^2(m_0^2 - M_\eta^2), \tag{B.19}$$

$$\epsilon^{v,8}_{pp} = \sqrt{3}(a_D - 3a_F)(D+F)^2 M_\pi^2(8m_0^2 - 5M_\pi^2), \tag{B.20}$$

$$\begin{aligned} \zeta^{v,8}_{pp} = M_K^2\Big[& (5D\Delta a_D - 3\Delta a_D F - 3D\Delta a_F + 9F\Delta a_F)(4m_0^2 - M_K^2) \\ & + 2a_D D(D-3F)(-8m_0^2 + 5M_K^2)\Big], \end{aligned} \tag{B.21}$$

$$\eta^{v,8}_{pp} = (a_D - 3a_F)(D-3F)^2 M_\eta^2(8m_0^2 - 5M_\eta^2), \tag{B.22}$$

$$\theta^{v,8}_{pp} = \sqrt{3}(a_D - 3a_F)(D+F)^2 M_\pi^2(8m_0^4 - 12m_0^2 M_\pi^2 + 3M_\pi^4), \tag{B.23}$$

$$\iota^{v,8}_{pp} = a_D D(D-3F) M_K^2(8m_0^4 - 12m_0^2 M_K^2 + 3M_K^4), \tag{B.24}$$

$$\kappa^{v,8}_{pp} = (a_D - 3a_F)(D-3F)^2 M_\eta^2(8m_0^4 - 12m_0^2 M_\eta^2 + 3M_\eta^4), \tag{B.25}$$

$$
\begin{aligned}
\lambda_{pp}^{v,8} = &-\frac{\sqrt{3}(a_D-3a_F)(D+F)^2(2m_0^2M_\pi^4-M_\pi^6)}{256\pi^2F_0^2m_0^4}\\
&+\frac{M_K^4}{1152\sqrt{3}\pi^2F_0^2m_0^4}\Big[-(5D\Delta a_D-3\Delta a_DF-3D\Delta a_F+9F\Delta a_F)\\
&\qquad\times(6m_0^2-M_K^2)\\
&\qquad+24a_DD(D-3F)(2m_0^2-M_K^2)\Big]\\
&-\frac{(a_D-3a_F)(D-3F)^2(2m_0^2M_\eta^4-M_\eta^6)}{768\sqrt{3}\pi^2F_0^2m_0^4}.
\end{aligned}
\tag{B.26}
$$

The only undefined element is the renormalization factor at the one-loop level, also called Z factor, Z_N here because it is the renormalization factor of the nucleon sector. We find that this factor at one-loop level takes the form

$$
\begin{aligned}
Z_N = 1 &- M_\pi^2\frac{3(D+F)^2}{32\pi^2F_0^2} - M_K^2\frac{5D^2-6DF+9F^2}{48\pi^2F_0^2} - M_\eta^2\frac{(D-3F)^2}{96\pi^2F_0^2}\\
&-\frac{3(D+F)^2M_\pi^3(-3m_0^2+M_\pi^2)}{16\pi^2F_0^2m_0^3\sqrt{4-\frac{M_\pi^2}{m_0^2}}}\arccos\left(-\frac{M_\pi}{2m_0}\right)\\
&-\frac{(5D^2-6DF+9F^2)M_K^3(-3m_0^2+M_K^2)}{24\pi^2F_0^2m_0^3\sqrt{4-\frac{M_K^2}{m_0^2}}}\arccos\left(-\frac{M_K}{2m_0}\right)\\
&-\frac{(D-3F)^2M_\eta^3(-3m_0^2+M_\eta^2)}{48\pi^2F_0^2m_0^3\sqrt{4-\frac{M_\eta^2}{m_0^2}}}\arccos\left(-\frac{M_\eta}{2m_0}\right)\\
&+\frac{3(D+F)^2M_\pi^2(-3m_0^2+2M_\pi^2)}{32\pi^2F_0^2m_0^2}\log\left(\frac{M_\pi}{m_0}\right)\\
&+\frac{(5D^2-6DF+9F^2)M_K^2(-3m_0^2+2M_K^2)}{48\pi^2F_0^2m_0^2}\log\left(\frac{M_K}{m_0}\right)\\
&+\frac{(D-3F)^2M_\eta^2(-3m_0^2+2M_\eta^2)}{96\pi^2F_0^2m_0^2}\log\left(\frac{M_\eta}{m_0}\right).
\end{aligned}
\tag{B.27}
$$

C Additional material for chapter 3

In section 3.3 we have mentioned that there is a systematic way to split off the finite part of an LEC from the divergent part, i.e.

$$d_i = \gamma_i^{\mathrm{IR}} \lambda + d_i^{(r)}(\mu). \tag{C.1}$$

In that way, we can define a completely scale independent quantity $\bar{d}_i$, which we define as

$$d_i^{(r)}(\mu) = \bar{d}_i + \frac{\gamma_i^{\mathrm{IR}}}{16\pi^2} \log\left(\frac{m_0}{\mu}\right). \tag{C.2}$$

In this appendix, we present these γ_i^{IR} which we have determined from our calculation. They read:

$$\gamma_1^{\mathrm{IR}} = \frac{1}{72F_0^2}\Bigg(b_D(14+69D^2+81F^2) + 162b_F DF + \frac{D^2-3F^2}{m_0} - (12b_1 - 4b_3 + 3b_8 - b_{10})\Bigg), \tag{C.3}$$

$$\gamma_2^{\mathrm{IR}} = \frac{1}{48F_0^2}\left(120b_D DF + b_F(4+60D^2+108F^2) + \frac{6DF}{m_0} + 3(4b_2+b_9)\right), \tag{C.4}$$

$$\gamma_3^{\mathrm{IR}} = \frac{1}{48F_0^2}\Bigg(6b_D(4+13D^2+9F^2) + 108b_F DF + \frac{3(D^2-3F^2)}{m_0} - (36b_1 + 4b_3 + 9b_8 + b_{10})\Bigg), \tag{C.5}$$

$$\gamma_4^{\mathrm{IR}} = \frac{1}{72F_0^2}\left(-4b_D(11+72D^2) - \frac{9(D^2-3F^2)}{m_0} + 108b_1 - 4b_3 + 27b_8 - b_{10}\right), \tag{C.6}$$

$$\gamma_5^{\mathrm{IR}} = \frac{1}{72F_0^2}\left(44b_F - \frac{26DF}{m_0} - 13(4b_2+b_9)\right), \tag{C.7}$$

$$\gamma_6^{\mathrm{IR}} = \frac{1}{432F_0^2}\left(264b_0 + b_D(132 - 144D^2) - \frac{35D^2 + 27F^2}{m_0}\right. \tag{C.8}$$
$$\left. - (108b_1 + 140b_3 + 264b_4 + 27b_8 + 35b_{10} + 66b_{11})\right),$$
$$\gamma_7^{\mathrm{IR}} = \frac{1}{144F_0^2}\left(120b_0 + b_D\Big(28 - 24(7D^2 + 9F^2)\Big) - 432b_F DF - \frac{17D^2 + 9F^2}{m_0}\right. \tag{C.9}$$
$$\left. - (36b_1 + 68b_3 + 120b_4 + 9b_8 + 17b_{10} + 30b_{11})\right).$$

These equations can be used to calculate the different low energy constants at different scales. The scale we have used in our work was $\mu = 1150\,\mathrm{MeV}$.

D Additional material for chapter 4

D.1 Loop integrals

Let us revisit the integral from eq. (A.7) and let us split it up into two parts:

$$H_{\mathrm{MV}}(s) = H_{\mathrm{MV}}(M_V^2) - \frac{s - M_V^2}{16\pi^2} J^{\mathrm{MV}}(s), \tag{D.1}$$

where

$$\begin{aligned} H_{\mathrm{MV}}(M_V^2) &= 2\lambda + \frac{1}{16\pi^2}\left(-1 + \log\left(\frac{M_V^2}{\mu^2}\right) + \frac{M^2}{M_V^2}\log\left(\frac{M}{M_V}\right)\right. \\ &\quad \left. + 2M\frac{\sqrt{4M_V^2 - M^2}}{M_V^2}\arctan\left(\frac{\sqrt{4M_V^2 - M^2}}{2M_V + M}\right)\right) \\ &= 2\lambda + \frac{1}{16\pi^2}\left(-1 + \log\left(\frac{M_V^2}{\mu^2}\right)\right) + \frac{M}{16\pi M_V} \\ &\quad + \frac{M^2}{16\pi^2 M_V^2}\left(\log\left(\frac{M}{M_V}\right) - 1\right) - \frac{M^3}{128\pi M_V^3} + \mathcal{O}(M^4), \end{aligned} \tag{D.2}$$

and $J^{\mathrm{MV}}(s)$ does not contain any divergencies

$$\begin{aligned} J^{\mathrm{MV}}(s) &= \int_{(M_V+M)^2}^{\infty} ds' \frac{\sqrt{(s' - (M_V + M)^2)(s' - (M_V - M)^2)}}{s'(s' - s)(s' - M_V^2)} \\ &= \frac{M^2 - M_V^2}{sM_V^2}\log\left(\frac{M}{M_V}\right) + \frac{4|\mathbf{q}|}{\sqrt{s}(s - M_V^2)}\arctan\left(\frac{2|\mathbf{q}|\sqrt{s}}{(M_V + M)^2 - s}\right) \\ &\quad + 2M\frac{\sqrt{4M_V^2 - M^2}}{M_V^2(s - M_V^2)}\operatorname{arctanh}\left(\frac{\sqrt{4M_V^2 - M^2}}{2M_V + M}\right). \end{aligned} \tag{D.3}$$

For $M \neq 0$ we find that this finite part can be expanded

$$J^{\mathrm{MV}}(M_V^2) = -\frac{1}{M_V^2}\left[1 + \log\left(\frac{M}{M_V}\right) - \frac{3\pi}{4}\frac{M}{M_V} + \frac{M^2}{M_V^2}\left(\frac{3}{4} - \log\left(\frac{M}{M_V}\right)\right) + \mathcal{O}(M^3)\right], \tag{D.4}$$

while for $s \neq M_V^2$ we find that the chiral expansion takes the following form:

$$\begin{aligned} J^{\mathrm{MV}}(s) = {} & \frac{1}{s}\log\left(\frac{M_V^2}{M_V^2 - s}\right) - \frac{\pi M}{M_V(M_V^2 - s)} - \frac{M^2}{M_V^2}\frac{(3M_V^2 - s)}{(M_V^2 - s)^2}\log\left(\frac{M}{M_V}\right) \\ & + \frac{M^2}{M_V^2(M_V^2 - s)^2}\left[2M_V^2 - s - (s + M_V^2)\frac{M_V^2}{s}\log\left(\frac{M_V^2}{M_V^2 - s}\right)\right] \\ & + \frac{\pi}{8}\frac{M^3}{M_V^3(M_V^2 - s)} + \mathcal{O}(M^4). \end{aligned} \tag{D.5}$$

As s approaches M_V^2, the convergence radius of this expansion vanishes and hence the expansion shown in eq. (D.4) should be used. We also find that the function $J^{\mathrm{MV}}(s)$ diverges logarithmically as both $s \to M_V^2$ and $M \to 0$. The integral $H^{\mathrm{MM}}(s)$ can be found immediately by replacing M_V with M. Analogously, one can find all integrals that contain the isosinglet vector mass by replacing M_V by M_S.
Let us also present the chiral limit values for these functions, as they are needed for the renormalization procedures described in chapter 4:

$$H_A^{\mathrm{MM}}(s) \to \frac{s}{192\pi^2}\left[\frac{5}{3} + \log\left(-\frac{\mu^2}{s}\right) - 32\pi^2\lambda\right] \tag{D.6}$$

$$\begin{aligned} H_A^{\mathrm{MV}}(s) \to {} & \frac{1}{192\pi^2 s}\Bigg[(3M_V^2 s - s^2)\left(32\pi^2\lambda + \log\left(\frac{M_V^2}{\mu^2}\right)\right) \\ & + \frac{(s - M_V^2)^3}{s}\log\left(\frac{M_V^2}{M_V^2 - s}\right) + \frac{1}{3}\left(5s^2 - 12M_V^2 s + 3M_V^4\right)\Bigg]. \end{aligned} \tag{D.7}$$

As a last point we want to show the chiral expansion of the full function H_A^{MV} in the case of $s \neq M_V^2$:

$$\begin{aligned} H_A^{\mathrm{MV}}(s) = {} & \frac{1}{192\pi^2 s}\Bigg[(3M_V^2 s - s^2)\left(32\pi^2\lambda + \log\left(\frac{M_V^2}{\mu^2}\right)\right) \\ & + \frac{(s - M_V^2)^3}{s}\log\left(\frac{M_V^2}{M_V^2 - s}\right) + \frac{1}{3}\left(5s^2 - 12M_V^2 s + 3M_V^4\right) \\ & + \frac{3M^2}{s}\Bigg(s^2\left(32\pi^2\lambda + \log\left(\frac{M_V^2}{\mu^2}\right)\right) + (M_V^4 - s^2)\log\left(\frac{M_V^2}{M_V^2 - s}\right) \\ & - s(s + M_V^2)\Bigg) + \mathcal{O}(M^4)\Bigg]. \end{aligned} \tag{D.8}$$

D.2 Dispersive representation of the $\pi\pi$ loop

The techniques employed in effective field theories match very well with the techniques of dispersion relations. There is a fruitful interplay when one mixes these two approaches to analyse low energy phenomena [141]. Let us start with the definition of the dispersive integral

$$\Pi(s) = \frac{1}{\pi}\int_{s_0}^{\infty} ds' \frac{\operatorname{Im}\Pi(s')}{s' - (s + i\varepsilon)}, \tag{D.9}$$

a representation which is valid for functions $\Pi(s)$ that vanish as $s \to \infty$ and that have a cut along the real, positive s axis, starting at s_0. This equation is usually called an unsubtracted dispersion relation. It is important to know $\operatorname{Im}\Pi(s')$ also for large values of s' in order to obtain $\Pi(s)$ for small s. One can also consider subtracted dispersion relations where the influence of the high-energy regions of $\operatorname{Im}\Pi(s')$ is reduced while the lower energies weigh in heavier. These subtractions are also needed if $\lim_{s\to\infty}\Pi(s) \neq 0$:

$$\Pi(s) = \sum_{n=0}^{N-1} c_n s^n + \frac{s^N}{\pi}\int_{s_0}^{\infty} ds' \frac{\operatorname{Im}\Pi(s')}{s'^N[s' - (s + i\varepsilon)]}, \tag{D.10}$$

When comparing these subtraction constants with the results obtained from ChPT we find that they are equivalent to the low energy constants.
Let us now show how this whole procedure works out in the case for the decay width $\Gamma[\rho \to \pi\pi]$ and the corresponding self-energy $\Pi_\rho^{\pi\pi}(s)$. From eq. (4.58) we obtain the energy dependence of the decay width

$$-iM_\rho\Gamma_\rho = -i\frac{g_V^2}{48\pi F_0^4}s^3\left[1 - \frac{4M_\pi^2}{s}\right]^{\frac{3}{2}}. \tag{D.11}$$

Let us now insert this expression in a dispersion relation with four subtractions, i.e.

$$\Pi_\rho^{\pi\pi}(s) = c_0 + c_1 s + c_2 s^2 + c_3 s^3 - \frac{g_V^2 s^4}{48\pi^2 F_0^4}\int_{4M_\pi^2}^{\infty}\frac{ds'}{s'(s' - s)}\left[1 - \frac{4M_\pi^2}{s'}\right]^{\frac{3}{2}}, \tag{D.12}$$

where we have dropped the ε-prescription but it is understood that the real values of s are approached from the upper complex plane for $s \in [4M_\pi^2, \infty)$. We can directly relate the expression in eq. (D.12) to the result of the bubble-type graph that we

have shown in fig. 4.3(a). The integral appearing in the above expression is given by

$$\begin{aligned} J_\rho^{\pi\pi} &= \int_{4M_\pi^2}^{\infty} \frac{ds'}{s'(s'-s)} \sqrt{1-\frac{4M_\pi^2}{s'}}^3 \\ &= \frac{1}{s}\left[\frac{8}{3} - \frac{8M_\pi^2}{s} + 2\sqrt{1-\frac{4M_\pi^2}{s}}^3 \operatorname{arctanh}\left(-\left[1-\frac{4M_\pi^2}{s}\right]^{-\frac{1}{2}}\right)\right]. \end{aligned} \tag{D.13}$$

We can perform a chiral expansion of this integral in the region $4M_\pi^2 < s$ and it is given to $\mathcal{O}(p^3)$ as

$$J_\rho^{\pi\pi} = \frac{1}{s}\left[\frac{8}{3} - \frac{8M_\pi^2}{s} + i\pi - \frac{6M_\pi^2}{s}\left(1 + \log\left(\frac{M_\pi^2}{s}\right) + i\pi\right)\right] + \mathcal{O}(M_\pi^4). \tag{D.14}$$

We can now perform the matching between the dispersion relation result eq. (D.12) to the pion part of the result of the dimensionally regularized loop graph presented in fig. 4.3(a), the first term in eq. (4.43) (d is the space-time dimension),

$$i\tilde{\Pi}_{\mu\nu}^{\pi\pi} = i\left[g_{\mu\nu} - \frac{k_\mu k_\nu}{k^2}\right]\tilde{\Pi}_\rho^{\pi\pi}, \qquad \tilde{\Pi}_\rho^{\pi\pi} = -\frac{4g_V^2}{F_0^4} s^2 I_A^{\pi\pi}(s). \tag{D.15}$$

We find that this yields simple expressions for the subtraction constants c_i:

$$c_0 = c_1 = 0, \tag{D.16}$$

$$c_2 = -\frac{g_V^2}{8\pi^2 F_0^4} M_\pi^2 \left[32\pi^2\lambda + \log\left(\frac{M_\pi^2}{\mu^2}\right)\right], \tag{D.17}$$

$$c_3 = \frac{g_V^2}{48\pi^2 F_0^4}\left[32\pi^2\lambda + \log\left(\frac{M_\pi^2}{\mu^2}\right) + 1\right]. \tag{D.18}$$

We find that the subtraction constant c_3 has a logarithmic divergence in the chiral limit, which is, however, counterbalanced by the infrared term in eq. (D.13). Obviously, we would need counterterms like $s^2 M_\pi^2$ and s^3 which are not yet present in our effective Lagrangian so to take care of the UV-divergencies present in λ in $c_{2,3}$. The construction of these terms that have more than one derivative acting on the vector meson field is in prinicple straightforward, as is shown in [126]. As a result, this would leave us with finite expressions for our subtraction constants

$$c_2 = -\frac{g_V^2}{8\pi^2 F_0^4} M_\pi^2 \left[r_2(\mu) + \log\left(\frac{M_\pi^2}{\mu^2}\right)\right], \tag{D.19}$$

$$c_3 = \frac{g_V^2}{48\pi^2 F_0^4}\left[r_3(\mu) + \log\left(\frac{M_\pi^2}{\mu^2}\right) + 1\right], \tag{D.20}$$

where the constants $r_{2,3}(\mu)$ are a priori unknown.

Bibliography

[1] J. Beringer *et al.* [Particle Data Group Collaboration], Phys. Rev. D **86** (2012) 010001

[2] D. J. Gross and F. Wilczek, Phys. Rev. Lett. **30** (1973) 1343

[3] H. D. Politzer, Phys. Rev. Lett. **30** (1973) 1346

[4] K. G. Wilson, Phys. Rev. D **10** (1974) 2445

[5] C. Gattringer and C. B. Lang, Lect. Notes Phys. **788** (2010) 1

[6] J. Gasser and H. Leutwyler, Annals Phys. **158** (1984) 142

[7] J. Gasser and H. Leutwyler, Nucl. Phys. B **250** (1985) 465

[8] S. Scherer and M. R. Schindler, arXiv:hep-ph/0505265

[9] M. A. Shifman, A. I. Vainshtein and V. I. Zakharov, Nucl. Phys. B **147** (1979) 385

[10] M. A. Shifman, Prog. Theor. Phys. Suppl. **131** (1998) 1

[11] E. H. Wichmann and J. H. Crichton Phys. Rev. **132** (1963) 2788

[12] S. Weinberg, In 'Boston 1996, Conceptual foundations of quantum field theory' 241, arXiv:hep-th/9702027

[13] Y. Nambu, Phys. Rev. Lett. **4** (1960) 380

[14] J. Goldstone, Nuovo Cim. **19** (1961) 154

[15] B. Kubis, arXiv:hep-ph/0703274

[16] S. R. Coleman, J. Wess and B. Zumino, Phys. Rev. **177** (1969) 2239

[17] C. G. Callan, Jr. *et al.*, Phys. Rev. **177** (1969) 2247

[18] H. Leutwyler, Annals Phys. **235** (1994) 165

[19] M. Gell-Mann, R. J. Oakes and B. Renner, Phys. Rev. **175** (1968) 2195

[20] M. D. Scadron, Rept. Prog. Phys. **44** (1981) 213

[21] A. Krause, Helv. Phys. Acta **63** (1990) 3

[22] B. Borasoy, Phys. Rev. D **59** (1999) 054021

[23] N. Cabibbo, E. C. Swallow and R. Winston, Ann. Rev. Nucl. Part. Sci. **53** (2003) 39

[24] H.-W. Lin and K. Orginos, Phys. Rev. D **79** (2009) 034507

[25] J. Gasser, M. E. Sainio and A. Švarc, Nucl. Phys. B **307** (1988) 779

[26] E. E. Jenkins and A. V. Manohar, Phys. Lett. B **255** (1991) 558

[27] V. Bernard *et al.*, Nucl. Phys. B **388** (1992) 315

[28] T. Becher and H. Leutwyler, Eur. Phys. J. C **9** (1999) 643

[29] H.-B. Tang, arXiv:hep-ph/9607436

[30] P. J. Ellis and H.-B. Tang, Phys. Rev. C **57** (1998) 3356

[31] T. Fuchs *et al.*, Phys. Rev. D **68** (2003) 056005

[32] V. Bernard, Prog. Part. Nucl. Phys. **60** (2008) 82

[33] M. Frink and U.-G. Meißner, JHEP **0407** (2004) 028

[34] M. Frink, *private communication*, Dec. 2011

[35] P. C. Bruns, L. Greil and A. Schäfer, Phys. Rev. D **87** (2013) 054021

[36] M. R. Schindler, J. Gegelia and S. Scherer, Phys. Lett. B **586** (2004) 258

[37] S. Gasiorowicz and D. A. Geffen, Rev. Mod. Phys. **41** (1969) 531

[38] M. Bando *et al.*, Phys. Rev. Lett. **54** (1985) 1215

[39] M. Bando, T. Kugo and K. Yamawaki, Nucl. Phys. B **259** (1985) 493

[40] S. Weinberg, Phys. Rev. **166** (1968) 1568

[41] G. Ecker *et al.*, Phys. Lett. B **223** (1989) 425

[42] G. Ecker *et al.*, Nucl. Phys. B **321** (1989) 311

[43] K. Kampf, J. Novotný and J. Trnka, Phys. Rev. D **81** (2010) 116004

[44] U.-G. Meißner, Phys. Rept. **161** (1988) 213

[45] M. C. Birse, Z. Phys. A **355** (1996) 231

[46] E. E. Jenkins, A. V. Manohar and M. B. Wise, Phys. Rev. Lett. **75** (1995) 2272

[47] J. Bijnens, P. Gosdzinsky and P. Talavera, Nucl. Phys. B **501** (1997) 495

[48] J. Bijnens, P. Gosdzinsky and P. Talavera, JHEP **9801** (1998) 014

[49] T. Fuchs *et al.*, Phys. Lett. B **575** (2003) 11

[50] P. C. Bruns and U.-G. Meißner, Eur. Phys. J. C **40** (2005) 97

[51] P. C. Bruns and U.-G. Meißner, Eur. Phys. J. C **58** (2008) 407

[52] D. Djukanovic *et al.*, Phys. Lett. B **680** (2009) 235

[53] T. Bauer *et al.*, Int. J. Mod. Phys. A **27** (2012) 1250178

[54] J. B. Kogut and L. Susskind, Phys. Rev. D **11** (1975) 395

[55] L. Susskind, Phys. Rev. D **16** (1977) 3031

[56] H. B. Nielsen and M. Ninomiya, Nucl. Phys. B **185** (1981) 20 [Erratum-ibid. B **195** (1982) 541]

[57] D. Friedan, Commun. Math. Phys. **85** (1982) 481

[58] D. B. Kaplan, Phys. Lett. B **288** (1992) 342

[59] D. B. Kaplan, Nucl. Phys. Proc. Suppl. **30** (1993) 597

[60] T. Banks, L. Susskind and J. B. Kogut, Phys. Rev. D **13** (1976) 1043

[61] R. Narayanan and H. Neuberger, Nucl. Phys. B **443** (1995) 305

[62] H. Neuberger, Phys. Lett. B **417** (1998) 141

[63] R. T. Scalettar, D. J. Scalapino and R. L. Sugar, Phys. Rev. B **34** (1986) 7911

[64] S. Duane *et al.*, Phys. Lett. B **195** (1987) 216

[65] J. Gasser and H. Leutwyler, Nucl. Phys. B **307** (1988) 763

[66] A. Ali Khan *et al.* [QCDSF-UKQCD Collaboration], Nucl. Phys. B **689** (2004) 175

[67] L. Greil, T. R. Hemmert and A. Schäfer, Eur. Phys. J. A **48** (2012) 53

[68] K. Symanzik, Nucl. Phys. B **226** (1983) 187

[69] K. Symanzik, Nucl. Phys. B **226** (1983) 205

[70] M. Lüscher and S. Schäfer, JHEP **1107** (2011) 036

[71] M. Lüscher and S. Schäfer, Comput. Phys. Commun. **184** (2013) 519

[72] R. Gupta, arXiv:hep-lat/9807028

[73] S. Chandrasekharan and U. J. Wiese, Prog. Part. Nucl. Phys. **53** (2004) 373

[74] M. Di Pierro, arXiv:hep-lat/0009001

[75] W. Bietenholz *et al.*, Phys. Rev. D **84** (2011) 054509

[76] B. Borasoy and U.-G. Meißner, Annals Phys. **254** (1997) 192

[77] J. Gasser, In 'Mainz 1997, Chiral dynamics: Theory and experiment' 12, arXiv:hep-ph/9711503

[78] J. F. Donoghue and B. R. Holstein, arXiv:hep-ph/9803312

[79] J. F. Donoghue, B. R. Holstein and B. Borasoy, Phys. Rev. D **59** (1999) 036002

[80] M. Mojžiš and J. Kambor, Phys. Lett. B **476** (2000) 344

[81] D. Djukanovic, J. Gegelia and S. Scherer, Eur. Phys. J. A **29** (2006) 337

[82] M. Mai *et al.*, Phys. Rev. D **80** (2009) 094006

[83] T. Meissner, Phys. Lett. B **340** (1994) 226

[84] A. Walker-Loud *et al.*, Phys. Rev. D **79** (2009) 054502

[85] K.-I. Ishikawa *et al.* [PACS-CS Collaboration], Phys. Rev. D **80** (2009) 054502

[86] P. C. Bruns, L. Greil and A. Schäfer, Eur. Phys. J. A **48** (2012) 16

[87] X.-D. Ji, Phys. Rev. Lett. **78** (1997) 610

[88] X.-D. Ji, J. Phys. G **24** (1998) 1181

[89] A. V. Belitsky and A. V. Radyushkin, Phys. Rept. **418** (2005) 1

[90] M. Diehl, Phys. Rept. **388** (2003) 41

[91] C. Alexandrou *et al.*, Phys. Rev. D **83** (2011) 114513

[92] A. Sternbeck *et al.*, PoS LATTICE **2011** (2011) 177

[93] M. Dorati, T. A. Gail and T. R. Hemmert, Nucl. Phys. A **798** (2008) 96

[94] W. S. Hellman and D. Mustaki, Phys. Rev. D **35** (1987) 3522

[95] N. Beisert and B. Borasoy, Eur. Phys. J. A **11** (2001) 329

[96] J. Gasser *et al.*, Phys. Lett. B **652** (2007) 21

[97] J. Gasser *et al.*, Phys. Lett. B **675** (2009) 49

[98] V. Bernard, T. R. Hemmert and U.-G. Meißner, Phys. Lett. B **565** (2003) 137

[99] E. E. Jenkins and A. V. Manohar, Phys. Lett. B **259** (1991) 353

[100] G. Colangelo *et al.*, Eur. Phys. J. C **71** (2011) 1695

[101] A. Bazavov *et al.* [MILC Collaboration], PoS LATTICE **2010** (2010) 074

[102] A. Bazavov *et al.* [MILC Collaboration], PoS CD **09** (2009) 007

[103] S. Aoki *et al.* [PACS-CS Collaboration], Phys. Rev. D **79** (2009) 034503

[104] M. Gell-Mann, CTSL-20

[105] S. Okubo, Prog. Theor. Phys. **27** (1962) 949

[106] R. L. Jaffe and A. Manohar, Nucl. Phys. B **337** (1990) 509

[107] F. E. Close and R. G. Roberts, Phys. Lett. B **316** (1993) 165

[108] A. Walker-Loud, Phys. Rev. D **86** (2012) 074509

[109] A. Semke and M. F. M. Lutz, Phys. Lett. B **717** (2012) 242

[110] P. C. Bruns, M. Mai and U.-G. Meißner, Phys. Lett. B **697** (2011) 254

[111] M. Mai, P. C. Bruns and U.-G. Meißner, Phys. Rev. D **86** (2012) 094033

[112] X.-L. Ren *et al.*, J. High Energy Phys. **12** (2012) 073

[113] V. Bernard and U.-G. Meißner, Phys. Lett. B **639** (2006) 278

[114] S. Durr *et al.*, arXiv:1310.3626 [hep-lat].

[115] M. F. M. Lutz and A. Semke, Phys. Rev. D **86** (2012) 091502

[116] J. Martin Camalich, L. S. Geng and M. J. Vicente Vacas, Phys. Rev. D **82** (2010) 074504

[117] A. Semke and M. F. M. Lutz, Phys. Rev. D **85** (2012) 034001

[118] H. Hellmann, Z. Phys. **85** (1933) 180

[119] R. P. Feynman, Phys. Rev. **56** (1939) 340

[120] R. Horsley *et al.* [QCDSF-UKQCD Collaboration], Phys. Rev. D **85** (2012) 034506

[121] L. Alvarez-Ruso *et al.*, Phys. Rev. D **88** (2013) 054507

[122] G. S. Bali *et al.*, Nucl. Phys. B **866** (2013) 1

[123] T. P. Cheng and R. F. Dashen, Phys. Rev. Lett. **26** (1971) 594

[124] J. Martin Camalich, J. M. Alarcon and J. A. Oller, Prog. Part. Nucl. Phys. **67** (2012) 327

[125] P. C. Bruns, L. Greil and A. Schäfer, Phys. Rev. D **88** (2013) 114503

[126] I. Rosell, J. J. Sanz-Cillero and A. Pich, JHEP **0408** (2004) 042

[127] H. W. Fearing and S. Scherer, Phys. Rev. C **62** (2000) 034003

[128] S. Okubo, Phys. Lett. **5** (1963) 165

[129] M. Benayoun *et al.*, Eur. Phys. J. C **17** (2000) 303

[130] R. Urech, Phys. Lett. B **355** (1995) 308

[131] D. B. Leinweber and T. D. Cohen, Phys. Rev. D **49** (1994) 3512

[132] C. C. Chiang and C. B. Chiu, Nuovo Cim. A **16** (1973) 511

[133] F.-K. Guo *et al.*, Phys. Lett. B **703** (2011) 510

[134] F. Klingl, N. Kaiser and W. Weise, Z. Phys. A **356** (1996) 193

[135] M. F. M. Lutz and S. Leupold, Nucl. Phys. A **813** (2008) 96

[136] C. Terschlüsen, B. Strandberg, S. Leupold and F. Eichstädt, Eur. Phys. J. A **49** (2013) 116

[137] F. Niecknig, B. Kubis and S. P. Schneider, Eur. Phys. J. C **72** (2012) 2014

[138] S. P. Schneider, B. Kubis and F. Niecknig, Phys. Rev. D **86** (2012) 054013

[139] S. Collins *et al.*, Phys. Rev. D **84** (2011) 074507

[140] A. Kucukarslan and U.-G. Meißner, Mod. Phys. Lett. A **21** (2006) 1423

[141] J. F. Donoghue, arXiv:hep-ph/9607351

Acknowledgments

First and foremost I would like to thank my supervisors Prof. Dr. Andreas Schäfer and Dr. Peter C. Bruns, who have guided me through the last three and a half years, allowing me to make use of their extensive knowledge. I would also like to thank Prof. Dr. Andreas Schäfer and Dr. Peter C. Bruns as well as my colleagues and friends Michael Gruber and Philipp Wein for proofreading and assessing this thesis.

Moreover I want to express my gratitude to my office mates Philipp Wein and Daniel Ostermeier for countless discussions and distractions during the last years. I also want to thank all the people at the institute I have worked and collaborated with.

For many fun evenings of watching movies, cooking, going out for dinner and lively discussions I would like to thank my closest friends Benjamin Koch, Michael Gruber, Anton Mühlhöfer and Dr. Holger Leutz and I hope for many more evenings to come. I wish them all the best for their future endeavors, whatever they may be.

Last but not least, I would like to extend my utmost gratitude to my family and loved ones Daniela, Maverick, Engelyna and Pheonix for their support and encouragement and bringing a lot of joy to my life. I also want to thank my parents for their long-lasting financial and emotional support.

All research presented in this work was supported by the Deutsche Forschungsgemeinschaft SFB/Transregio 55 and the research presented in ch. 3 was partly supported by the European Union under Grant No. 256594 (IRG).